

This file is part of the following work:

**Dastpeyman, Mohadeseh (2019) *Structure-function relationships of disulfide-rich peptides*. PhD Thesis, James Cook University.**

Access to this file is available from:

<https://doi.org/10.25903/5ea659714d9ab>

Copyright © 2019 Mohadeseh Dastpeyman.

The author has certified to JCU that they have made a reasonable effort to gain permission and acknowledge the owners of any third party copyright material included in this document. If you believe that this is not the case, please email

[researchonline@jcu.edu.au](mailto:researchonline@jcu.edu.au)

# **Structure-Function Relationships of Disulfide-Rich Peptides**

Thesis submitted by

**Mohadeseh Dastpeyman**

M.Sc. Molecular Cell Biology

B.Sc. Biology

For the degree of Doctor of Philosophy in Medical and Molecular Sciences

College of Public Health, Medical and Veterinary Sciences

James Cook University

March 2019

## Acknowledgements

First and foremost, I would like to express my profound gratitude to my supervisor, Professor Norelle Daly, for her inspiring guidance, immense dedication and meticulous care throughout my PhD journey. She was the one who introduced me to the fascinating world of NMR spectroscopy of peptides and taught me NMR from the ground up.

I also would like to express my sincerest gratitude to my secondary supervisors: To Dr. Michael Smout for his enthusiasm for my work and excellent guidance on the *Ov*-GRN-1 part of the study; To Dr. David Wilson whose great insights and sound knowledge of HPLC analysis, mass spectroscopy, computer problems and IT helped me in the course of my PhD.

I would like to extend my gratitude to Dr. Paramjit Bansal for his invaluable advice on the chemistry side of the study, especially in peptide synthesis. I am also grateful to Dr. Paul Giacomini, Dr. Roland Ruscher, Mrs. Martha Cooper and Mrs. Jamie Brady for their kind advice and expertise in flow cytometry, to Mr. Phill Walsh for technical advice on chemical synthesis of chlorotoxin and to Dr. Javier Sotillo for collaboration in *in vivo* wound healing assay in *Ov*-GRN-1 project; Likewise, I would like to thank Distinguished Prof. Alex Loukas for his invaluable suggestions on *Ov*-GRN-1 manuscripts.

I would like to appreciate the support of the Australian Institute for Tropical Health and Medicine (AITHM) for granting me the scholarship throughout my PhD study. Many thanks must go to the many AITHM staff members, PhD and undergrad students in Daly's and Loukas's group who I have had the pleasure of working with. Especially Dr. Claudia Caceres Cobos for her friendship and support in the laboratory. Without you all, these years would not have been the same. I wish you all the best in your own adventures ahead.

I also would like to express my absolute gratitude to my beloved husband, Dr. Mojtaba H. Zadeh whose encouragement, endless support has meant a lot to me during the pursuit of my PhD. Last but not least, a heartfelt thanks to my dearest

family and close friends for their constant love and encouragement to pursue my goals and ambitions.

It's a moment of joy and fulfillment for me that this task has been accomplished. I would be proud if this work has added even a little to the current knowledge of science to enhance the quality of human life. I look forward to commencing the next phase of my career as a life scientist.

M. Dastpeyman

***“Let us fight for every woman and every man to have the opportunity to live  
healthy, secure lives, full of opportunity and love.  
We are all time travellers, journeying together into the future. But let us  
work together to make that future a place we want to visit.  
Be brave, be curious, be determined, overcome the odds. It can be done.”***

*Brief answers to the big questions by Stephen Hawking; 2018;p. 22*

## **Statement of the Contribution of Others**

During my PhD candidature my thesis work has included:

- 1) Synthesis of peptides (synthesis, oxidation, purification, mass analysis)
- 2) Structural analysis and calculation of peptides (NMR spectroscopy, CYANA, MOLMOL)
- 3) Biological assay (Cell culture, migration assay, invasion assay, xCELLigence cell proliferation assay, Flow cytometry assay, cell cytotoxicity assay, mouse wounding assay)
- 4) Thesis write-up

I had a James Cook University PhD scholarship and travel grants. I have attached a list outlining the contributions from others in the following table.

Nature of Assistance	Contribution	Names, Titles ( <i>if relevant</i> ) and Affiliations of Co-Contributors
Intellectual Support	Project plan and development	Prof. Norelle Daly, AITHM
	Data analysis assistance	Prof. Norelle Daly, AITHM Dr. Michael Smout, AITHM Dr. David Wilson, AITHM Dr. Paul Giacomin, AITHM
	Editorial support	Prof. Norelle Daly, AITHM Dr. Michael Smout, AITHM Dr. David Wilson, AITHM
	Stipend	Australian Institute for Tropical Health and Medicine (AITHM) PhD scholarship
	Conference travel assistance	<ul style="list-style-type: none"> <li>• 2018 College of Public Health, Medical and Veterinary Sciences Higher Degree Research Enhancement Scheme grant – Round 2 to attend Lorne 2019 conference</li> <li>• Travel grant for the Australian and New Zealand Society for Magnetic Resonance (ANZMAG), 2017</li> <li>• Travel grant for 12<sup>th</sup> Australian Peptide Conference, 2017</li> <li>• Travel grant for 3<sup>rd</sup> International Conference on Circular Proteins (ICCP), 2015</li> <li>• College of Public Health, Medical and Veterinary Science, James Cook University-Student Allowance</li> </ul>
Write-up grant	Doctoral Completion Grant, College of Public Health, Medical and Veterinary Science, James Cook University.	

<b>Research Assistant</b>	xCELLigence cell Proliferation assay, Mouse wounding assay	Dr. Michael Smout, AITHM
	Mouse wounding assay	Dr. Javier Sotillo, AITHM
	Flow cytometry	Dr. Paul Giacomin, AITHM
	Peptide synthesis	Dr. Paramjit Bansal, AITHM
	Mass spectrometry, Peptide synthesizer	Dr. David Wilson, AITHM
	NMR, Structure calculation	Prof. Norelle Daly, AITHM



## Published Works by the Author Incorporated into the Thesis

- **Part of Chapter 1: Dastpeyman, M.**, Smout, M.J., Wilson, D., Loukas, A., and Daly, N.L. Folding of granulin domains. *Peptide Science*, 2018, Doi:10.1002/pep1002.24062.

### **Author contributions:**

MD and NLD wrote the paper. MJS, DW and AL contributed to the final version of the manuscript.

- **Chapter 2: Dastpeyman, M.**, Giacomini, P., Wilson, D., Nolan M.J., Bansal, P.S., and Daly, N.L. A C-terminal fragment of chlorotoxin retains bioactivity and inhibits cell migration. *Frontiers in Pharmacology*, 2019, Doi:10.3389/fphar.2019.00250 (*in press*)

### **Author contributions:**

NLD, **MD** and PG conceived and designed the study. **MD** synthesized the chlorotoxin fragments and performed all the cell assays and structural studies. **PB** synthesized the chlorotoxin chemically. MJN and DW performed the protein array analysis. **MD** and NLD wrote the paper. All authors discussed the results and commented on the manuscript.

- **Chapter 3: Bansal, P.S.**, Smout, M.J., Wilson, D., Cobos Caceres, C., **Dastpeyman, M.**, Sotillo, J., Seifert, J., Brindley, P.J., Loukas, A., and Daly, N.L. Development of a potent wound healing agent based on the liver fluke granulin structural fold. *Journal of Medicinal Chemistry*, 2017 (60), 4258-4266.

### **Author contributions:**

MJS, AL, NLD conceived and designed the study. PSB, CCC and DW carried out the chemical synthesis and characterisation of the peptides. MJS carried out the recombinant expression of protein and cell proliferation assay. MJS and JS performed the *in vivo* mouse wounding study and analyzed the data. **MD** and ND performed NMR studies and structure calculation. NLD, AL, MJS supervised the

project. NLD and MJS wrote the paper. All authors discussed the results and commented on the manuscript.

- **Chapter 4: Dastpeyman, M.**, Bansal, P.S., Wilson, D., Sotillo, J., Brindley, P.J., Loukas, A., Smout, M.J., and Daly, N.L. Structural variants of a liver fluke derived granulin peptide potently stimulate wound healing. *Journal of Medicinal Chemistry*, 2018 (61), 8746-8753.

**Author contributions:**

NLD designed the project. **MD** synthesized and oxidized the peptides. PSB synthesized the GRN<sub>P2A</sub>. **MD** and NLD determined the structure. **MD** and MJS carried out the cell proliferation assay. **MD** aided in performing the *in vivo* studies by MJS and JS. MJS and JS analyzed the *in vivo* mouse wounding data. **MD** and NLD wrote the paper. All authors discussed the results and commented on the manuscript.

## Unpublished Works by the Author Incorporated into the Thesis

- **Chapter 5: Dastpeyman, M., Bansal, P.S., Wilson, D., Loukas, A., Smout, M.J., and Daly, N.L.** Distinct structural and biological differences between the N- and C-terminal regions of granulins. 2019.

### **Author contributions:**

NLD and **MD** conceived and designed the study. **MD** carried out peptide synthesis, oxidation and purification. **BSP** synthesized hGRNA. **MD** and NLD determined the structure. **MD** carried out the cell proliferation assay. **MD** and NLD wrote the paper. All authors discussed the results and commented on the manuscript.

## Abstract

This thesis focuses on applying the approach of downsizing disulfide-rich peptides for the development of potential drug leads, and providing insight into important structural features for bioactivity. Disulfide-rich peptides are widely distributed in nature and several hold promise for the development of novel therapeutics and diagnostic agents. This thesis explores the structure-function relationships of two disulfide rich peptides; the scorpion venom peptide chlorotoxin, and the parasitic liver fluke protein *Ov*-GRN-1.

Chapter 2 focuses on chlorotoxin, a potent tumour-imaging agent that selectively binds to tumour cells. Interestingly, it has been shown that chlorotoxin can have biological effects without disulfide bonds stabilising the native fold. This finding suggests that smaller regions, the inter-cysteine loops, might be responsible for the bioactivity of chlorotoxin. To explore this hypothesis, four small fragments of chlorotoxin were chemically synthesised using Fmoc solid-phase peptide synthesis method. As expected for such small peptides, NMR analysis indicated that the peptides were unstructured in solution. The bioactivity of the fragments was assessed by cell migration and invasion assays, alongside cell surface binding and internalization assays. Our results indicate that a small, unstructured fragment from the C-terminal region plays a critical role in the bioactivity of chlorotoxin. This is an unusual finding as structure is often critical for bioactivity in disulfide-rich peptides.

The remaining experimental chapters focus on the characterization of *Ov*-GRN-1, a protein isolated from the excretory/secretory (ES) products of the carcinogenic liver fluke *Opisthorchis viverrini*. *Ov*-GRN-1 belongs to the granulin family, which are growth factor proteins with a wide range of functions mainly involved in cell modulation. A recombinant version of *Ov*-GRN-1 causes proliferation of host (human) cells and can accelerate the repair of wounds in animals. However, recombinant expression of *Ov*-GRN-1 is challenging and leads to a low product yield, impeding its utility as a drug lead.

Chapter 3 focuses on the design, structure and functional analysis of minimized analogues from the N-terminal region of *Ov*-GRN-1. A series of analogues from the N-

terminal region of *Ov*-GRN-1 were chemically synthesised by solid-phase peptide synthesis, oxidized by air oxidation, purified by HPLC and characterized by mass spectroscopy. The structure of peptides was studied by NMR spectroscopy and the 3D structure was calculated by CYANA and visualized by MolMol. Cell proliferation and wound healing activity were assessed by an *in vitro* xCELLigence cell proliferation assay and an *in vivo* mouse-wounding model, respectively. The structural characterization of the *Ov*-GRN-1 N-terminal truncated peptides indicated that the introduction of a non-native disulfide bond appears to stabilize the fold and allow the peptide to form a  $\beta$ -hairpin structure. This analogue, which is called *Ov*-GRN<sub>12-35\_3s</sub>, induced cell proliferation and *in vivo* wound healing with similar potency to the full-length *Ov*-GRN-1.

NMR analysis of *Ov*-GRN<sub>12-35\_3s</sub> indicated the presence of multiple conformations, most likely from proline *cis/trans* isomerisation. In Chapter 4, a series of analogues involving mutation of the proline residues was synthesised to investigate the role of proline residues in adopting the multiple conformations by *Ov*-GRN<sub>12-35\_3s</sub>. Utilising the same techniques and methods used in Chapter 3, proline residues were shown to have a significant influence on the structure, activity and folding of *Ov*-GRN<sub>12-35\_3s</sub>. The results obtained for this chapter led to the development of a more potent analogue, GRN<sub>P4A</sub>, with improved folding yield.

Chapter 5 further explores the structure-function relationships of granulin peptides through analysis of the N-terminal region of human granulin A, as well as the C-terminal region of *Ov*-GRN-1. The former peptide was designed to determine if the non-native disulfide bond present in *Ov*-GRN<sub>12-35\_3s</sub> could also be accommodated in a granulin from another species, whereas the latter represents the first truncation study of the C-terminal region of a granulin peptide. The same techniques and methods as Chapter 4 were used to synthesise and characterise the analogues. Bioactivity of analogues were assessed using an *in vitro* xCELLigence cell proliferation assay. The results indicated that accommodation of a non-native disulfide bond might be a general phenomenon in the granulin family, as the N-terminal half of the human granulin A protein also folds independently with three disulfide bonds, despite significant sequence differences to the *Ov*-GRN-1 peptide. We also show for the first time that the equivalent C-terminal half of *Ov*-GRN-1 does not fold into a well-

defined structure, but still displays cell proliferative activity. Our results indicate that well-defined structures are not critical for granulin bioactivity.

In summary, the results highlight the potential of the “downsizing” approach for elucidating bioactive sequences, providing insight into folding processes and the development of novel drug leads. One of the major findings from this thesis is the development of a truncated form of *Ov*-GRN-1 that is likely to have lower immunogenicity than the full-length protein because of its smaller size, is significantly easier to produce and more potent in a mouse wound healing assay. These features make it a more viable drug lead for wound healing applications, and it is currently being considered for commercial development.

# Table of Contents

<b>Acknowledgements</b> .....	<b>ii</b>
<b>Statement of the Contribution of Others</b> .....	<b>v</b>
<b>Published Works by the Author Incorporated into the Thesis</b> .....	<b>viii</b>
<b>Unpublished Works by the Author Incorporated into the Thesis</b> .....	<b>x</b>
<b>Abstract</b> .....	<b>xi</b>
<b>Table of Contents</b> .....	<b>xiv</b>
<b>List of Tables</b> .....	<b>xviii</b>
<b>List of Figures</b> .....	<b>xix</b>
<b>Chapter 1. Introduction</b> .....	<b>1</b>
<b>1.1 Disulfide-rich peptides as therapeutics</b> .....	<b>2</b>
<b>1.2 Chlorotoxin: A naturally occurring peptide from scorpion venom</b> .....	<b>3</b>
1.2.1 Chlorotoxin selectively binding to tumour cells.....	4
1.2.2 Elucidating the biological target of chlorotoxin .....	7
1.2.3 Structure activity relationships of chlorotoxin.....	10
<b>1.3 <i>Ov</i>-GRN-1: A liver fluke granulin protein</b> .....	<b>12</b>
<b>1.4 Granulins</b> .....	<b>14</b>
1.4.1 Granulin structure .....	16
1.4.2 Truncation of granulin peptides.....	19
1.4.3 Related proteins – from plants to cone snails .....	26
1.4.4 Conclusions.....	27
<b>1.5 Scope of the thesis</b> .....	<b>28</b>
<b>1.6 References</b> .....	<b>30</b>
<b>Chapter 2. A C-terminal Fragment of Chlorotoxin Retains Bioactivity and Inhibits Cell Migration</b> .....	<b>43</b>
<b>2.1 Abstract</b> .....	<b>44</b>
<b>2.2 Introduction</b> .....	<b>45</b>
<b>2.3 Experimental section</b> .....	<b>48</b>
2.3.1 Peptide synthesis, purification and characterization.....	48
2.3.2 NMR spectroscopy and structure analysis.....	48

2.3.3	Serum stability assay .....	48
2.3.4	Mammalian cell culture .....	49
2.3.5	Cytotoxicity assay .....	50
2.3.6	Peptide biotinylation .....	50
2.3.7	Cell surface binding and internalization assay .....	51
2.3.8	Cell migration/invasion assay .....	52
2.3.9	Protein array analysis of chlorotoxin .....	53
<b>2.4</b>	<b>Results .....</b>	<b>54</b>
2.4.1	Design and synthesis of chlorotoxin fragments .....	54
2.4.2	Structural analysis with NMR spectroscopy .....	54
<b>2.5</b>	<b>Discussion .....</b>	<b>62</b>
<b>2.6</b>	<b>Acknowledgements .....</b>	<b>65</b>
<b>2.7</b>	<b>Non-standard abbreviations .....</b>	<b>65</b>
<b>2.8</b>	<b>References.....</b>	<b>66</b>

### **Chapter 3. Development of a Potent Wound Healing Agent Based on the Liver**

<b>Fluke Granulin Structural Fold .....</b>	<b>70</b>
<b>3.1 Abstract.....</b>	<b>71</b>
<b>3.2 Introduction.....</b>	<b>72</b>
<b>3.3 Experimental section .....</b>	<b>75</b>
3.3.1 Peptide synthesis and purification .....	75
3.3.2 Auto-induction of recombinant protein expression in <i>E. coli</i> .....	76
3.3.3 Recombinant protein purification .....	76
3.3.4 Protein refolding and purification.....	76
3.3.5 NMR spectroscopy and structure determination .....	77
3.3.6 Mammalian cell culture .....	77
3.3.7 Cell proliferation monitoring in real time using xCELLigence.....	78
3.3.8 Mouse wounding assay .....	79
<b>3.4 Results.....</b>	<b>80</b>
3.4.1 Design and synthesis of truncated <i>Ov</i> -GRN-1 peptides .....	80
3.4.2 Structural analysis with NMR spectroscopy.....	82
3.4.3 Cell proliferation.....	87
3.4.4 Mouse wound healing model.....	89
<b>3.5 Discussion .....</b>	<b>91</b>
<b>3.6 Acknowledgements .....</b>	<b>93</b>
<b>3.7 Supporting information.....</b>	<b>93</b>



3.8	Non-standard abbreviations .....	93
3.9	References.....	94
<b>Chapter 4. Structural Variants of a Liver Fluke Derived Granulin Peptide</b>		
<b>Potently Stimulate Wound Healing..... 97</b>		
4.1	Abstract.....	98
4.2	Introduction.....	99
4.3	Experimental section .....	101
4.3.1	Peptide synthesis, purification and characterisation .....	101
4.3.2	Disulfide formation.....	101
4.3.3	NMR spectroscopy and structure analysis .....	101
4.3.4	Mammalian cell culture .....	102
4.3.5	Cell proliferation monitoring in real time using xCELLigence.....	102
4.3.6	Mouse wounding assay .....	103
4.4	Results .....	104
4.4.1	Design and synthesis of <i>Ov</i> -GRN <sub>12-35_38</sub> mutants.....	104
4.4.2	Structural analysis with NMR spectroscopy.....	106
4.4.3	Cell proliferation monitoring in real time using xCELLigence.....	109
4.4.4	Mouse wounding assay .....	111
4.5	Discussion .....	112
4.6	Conclusions.....	116
4.7	Acknowledgements .....	117
4.8	Supporting information.....	117
4.9	Non-standard abbreviations .....	117
4.10	References .....	118
<b>Chapter 5. Distinct Structural and Biological Differences Between the N- and C-terminal Regions of Granulins .....</b>		
<b>123</b>		
5.1	Abstract.....	124
5.2	Introduction.....	125
5.3	Experimental section .....	127
5.3.1	Peptide synthesis, purification and characterisation .....	127
5.3.2	Disulfide bond formation.....	127
5.3.3	NMR spectroscopy .....	128
5.3.4	Structure calculations.....	128
5.3.5	Mammalian cell culture .....	128

5.3.6	Cell proliferation monitoring in real time using xCELLigence.....	129
<b>5.4</b>	<b>Results.....</b>	<b>130</b>
5.4.1	Design and synthesis of granulin peptide analogues .....	130
5.4.2	Structural analysis with NMR spectroscopy.....	133
5.4.3	Cell proliferation monitoring in real time using xCELLigence.....	137
<b>5.5</b>	<b>Discussion .....</b>	<b>138</b>
<b>5.6</b>	<b>Acknowledgements .....</b>	<b>142</b>
<b>5.7</b>	<b>Non-standard abbreviations .....</b>	<b>142</b>
<b>5.8</b>	<b>References.....</b>	<b>143</b>
<b>Chapter 6.</b>	<b>Conclusions and Future Directions .....</b>	<b>146</b>
<b>6.1</b>	<b>Conclusions.....</b>	<b>147</b>
<b>6.2</b>	<b>Future directions.....</b>	<b>151</b>
<b>6.3</b>	<b>References.....</b>	<b>154</b>

# List of Tables

## CHAPTER 1

Table 1-1 The sequence alignment of chlorotoxin and selected chlorotoxin-like peptides.....	11
---	----

## CHAPTER 3

Table 3-1 Structural statistics for the <i>Ov</i> -GRN-1 peptides ensemble .....	84
Table 3-2 CYANA target functions for the 15 possible disulfide bond connectivities present in <i>Ov</i> -GRN <sub>12-35_3s</sub> . .....	86

## CHAPTER 4

Table 4-1 Sequences of <i>Ov</i> -GRN-1 peptides .....	104
Table 4-2 Oxidative folding yields for the granulin peptides.....	105
Table 4-3 Structural statistics for GRN <sub>3Ala</sub> .....	108
Table 4-4 Sequence alignment of human granulins. ....	114

## CHAPTER 5

Table 5-1 Sequences of granulin peptides.....	131
Table 5-2 Structural statistics for hGRNA <sub>4-28_3s</sub> .....	135

## List of Figures

### CHAPTER 1

Figure 1-1 Schematic three-dimensional structure of chlorotoxin.....	4
Figure 1-2 (A) The order of the granulin motifs in human PGRN. (B) Granulin cysteine framework.....	15
Figure 1-3 Three-dimensional structure of full-length human GRN-4..	18
Figure 1-4 Sequence and three-dimensional structure of truncated carp granulin-1...	21
Figure 1-5 (A) The sequence of the 30-residue amino terminal sub-domain of GRN- 4..	23
Figure 1-6 Sequence and three-dimensional structures of the liver fluke <i>Ov</i> -GRN-1 truncated analogues. ....	25
Figure 1-7 Three-dimensional structures of peptides with granulin-like structures....	27

### CHAPTER 2

Figure 2-1 Schematic three-dimensional structure of chlorotoxin .....	45
Figure 2-2 Secondary shifts of chlorotoxin fragments. ....	54
Figure 2-3 Stability of the peptides in human serum.....	55
Figure 2-4 Cell viability assay of chlorotoxin and fragments treated U87-MG cells for 24 hours. ....	56
Figure 2-5 <i>In vitro</i> cell surface binding of chlorotoxin fragments. ....	58
Figure 2-6 <i>In vitro</i> cell internalization of chlorotoxin fragments.....	61

### CHAPTER 3

Figure 3-1 Three-dimensional structure of a 30 residue N-terminal domain of carp granulin-1.....	74
Figure 3-2 Sequences and secondary shifts of the <i>Ov</i> -GRN-1 truncated analogues. ...	81
Figure 3-3 Structural analysis of <i>Ov</i> -GRN <sub>12-34</sub> and <i>Ov</i> -GRN <sub>12-35_3s</sub> . ....	83
Figure 3-4 Chemical shift comparison between the published shifts of a truncated form of carp granulin and the mutant with C17A and C27A mutations. ....	85
Figure 3-5 Liver fluke granulin peptides induce cell proliferation. ....	88
Figure 3-6 Mouse wound healing activity of <i>Ov</i> -GRN-1 and peptides.....	89
Figure 3-7 Mouse wound healing day 4 images.....	90

## CHAPTER 4

Figure 4-1 Conserved cysteine framework in the granulin family.....	100
Figure 4-2 Regions of the TOCSY spectra of <i>Ov</i> -GRN <sub>12-35_3s</sub> and GRN <sub>3Ala</sub> .....	106
Figure 4-3 Secondary shifts of <i>Ov</i> -GRN <sub>12-35_3s</sub> engineered peptides.....	107
Figure 4-4 Three-dimensional structure of <i>Ov</i> -GRN <sub>12-35_3s</sub> (A) and GRN <sub>3Ala</sub> (B).....	109
Figure 4-5 Granulin peptide variants stimulated <i>in vitro</i> cell proliferation.....	110
Figure 4-6 Granulin peptides stimulated mouse wound healing.....	111

## CHAPTER 5

Figure 5-1 Granulin cysteine framework and structure.....	125
Figure 5-2 HPLC analysis of the oxidation reaction of granulin N-terminal truncated analogues, <i>Ov</i> -GRN <sub>9-35_3s</sub> and hGRNA <sub>4-28_3s</sub> .....	132
Figure 5-3 HPLC and mass analysis of the <i>Ov</i> -GRN <sub>39-66_3s</sub> oxidation reaction.....	133
Figure 5-4 One-dimensional proton NMR spectra for granulin N-terminal truncated analogues.....	134
Figure 5-5 $\alpha$ H Secondary-shift comparison for truncated granulin analogues.....	135
Figure 5-6 A comparison of the three-dimensional structure of (A) hGRNA <sub>4-28_3s</sub> and (B) <i>Ov</i> -GRN <sub>12-35_3s</sub> .....	136
Figure 5-7 xCELLigence fibroblasts cell proliferation assay.....	137
Figure 5-8 Superposition of the structures of the hGRNA <sub>4-28_3s</sub> and the hybrid hGRNA N-terminal truncated peptides.....	140

# **Chapter 1. Introduction**

## 1.1 Disulfide-rich peptides as therapeutics

Interest in peptides as pharmaceuticals or biological tools has increased recently. This interest reflects the importance of peptides in physiological processes in living systems, as well as certain properties that make them excellent potential drug candidates such as the ability to diffuse easily through tissue unlike antibodies, low toxicity, and high affinity and specificity for targets (1). In addition, they can be synthesized chemically. The list of peptides that have been investigated for therapeutic potential is enormous (1, 2). Peptides and their homologues are, or have the potential to be, used in medicine to treat several kinds of diseases and conditions, including: osteoporosis, cancer, cardiovascular and cardiovascular diseases (coronary syndrome and angina), diabetes, allergy and asthma, analgesia, epilepsy, gastrointestinal, baldness, growth problems, arthritis, impotence, haemostasis immunity, inflammation, obesity and vaccines (1-5).

Peptide-based drugs have been derived from three sources. The first group includes naturally occurring bioactive peptides, which are extracted from animals or plants. Those bioactive peptides include toxins, hormones and neurotransmitters. The second and third groups are non-naturally occurring peptides produced from either genetic libraries or chemical libraries (6, 7). Among these, the first group is the most preferred because naturally occurring peptides are optimized functionally against their ligands (6). Indeed, peptides based on naturally occurring drugs are a sensible option for addressing new therapeutic challenges in the coming years.

Despite the potential of peptides as drug leads, they often have low stability and significant effort has been directed at overcoming this limitation. Both naturally occurring and non-native modifications can stabilize peptides. One of the most common naturally occurring features that can stabilize peptides is a disulfide bond. Recently, disulfide-rich peptides have generated considerable interest in the development of peptide-based therapeutics owing to their remarkable stability toward chemical, enzymatic, or thermal extremes brought about by their highly folded structures (8). Examples of disulfide rich peptides currently used in the clinic include ziconotide (9) and linaclotide (10) for the treatment of chronic pain and constipation, respectively. Numerous other peptides are being assessed as potential drug treatments

but also for use as imaging agents.

Chlorotoxin (CTX), a disulfide-rich peptide extracted from the venom of a scorpion (*Leiurus quinquestriatus*), and granulin (*Ov*-GRN-1), a small disulfide-rich protein from the carcinogenic liver fluke *Opisthorchis viverrini*, have potential as diagnostic and/or therapeutic applications. Exploring the potential of chlorotoxin and peptides derived from *Ov*-GRN-1 is the focus of this thesis. Details regarding their biology, activity and structures are given in the following sections.

## **1.2 Chlorotoxin: A naturally occurring peptide from scorpion venom**

Scorpions were among the first habitant arthropods of the earth (11). Their venoms contain a variety of compounds, with the majority being small peptides containing 30-70 residues (12-14). There are approximately 1500 scorpion species, and despite the reputation for being dangerous, only 30 are considered life threatening to humans (15).

Scorpion envenomation results in stimulation of the nervous system and the adrenal medulla causing a massive release of sympathetic and parasympathetic neurotransmitters (15-17). Recent studies have shown scorpion venom peptides can influence a range of proteins including platelet activating factor (PAF), complement system interleukins, cytokines and tumour necrosis factor (TNF) (18). Although only a limited number have been pharmacologically and biochemically characterized, there has been interest in scorpion venom peptides as potential sources for drug design for decades.

One of the most well-studied scorpion venom peptides is chlorotoxin, which was originally purified from the venom of the Israeli scorpion *Leiurus quinquestriatus* in 1993 (19). Chlorotoxin is a 4 kDa neurotoxin that contains 36 amino acids and with four disulfide bonds at the core of its structure it is tightly folded and highly stable. The tertiary structure is composed of a  $\beta$ -hairpin and an  $\alpha$ -helix as shown in Figure 1-1 (19-21).



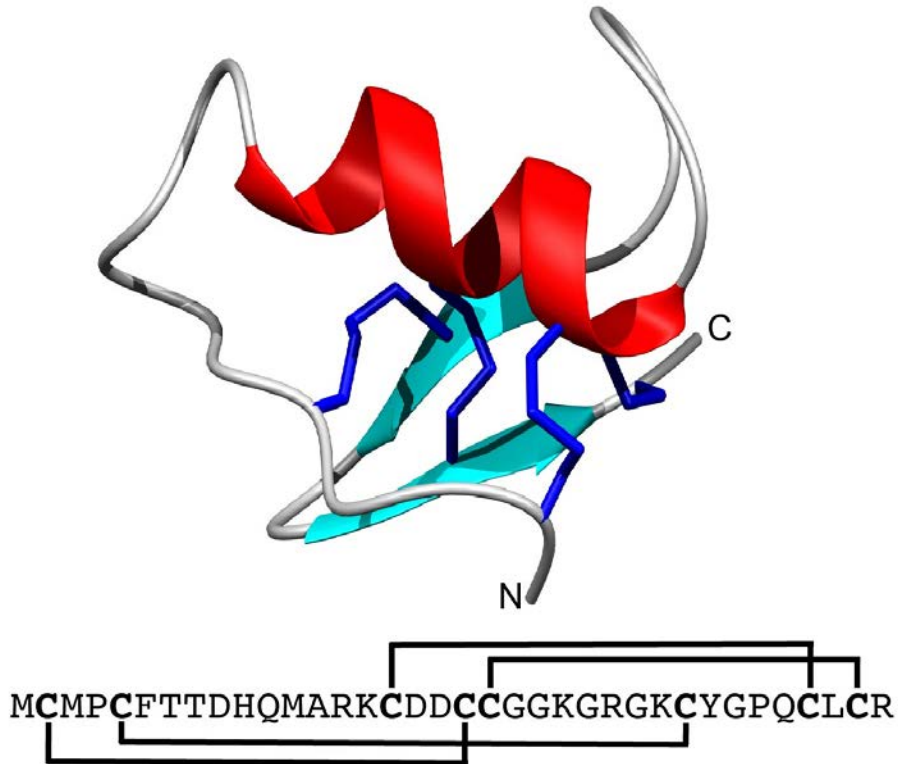


**Figure 1-1 Schematic three-dimensional structure of chlorotoxin (PDB code 5L1C).** The chlorotoxin sequence and disulfide bond connectivity is given below the structure.

### 1.2.1 Chlorotoxin selectively binding to tumour cells

It was initially shown that chlorotoxin selectively binds to glioma cells but not normal healthy brain cells (22). Later, it has been demonstrated that it can also bind to other embryologically related cells and derived tumours of neuroectodermal origin (23). An explanation for this result is that these cells, and the tumours that originate from them, have a common embryologic stem, so they share genetic and antigenic phenotypes that appears to contribute to selective binding of chlorotoxin. In contrast to the high-affinity of chlorotoxin for tumour cells, more than fifteen normal human tissues have been shown to be negative for chlorotoxin binding. The only exception is human umbilical vein endothelial cells (HUVEC) (24). Chlorotoxin showed anti-angiogenic activity on HUVEC cells *in vivo* and *in vitro*, and can also significantly inhibit tumour cell migration and invasion (24, 25) highlighting the potential of chlorotoxin in cancer treatment.

The selective binding of chlorotoxin to tumour cells bodes well for its application in cancer therapy as a tumor imaging agent (23). Tumour imaging agents have great potential in the treatment of cancer, particularly for brain cancer. The primary treatment of cancerous tissue is resection and this requires accurate imaging. Cancers of the brain are one of the most critical forms influenced by the success of surgical procedures, with more than 80% of malignant cancers recurring as a result of a residual tumour (26). Brain tumours are neoplasms in the pediatric and adult population that are often associated with considerable morbidity and mortality (27). Successful imaging has several benefits for both patients and surgeons:

- Guaranteeing a long-term survival of the patient because only one remaining cancer cell can cause regrowth of a new tumour so by precisely defining the tumor boundaries tumour removal will be optimized (28, 29).
- Maximizing radiotherapy efficiency.
- By determining the exact size and extent of the tumour, local delivery of therapeutics will be enhanced.

Whereas adequate imaging is nearly impossible due to limitations in traditional imaging methods such as MRI, magnetic resonance spectroscopy (MRS), and <sup>18</sup>F-FDG PET<sup>1</sup> (30-34), specific binding activity of chlorotoxin to tumour cells make this peptide an effective optical imaging contrast agent. While most of available radiopharmaceuticals such as 81C6 antibodies cannot pass through the blood barrier brain (BBB) (33, 35, 36), it is reported that chlorotoxin and its conjugated biomolecules such as radiolabeled-chlorotoxin can diffuse in brain tumour cells and selectively bind to tumour cells, not normal cells (22, 33, 36). However, Kovar and colleagues used the Evan's Blue perfusion assay to test the integrity of the BBB after administration of IRDye800CW chlorotoxin, and reported that the BBB was compromised at the site of the tumours (36), indicating this aspect of chlorotoxin needs more study.

Several methods have been used to detect chlorotoxin binding to tumours, both *in vitro* and *in vivo*, including radiolabelling and fluorescent labels such as Cy5.5 (37), Alexa-488 (38) and IRDye800CW (36). Initial studies used labelling of chlorotoxin with different I-radioisotopes in order to develop chlorotoxin as both a tumour

---

<sup>1</sup> Fluorodeoxyglucose(<sup>18</sup>F-FDG) Positron Emission Tomography(PET)

imaging agent and a cell proliferation controlling medicine. The tyrosine residue at position 29 of chlorotoxin was labelled with  $^{131}\text{I}$  or  $^{125}\text{I}$  and analyses confirmed chlorotoxin could selectively bind to glioma cells and serve as a glioma-specific marker with diagnostic and therapeutic potential (22, 33, 39). The activity of chlorotoxin does not change by labelling with either  $^{131}\text{I}$  or  $^{125}\text{I}$ . Further investigation showed  $\gamma$  emittance, energy level and consequently penetration properties of  $^{131}\text{I}$  is higher and deeper than other radioisotopes such as  $^{123}\text{I}$  and  $^{124}\text{I}$  (22, 33).  $^{131}\text{I}$ -Chlorotoxin has been termed  $^{131}\text{I}$ -TM-601 and successfully passed human clinical trial phase I (40, 41). The results from the phase I trial were promising as  $^{131}\text{I}$ -radiolabeled chlorotoxin was detectable for up to 8 days after drug injection *in vivo* (41, 42).

Despite the potential of radiolabelled chlorotoxin, significant effort has been put into developing alternative forms of chlorotoxin for binding to tumour cells. Chlorotoxin conjugated to the near-infrared (NIR) fluorescent dye Cy5.5 has been termed “Tumour Paint”(37). Chlorotoxin-Cy5.5 effectively identifies the margin between tumour and normal tissue on genetically engineered or orthotopically xenografted mouse models of brain cancer (37). Further studies have shown that labelled chlorotoxin can be used to discriminate prostate cancer, intestinal cancer and sarcoma from normal tissue in mouse models, indicating its significant potential in the treatment of a range of cancers (37). There are three lysine residues at positions 15, 23, and 27 in chlorotoxin that can react with Cy5.5. The presence of multiple lysine residues complicates the conjugation with Cy5.5 leading to the presence of di- and tri- labelled peptide (37). Although it is possible to have mixtures such as this approved by the US Food and Drug Administration (FDA) and similar regulatory agencies elsewhere, commercialisation is hindered by the fact that it is expensive and difficult to match the ratio of mono-, di- and tri-labelled batches in the future. Lysine 15 and lysine 23 have been substituted with either alanine or arginine residues, which resulted in mono-labelled peptide that was still functional in *in vivo* assays (43). Mono-conjugated chlorotoxin is anticipated to have fewer regulatory hurdles for human applications than a mixture of conjugation forms, highlighting the significance of the results. Chlorotoxin labelled with IRDye800CW, has also successfully been used as a tumour-imaging agent in a spontaneous mouse model of medulloblastoma (36).

Chlorotoxin has also been used for targeting ligands in drug delivery systems (44). It has been shown that coating nanoparticles with Cy5.5-chlorotoxin, in order to visualize and image tumours, improves their uptake by tumour cells and enhances the effect of the loaded medicine (37, 44-53). In addition, tumors treated with chlorotoxin nanoparticles are detectable longer, inferring that conjugating chlorotoxin to nanoparticles probably changes its internalization pathway making it more resistant to lysosomal degradation enzymes (38).

### **1.2.2 Elucidating the biological target of chlorotoxin**

Given the potential of chlorotoxin as a therapeutic it is of significant interest to understand how it is acting *in vivo* and to determine the biological target. However, elucidating the actual target for chlorotoxin has not been straightforward. It was initially thought that chloride channels were the specific receptor for chlorotoxin (54), but later matrix metalloproteinase-2 and annexin A2 have been proposed as other possible targets for chlorotoxin (39, 55).

#### **1.2.2.1 Chloride ion channel**

Chlorotoxin can effectively block glioma-specific chloride ion channel (ClC-3) (56, 57). ClC-3 is one of nine subtypes of chloride ion channels (ClC) situated in various and widespread sub-cellular places. A few of ClCs that are plasma membrane channel have an essential role in ion transportation. The other ClC proteins are situated in the endosomal-lysosomal apparatus to either acidify or modify chloride concentration of the vesicles (58).

The ClC-3 voltage-gated chloride channel is highly and selectively expressed in glioma cells (57, 59) and end-stage patient biopsies (59), consistent with it being a target for chlorotoxin. ClC-3 is a type of Cl<sup>-</sup>/H<sup>+</sup> exchanger that is mainly expressed in the membrane of endosomal/lysosomal vesicles and synaptic vesicles (58, 59) and is involved in cell cytoskeleton rearrangements and consequently cell shape and movements during cell migration and invasion (22, 60, 61). Interestingly, it is reported that chlorotoxin can inhibit rat colonic enterocyte Cl<sup>-</sup> channels when only applied to the cytoplasmic surface (62).

### **1.2.2.2 Matrix metalloproteinase-2**

MMP-2 belongs to a superfamily of zinc-dependent endopeptidases, and has been identified as another target for chlorotoxin (55). There are four variations of MMPs (MMP-1, MMP-2, MMP-3 and MMP-9), which are not normally expressed in normal brain cells, but they are overexpressed in tumour cells (63-65) consistent with it being a target for chlorotoxin. Interestingly, chlorotoxin appears to interact with MMP-2 but not other isoforms of MMPs (55).

MMP-2 is part of a lipid raft-anchored complex, which is involved in cell migration and invasion. The other components of this complex are membrane type-I MMP (MT1-MMP), a transmembrane inhibitor of metalloproteinase-2 (TIMP2),  $\alpha_v\beta_3$  integrin, and other proteins (55, 66). MT1-MMP converts MMP-2 to an active enzyme by proteolytic cleavage of the MMP-2 proenzyme (67-69). The MMP-2 complex is internalized via clathrin-mediated endocytosis into cells following binding of chlorotoxin (38, 64). Receptor-mediated endocytosis was also observed when chlorotoxin was conjugated to nanoparticles (70). The interaction between chlorotoxin with MMP-2 decreases the surface expression of CIC-3 and potentially de-functionalizes CIC-3 channels (60), suggesting a pathway for how chlorotoxin can effectively inhibit tumour cell migration and invasion (25, 55, 61). Further investigation showed that after internalization of chlorotoxin, it localizes near the trans-Golgi in human glioma, lung carcinoma and normal vascular endothelial cells, while in normal human dermal fibroblast (NDHF) and astrocytes the chlorotoxin vesicle trafficking pattern is different and chlorotoxin is distributed throughout the cytoplasm (38).

There is a direct relation between the high level of MMP's expression and malignancy of tumours (71-73). Also, MMP-2 has a key role in migration and invasion of glioma cells (74). It is reported that chlorotoxin can inhibit MMP-2 via two main mechanisms, firstly it reduces the surface expression of active MMP-2 due to internalization of MMP-2 upon chlorotoxin exposure, furthermore it inhibits its enzymatic activity (55). Chlorotoxin can inhibit MMP-2 activation in pancreatic cancer cells via the same mechanism (75).

Although MMP-2 appears to be involved in chlorotoxin binding to tumor cells, the evidence on how these two molecules specifically bind is controversial (37, 55). Although recombinant His-CTX co-purified with MMP-2 using affinity chromatography (55), in another study recombinant MMP-2 did not show any specific binding to CTX:cy5.5 conjugates in pull down experiments (37).

### **1.2.2.3 Annexin A2**

Subsequent studies have identified annexin A2 as a novel binding partner of chlorotoxin in multiple tumour cell lines as well as human umbilical vein endothelial cells (HUVEC) (39). Annexin A2 is overexpressed in several human cancers including high-grade glioma consistent with it being a target for chlorotoxin (39). Although chlorotoxin binds to HUVECs it has higher affinity for glioma cells and when conjugated has very high selectivity for tumour cells in *in vivo* assays (36, 37).

Annexins are ubiquitous soluble proteins with the hallmark feature of calcium-dependent binding to phospholipid membranes. They are important for the health of organisms, and the term ‘annexinopathies’ has been coined for annexin-related diseases (76). All known members of this protein family possess a distinctive, highly conserved fold (77). This fold enables general adapter-like functions at the surface of phospholipid membranes (78) and confers diverse roles to these proteins including vesicular transport (endo- and exocytosis), and membrane attachment of the cytoskeleton (79). Several annexins, and in particular annexin A2, have also been implicated in extracellular functions (80) but always with the involvement of membrane surfaces.

Annexin A2 is involved in a multitude of cellular signaling processes, including the endocytic transport and localisation of activated epidermal growth factor receptor. Activation of the receptor at the cell surface elicits signaling events that regulate a variety of cellular processes. For signal termination, the receptor needs to be internalized and targeted to lysosomes for degradation –a process which is regulated by calcium-binding proteins, including annexin A2 (79). In the context of chlorotoxin internalisation, the involvement of annexin A2 in early endocytosis, i.e. the formation and pinching off of clathrin-coated vesicles (81) is of particular interest. Structurally,

annexin A2 has features that are not shared by other members of this family (82). Its N-terminal region binds with high affinity to the small S100A10 protein (also called p11), a member of the S100-family of proteins (83). The annexin A2 N-terminus is  $\alpha$ -helical and binds p11 only in the acetylated form. The binding of p11 modulates the *in vitro* properties of annexin A2 and probably also its *in vivo* function (84).

### 1.2.3 Structure activity relationships of chlorotoxin

In addition to understanding the biological target, understanding the structural features important for function is likely to facilitate the development of chlorotoxin as a therapeutic. Peptides such as chlorotoxin are well suited to structural analysis with NMR spectroscopy because of their small size, solubility in water and well-defined structures. The methods used for NMR analysis of peptides have been reviewed and several studies have highlighted the potential of this technique in elucidating structure/function relationships of peptides (85-88).

There has been limited structure function studies done on chlorotoxin but there are related peptides that provide the opportunity to assess the natural structural and functional variation. Three chlorotoxin-like peptides have been reasonably well studied. The sequence of these peptides is compared to chlorotoxin in Table 1-1.

AaCTx, a 34-residue peptide from the venom of *Androctonus australis*, has four disulfide bonds and shares 61% identity to chlorotoxin (Table 1-1). AaCTx is less potent at inhibiting glioma cell migration and invasion than chlorotoxin (89). BmK CT, a 35 amino acid peptide with four disulfide bonds and 68% amino acid identity to chlorotoxin was purified from the Chinese scorpion *Buthus martensii Karsch* venom. BmK CT showed similar activity to chlorotoxin regarding inhibition of migration and invasion of glioma cells via interaction with the MMP-2 receptor and blocking of CIC-3 in glioma cells (52). GaTx1 is a 34 amino acid peptide extracted from the venom of the scorpion *Leiurus quinquestriatus hebraeus*. It shares 79% homology sequence identity with chlorotoxin and acts on a receptor from the ATP-binding cassette transporters (ABC) family. This receptor can act as a CIC (90).

The activity of these three peptides provides insight into the structure function

activity particularly with AaCTx displaying lower bioactivity than chlorotoxin. However, further study is required to more fully understand the important structural features for binding to tumour cells.

**Table 1-1 The sequence alignment of chlorotoxin and selected chlorotoxin-like peptides.**

Peptide	Sequence
Chlorotoxin	MCMP <b>C</b> FTTD <b>H</b> QMARK <b>C</b> DD <b>C</b> CGGKGRGK <b>C</b> YGPQ <b>C</b> LCR--
AaCTx	MCIP <b>C</b> FTTNPNMAAK <b>C</b> NAC <b>C</b> GSRR-G <b>S</b> CRGPQ <b>C</b> IC---
BmK CT	- <b>C</b> GP <b>C</b> FTTDANMARK <b>C</b> RE <b>C</b> CGGIG--K <b>C</b> FGPQ <b>C</b> LCNR <b>I</b>
GaTx1	- <b>C</b> GP <b>C</b> FTTD <b>H</b> QMEQ <b>K</b> CAE <b>C</b> CGGIG--K <b>C</b> YGPQ <b>C</b> LCNR-

The sequence of the chlorotoxin (19), AaCTX (89), BmK CT (52) and GaTx1 (90) are cited accordingly.

A recent study has shown that the structure function relationships of chlorotoxin might be quite complicated. Ojeda and colleagues explored the importance of each of the four disulfide bonds in chlorotoxin structure and activity. Briefly, they replaced each cysteine pair or all of the cysteine residues with L- $\alpha$ -aminobutyric acid and found that the disulfide bonds of chlorotoxin are essential for its stability and structure but not for its migration inhibitory effect (24). This interesting finding implies that one of the individual inter-cysteine loops might play a role in the activity. This hypothesis will be explored in this thesis.



### 1.3 *Ov*-GRN-1: A liver fluke granulin protein

*Ov*-GRN-1 is a protein from the carcinogenic liver fluke *Opisthorchis viverrini*, which is one of only three known carcinogenic eukaryotic pathogens (91) and is classified as a group 1 carcinogen by the international agency for research on cancer (IARC) (92). *O. viverrini* transmits to humans through eating raw cyprinid fishes containing the metacercarial stage of *O. viverrini* (93) and stimulates cellular proliferation and tumorigenesis of cholangiocytes in bile ducts via excretory-secretory products (ES) (91, 94, 95) that can finally lead to cholangiocarcinoma (CCA), bile duct cancer after 30-40 years of infection (94). CCA is invasive, highly metastatic with a dismal prognosis and patients die within 3-6 months of diagnosis (94, 96). The association between the occurrence of CCA and the presence of liver flukes has been known for about 50 years (97) and confirmed by WHO (98).

Analysis of the ES products of *O. viverrini* has revealed a complex mixture of proteins that have been associated with cancer and cell proliferation, including proteases of different mechanistic classes and orthologues of mammalian growth-factor like proteins and anti-apoptotic proteins (99, 100). Transcriptome analysis and the ES proteome screening have shown that a homologue of human granulin, a growth factor protein, exists in the ES products and it has been termed *Ov*-GRN-1 (100, 101).

*Ov*-GRN-1 plays a potential role in establishing a tumorigenic environment during chronic infection (99, 101) and is the first helminth-derived growth factor described from a pathogen to cause proliferation of mammalian cells (99, 101). This finding led to the hypothesis that the natural physiological role for *Ov*-GRN-1 is to stimulate wound healing in bile duct epithelia damaged by feeding and other activities of the liver flukes (101, 102). Based on this hypothesis it was shown that the ES products of *O. viverrini* can accelerate the repair of wounds in cultured human cholangiocytes (101, 102), and wound repair is significantly diminished by silencing *Ov-grn-1* gene expression in the fluke (101, 102). Picomolar concentrations of recombinant *Ov*-GRN-1 induced angiogenesis and significantly accelerated wound repair in mice (101).

Although the exact mechanism of action of *Ov*-GRN-1 has not been fully determined several studies have provided details regarding changes in gene expression profiles. Investigation on *Ov*-GRN-1 downstream signaling pathways showed it induce gene expression of proteins involved in carcinogen pathway alongside with wound healing pathways (102). Three pathways appear to be involved. Firstly, *Ov*-GRN-1 principally over expresses proteins involved in spliceosomes, endoplasmic reticulum (ER) protein processing and metabolic pathways (102). The main role of the spliceosome is splicing pre-RNA to mRNA (103). As RNA splicing has the main role in the epithelial-mesenchymal transition (EMT) process, *Ov*-GRN-1 can indirectly regulate EMT (102). EMT is a biological process including multiple biochemical changes in epithelial cells that finally lead to acquiring mesenchymal cell phenotype including migration and invasion capacity and resistance to apoptosis (104). Mesenchymal cells are involved in both wound repair and tumor metastasis but the mechanism is still unclear (104). Therefore, by overexpressing spliceosome proteins, *Ov*-GRN-1 can indirectly contribute to both wound healing and tumorigenesis.

Secondly, *Ov*-GRN-1 up regulates genes encoding proteins from the CXCL family of cytokines (CXCL1, 2, 5 and 8). The CXCL chemokine family has an important role in wound healing and angiogenesis (105, 106) and the receptor (CXCR<sub>2</sub>) for this family shares downstream signaling pathways with epidermal growth receptor (EGFR) and MAPK pathways that are the main signaling pathways for cell proliferation induction (107-110). *Ov*-GRN-1 triggers the MAPK pathway (101) which is consistent with the initiation of CCA in people with chronic *O. viverrini* infection [99].

Thirdly, *Ov*-GRN-1 induces gene expression of STK11 (liver kinase B1), which is involved in wound healing by triggering inflammatory pathways and chemotaxis regulation (111, 112).

The wound healing properties of *Ov*-GRN-1 has potential in the treatment of diabetic ulcers where the normal tissue repair mechanisms are overwhelmed and topical treatment is required for a short term. There are staggering statistics related to diabetes, with estimates of 280 Australians developing the disease every day and predictions that 3.3 million Australians will have type 2 diabetes by 2031 (113). More

than 8% of diabetic deaths are related to diabetic ulcers, (reviewed in (113)) making the need for more effective wound healing treatments of critical importance.

Despite the potential of *Ov*-GRN-1, complications might arise in its development as a wound healing agent because it is difficult to produce in substantial quantities (114). An approach that might be effective in developing more viable wound healing agents based on *Ov*-GRN-1, involves using chemical synthesis to make truncated forms of the full-length protein. Minimising proteins can enhance their potential in drug design by improving stability and making them cheaper to manufacture (115). Furthermore, smaller peptides are less likely to be immunogenic than larger proteins. The background to the granulin family and details of the truncation studies on granulins are given in 1.4 and is taken from a published review on “Folding of Granulin Domains” (116).

#### **1.4 Granulins**

Granulins were initially identified in the granules of human leukocytes (117) and are now known to occur in a wide range of organisms (118) with examples in particular species of oyster (119), insects (120), parasites (101), ascidians (121), mollusks (122) and plants (123). They are involved in several physiological functions and disease processes (124, 125) such as cell growth modulatory effects (125-127), wound repair (114, 128), inflammation (129) and tumour growth (130-132). We have recently shown that a granulin from a liver fluke, and peptides engineered based on this protein, have potent wound healing properties in a mouse model (128). The peptides in particular have significant potential in the development of new therapeutics for wound healing in conditions such as diabetes, which is often associated with chronic wounds.

The precursor proteins of granulins either have a single granulin domain, or multiple domains. The precursor protein of human granulin is progranulin (PGRN) (126), also known as proepithelin (133, 134), PC-cell-derived growth factor (135) and acrogranin (136). PGRN comprises a signal peptide and tandem repeats of seven-and-a-half granulin motifs in the order P-G-F-B-A-C-D-E, where P is the half-motif and A-G are full repeats (129, 137, 138). The full repeats have also been referred to as 1-7, in the

order they occur in the precursor protein, as shown in Figure 1-2A. The numerical nomenclature will be used in this review. The precursor protein is proteolytically processed by elastase into individual granulin modules, which each have masses in the 6 kDa range, after secretion from the cell (137, 138). PGRN has similar activities to granulin including roles in cellular proliferation (134), controlling embryogenesis (139), tissue repair (140), cancer (141, 142) and inflammation (129, 137, 143).

Granulins have a conserved cysteine framework comprising four pairs of cysteine residues flanked by two separated cysteine residues at both the N and C terminal regions (129), as shown in Figure 1-2B.

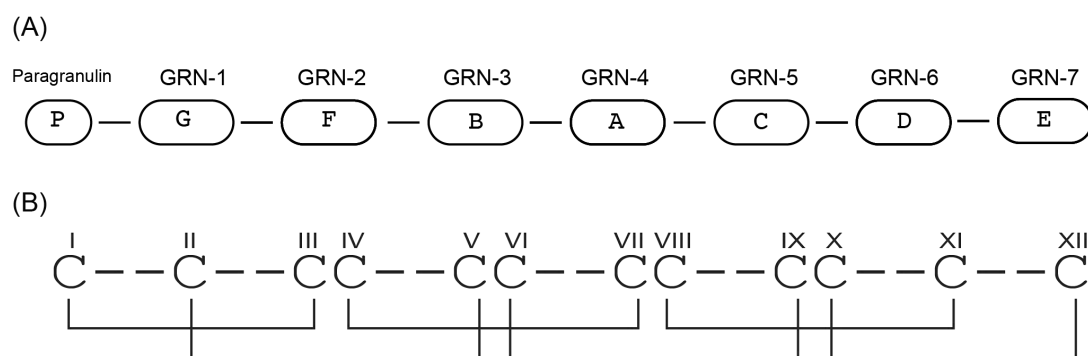


**Figure 1-2 (A) The order of the granulin motifs in human PGRN. (B) Granulin cysteine framework.** Granulins comprise 12 cysteine residues, with four cysteine pairs and two separated cysteine residues at the N- and C-terminal regions. The disulfide bonds shown in the figure are based on the connectivity determined for carp granulin-1 (144).

Despite the conserved cysteine framework, there is limited sequence conservation amongst the granulin family and consequently there is variation in the structures and biological activities. The three-dimensional structures and folding properties of granulins from carp, human and a liver fluke have been studied. This review provides an overview of these studies and the insight gained on the structure-function relationships for these peptides. Understanding the structure-function relationships is likely to be useful for developing lead molecules for conditions such as wound healing.

## 1.4.1 Granulin structure

### 1.4.1.1 *Three-dimensional structure of carp granulin-1*

The first three-dimensional structure determined in the granulin family was of carp granulin-1, and used native material isolated from extracts of spleen and head kidney of *Cyprinus carpio* (144, 145). The structure, determined using NMR spectroscopy, comprises four  $\beta$ -hairpins (I-IV) that are cross-linked by six disulfide bonds resulting in a ladder-shaped arrangement of the disulfide bonds (144). Residues 1-11 (I), 14-28 (II), 31-43 (III) and 46-57 (IV) are involved in forming the four  $\beta$ -hairpins (I-IV). The structures are relatively well defined with an RMSD over the backbone atoms of  $0.52 \pm 0.2 \text{ \AA}$  (144).

Carp granulin-1 appears to be highly stable to thermal denaturation as there were no changes in the NMR spectra following a heating and cooling cycle (144). This stability is likely to be associated with hydrophobic interactions involving the side chains of Val 1, His 3 and Ile 9, as well as interactions between the side chains of Ile 2, Trp 24 and the two disulfide bridges Cys I-Cys III and Cys II-Cys V, which link the first two  $\beta$ -hairpins together (144). The side chain of Trp 24 also interacts with the side chains of Asp 5, Thr 8 and Leu 18, which is likely to be contributing to the stability (146).

### 1.4.1.2 *Three-dimensional structures and activities of human granulins*

The seven full-length human granulin modules (1-7) have each been expressed recombinantly as thioredoxin fusion proteins using an *E. coli* strain that promotes formation of disulfide bonds (147). Enterokinase was used to cleave the fusion proteins to yield the individual modules. The disulfide isomers present in the recombinant granulin modules were analysed using reversed-phase HPLC, mass spectrometry and NMR spectroscopy (147). Three of the seven peptides (GRN-2, GRN-4 and GRN-5) displayed relatively sharp peaks on HPLC and significant dispersion in the amide region of NMR spectra. By contrast GRN-3 and GRN-7 did not display significant dispersion in the NMR spectra, indicating a lack of well-defined structure. The fractions from GRN-1 and GRN-6 were not spectrally homogeneous. GRN-1 contains only ten cysteine residues rather than the twelve

present in the majority of granulins (147). It would be of interest to further characterize the folding of this peptide to determine the influence of a reduced number of disulfide bonds on structure.

Given the significant dispersion in the amide region for GRN-2, GRN-4 and GRN-5, isomers were purified by RP-HPLC and analysed using two-dimensional NMR spectroscopy (147). A single peak from GRN-4 was purified, whereas two peaks were purified for GRN-5 and GRN-2. All of the purified forms were full-length, with the exception of one of the fractions from GRN-2, which had a molecular weight of approximately half that of the full-length peptide (147). The GRN-5 peaks had the same mass and appeared to be different disulfide bond isomers. Analysis of the NOEs (Nuclear Overhauser Enhancement) in the NMR data indicated that Cys I-Cys III and Cys II-Cys V formed disulfide bonds in GRN-2, GRN-4 and GRN-5, consistent with the carp granulin-1 structure, but did not allow definitive elucidation of the other disulfide bonds. Similarly, proteolytic cleavage and partial reduction approaches did not provide evidence for the complete disulfide connectivity (147).

The three-dimensional structures of GRN-2, GRN-4 and GRN-5 were determined using the disulfide connectivity elucidated for carp granulin-1 and indicated the presence of two well-defined  $\beta$ -hairpins in the N-terminal region but the C-terminal regions were more disordered (147). Despite the well-defined N-terminal region, the first hairpin was less well defined than the second hairpin (147). The three-dimensional structure of GRN-4 is shown in Figure 1-3, highlighting the well-defined N-terminal region in contrast to the C-terminal region. The root mean square deviation (RMSD) for GRN-4 is  $7.0 \pm 1.9 \text{ \AA}$  over the backbone atoms, which is significantly higher than that observed for carp granulin-1, highlighting the disorder present in the C-terminal region of GRN-4.

In addition to the structural variation, there was also significant variation in the bioactivity of the GRN peptides. GRN-4 displayed inhibition of the growth of a breast cancer cell line, whereas GRN-2 showed stimulatory activity (147). The poorly folded isomers, which were present in GRN-1, GRN-3, GRN-6 and GRN-7, generally had weak activity (148). The differences in structure and activity across the human

granulin peptides indicate that the sequence diversity has a significant impact on the structure-function relationships. The role of the disulfide bonds in structure and activity has been further evaluated for GRN-3 using experimental and computational approaches (148, 149). Structural analysis of fully reduced GRN-3 indicated the peptide was disordered (149).

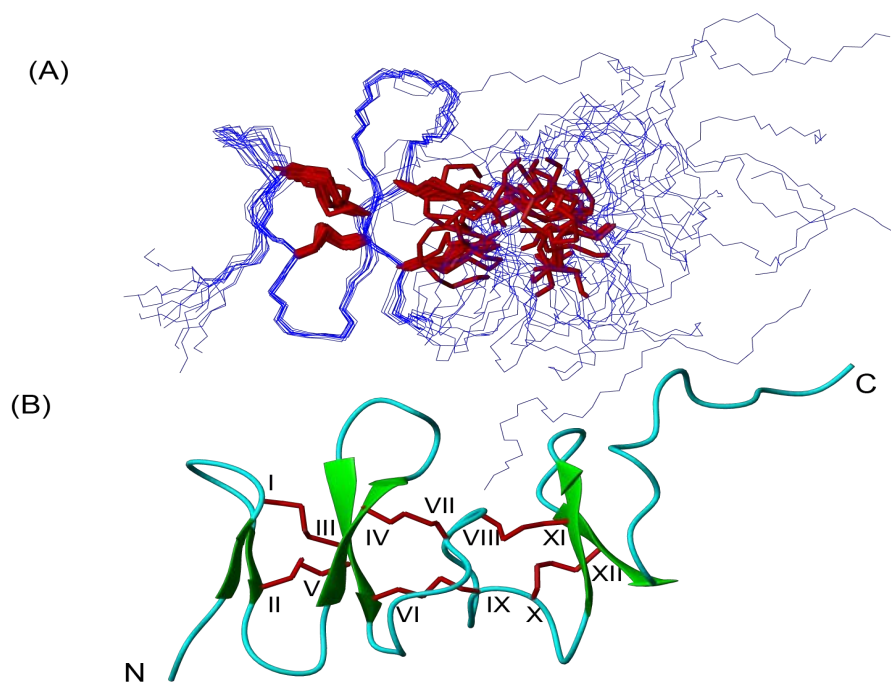


**Figure 1-3 Three-dimensional structure of full-length human GRN-4.** (A) An overlay of the ten lowest energy structures of full-length GRN-4 (PDB code 2JYE). The disulfide bonds are shown in red. (B) Ribbon representation of the secondary structure present in a single structure of GRN-4 (PDB code 2JYE).

This is perhaps not surprising given the role of disulfide bonds in stabilizing the structures of small peptides. Intriguingly though, the fully reduced GRN-3 had biological activity, as it was able to trigger an inflammatory response in SY-SH5Y human neuroblastoma cells by activation of NF- $\kappa$ B, in a dose dependent manner (149). It appears a well-defined structure is not necessary for this bioactivity, but further study on the structure-function relationships are required to understand the important structural features.

Computational analysis of the structures of PGRN and the human granulin domains

indicates the presence of disorder, and in particular there appears to be disorder between the granulin domains (148). It has been suggested that this disorder is associated with facilitating the cleavage of the granulin domains from the precursor protein (148). In addition, it has been suggested that the predicted disordered regions surrounding individual GRNs in PGRN could provide a binding site for specific protein disulfide isomerases to impart correct disulfide bonding in PGRN (148). Highly flexible/disordered regions have also been suggested to be involved in the multi-functionality of granulin modules, since the plasticity in disordered conformations can facilitate interaction with other proteins (148).

GRN-3 showed the greatest disorder in the computational analysis (148), consistent with the original study by Ghag et al, 2016 which showed that GRN-3 had limited dispersion in the amide region of the NMR spectra (149). However, the disorder predicted by the computational analysis in the Ghag et al, 2017 study was not unequivocally confirmed by experimental analysis, as the circular dichroism (CD) spectroscopy and NMR data were inconsistent (148). The CD data indicated a lack of structure whereas the NMR data showed the oxidized peptide was more structured than the fully reduced peptide (148). Although there is evidence that GRN-3 might not be well structured in solution, it was shown to be highly thermally stable (146, 150). The interplay between structure and stability is unclear in this case, but an experimental structure, not presently available, is likely to provide insight into the disorder/flexibility present in GRN-3.

## **1.4.2 Truncation of granulin peptides**

### **1.4.2.1 *Carp granulin-1***

Following on from the elucidation of the three-dimensional structure of carp granulin-1, its folding has been explored to determine if the N-terminal region can fold independently. The rationale for these studies was based on the N-terminal region of carp granulin-1 resembling a disulfide  $\beta$ -cross motif and the two hydrophobic clusters that appear to stabilize the first two  $\beta$ -hairpins (146).

A 30-residue peptide corresponding to the N-terminal fragment of the carp granulin protein (CG1 1-30) with Cys IV and Cys VI, the disulfide connecting the N-terminal



to the C-terminal domain of the full-length protein, replaced with serine residues has been chemically synthesised (see Figure 1-4A) (151). The peptide was oxidized in a single step reaction to form two disulfide bonds and, based on NMR and mass spectrometry data, the disulfide bond connectivity was determined to be Cys I-Cys III and Cys II-Cys V, and is identical to full-length carp granulin-1. The three-dimensional structure is also consistent with the structure present in the full-length protein, as CG1 1-30 contains two  $\beta$ -hairpins as shown in Figure 1-4(B-C). These results indicate that the N-terminal region of carp granulin-1 can fold independently, and that only two disulfide bonds are required to allow formation of the native-like structure (151).

A smaller peptide, termed CG1 3-30 and corresponding to residues 3-30 of carp granulin-1, has also been synthesised and structurally characterised (151). A comparison of the  $C^\alpha$ ,  $C^\beta$  and  $H^\alpha$  chemical shifts of CG1 1-30 and CG1 3-30 showed significant differences in the N-terminal region of the two peptides (151). Consistent with the observed chemical shift differences, the structures also differ with CG1 3-30 only containing one  $\beta$ -hairpin in contrast to the two  $\beta$ -hairpins of CG1 1-30 (Figure 1-4D-E). Furthermore, the structures of CG1 3-30 are less well defined than the CG1 1-30 structures. The structural differences are thought to result from differences in the hydrophobic interactions present in the two peptides. The first two residues in CG1 1-30 are involved in hydrophobic clusters and it appears that these residues have a critical role in folding (151).

The lack of structural definition for the first  $\beta$ -hairpin in CG1 3-30 was consistent with the lack of slowly exchange amide protons observed for residues 1-14, indicating that this region is not stabilized by hydrogen bonds (151). In contrast, H/D exchange experiments indicated the presence of a number of slowly exchanging amide protons for residues 15-25 that correspond to the second  $\beta$ -hairpin region in CG 1-30 (151). Therefore, it is likely that this region is stabilized by hydrogen bonds, as expected for  $\beta$ -sheet structure (151).

Overall, the analysis of the truncated carp granulin-1 peptides suggested that although the N-terminal region can fold independently with only two disulfide bonds,

removing the first two residues prevents formation of the first  $\beta$ -hairpin, most likely as a result of disrupting hydrophobic interactions (151). Consequently, it appears that the disulfide bonds alone are not sufficient for the conformational stability of the  $\beta$ -hairpin stack in carp granulin-1 N-terminal truncated peptides.

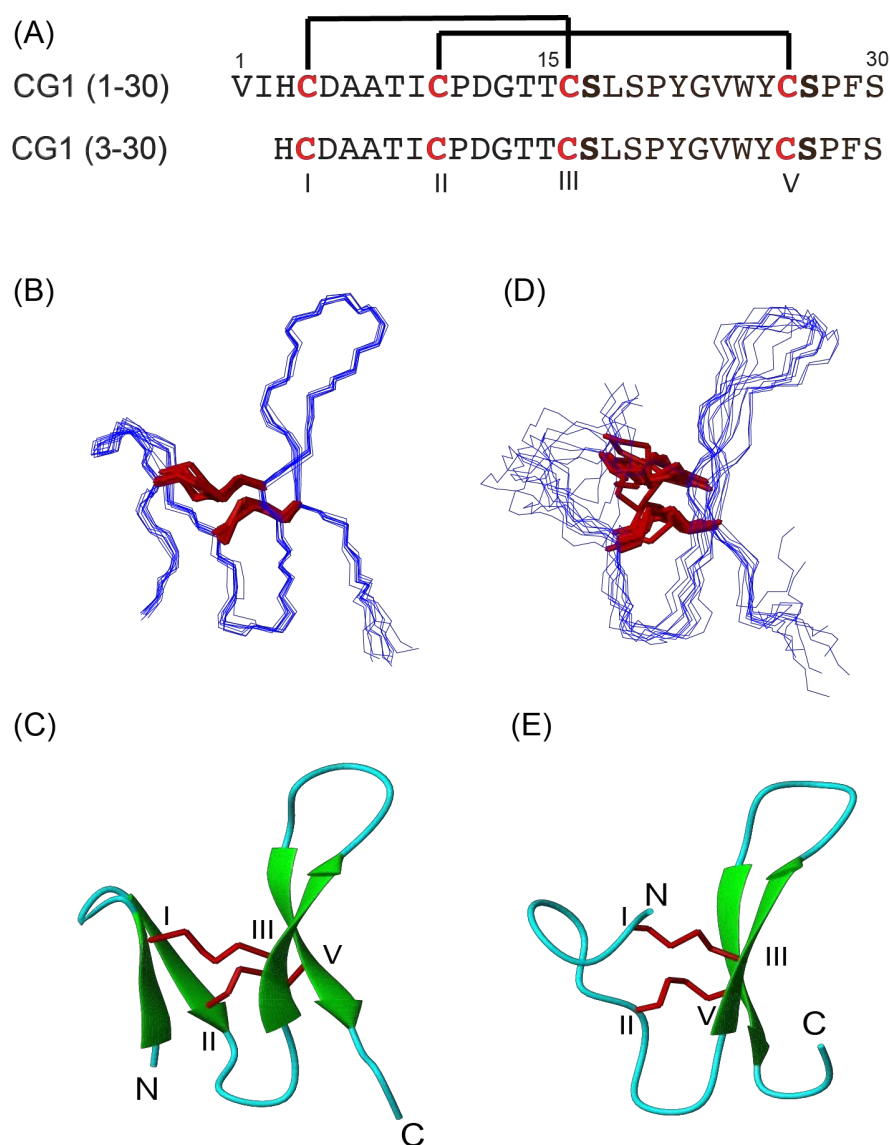


**Figure 1-4 Sequence and three-dimensional structure of truncated carp granulin-1.** (A) Sequences of N-terminal truncated analogues of carp granulin-1 from residues 1-30 and 3-30. Cys IV and Cys VI were replaced with serine residues; the cysteines are highlighted in red, and the substitutions are in bold letters. (B) Superposition of the ten lowest energy structures of CG1 1-30 (PDB code 1I8X) over the backbone atoms. (C) The ribbon representation of the secondary structure present in CG1 1-30. (D) Superposition of the ten lowest energy structure of CG1 3-30 (PDB code 1I8Y). (E) The ribbon representation of the secondary structure present in CG1 3-30. Figure generated using MOLMOL (152).

#### ***1.4.2.2 Truncation of a human granulin – GRN-4***

As mentioned in section 1.4.1.2, full length human GRN-4 has a  $\beta$ -hairpin structure similar to the N-terminus of carp granulin-1, but significant structural disorder in the C-terminal region (147). However, the amino-terminal domain of GRN-4 has a distinctly more flexible conformation in solution than its carp granulin-1 homologue as a consequence of low sequence identity (50%) (146, 147). GRN-4 lacks several hydrophobic and turn-stabilizing residues that are predicted to contribute to the conformational stability of carp granulin-1 and its N-terminal subdomain (153).

Based on the structural differences between GRN-4 and carp granulin-1, truncated, hybrid GRN-4 peptides have been designed and synthesized (153). These truncated peptides included incorporation of the hydrophobic cap of carp granulin-1 into GRN-4 by replacing residues Asp 1, Lys 3 and Ser 9 with the corresponding residues, Val 1, His 3, and Ile 9, and replacement of Gln 20 of GRN-4 with Pro 20, the corresponding residue in carp granulin-1 as shown in Figure 1-5A (153). The latter change was made in an attempt to stabilise the  $\beta$ -turn linking the two antiparallel strands of the second  $\beta$ -hairpin (153).

Disulfide bond mapping and proteolytic digestion experiments showed that the disulfide bond pairing in the hybrid peptides was identical to that found in carp granulin-1 N-terminal fragment (146, 153). Despite containing the native-like disulfide connectivity, the majority of the hybrid peptides did not display the regular secondary structure present in the native peptide. Only the hybrid peptide that incorporated the hydrophobic cap with Pro 20 resulted in a well-defined structure similar to the carp granulin-1 truncated peptide, as shown in Figure 1-5B (153). These findings emphasize that both hydrophobic and turn-stabilizing interactions are important for deriving the correct disulfide pairing alongside the structural integrity of the stack of two  $\beta$ -hairpins in GRN-4.

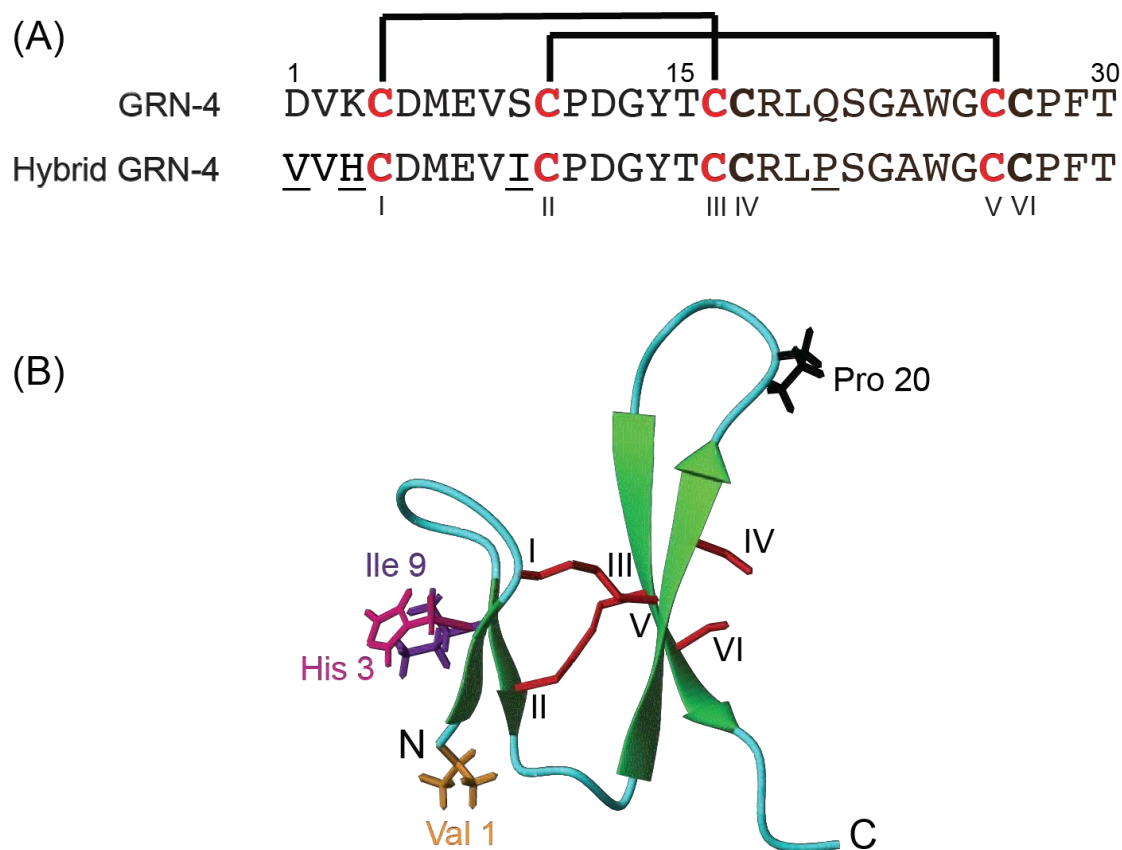


**Figure 1-5 (A) The sequence of the 30-residue amino terminal sub-domain of GRN-4.** Residues D1, K3, S9 and Q20 were replaced with V1, H3, I9 and P20, respectively, in the hybrid peptide. The SH groups of Cys IV and Cys VI were protected by S-acetamidomethyl in the hybrid peptide. (B) Three-dimensional structure of hybrid truncated GRN-4 peptide (PDB code 1G26). The side chains of replaced amino acids are highlighted. The Cys IV and Cys VI ACM protecting groups were left unmodified. Figure generated using MOLMOL (152).

#### 1.4.2.3 Truncation of human progranulin

Truncation studies have also been carried out on human PGRN. An engineered protein, termed Atsttrin, has been recombinantly expressed in bacteria containing partial segments of GRN 2, 4 and 5 and linker regions between the segments (154). The full-length protein exerts anti-inflammatory effects via binding to tumor necrosis factor receptors (TNFRs) and inhibits the TNF $\alpha$ -TNFR interaction (154). Although this interaction has been questioned it has been confirmed by several groups (155). PGRN has been reported to have potential for treating TNF $\alpha$ -mediated pathologies and conditions such as rheumatoid arthritis (154-156). Interestingly, Atsttrin showed even better anti-inflammatory effects with higher binding affinity to TNFR and a longer half-life (~120 hours) compared to PGRN (~40 hours) (154).

The PGRN-TNFR interaction appears to be highly dependent on PGRN folding, as the PGRN-TNFR interaction was abolished by treating PGRN with the reducing agent DTT (157). Given that Atsttrin also has anti-inflammatory activity suggests that it is folded in a similar way but no three-dimensional structural data has been reported. Atsttrin contains an uneven number of cysteine residues (17) suggesting that the oxidative folding could be complicated. This complexity appears to be reflected in the purification, as the reverse phase HPLC trace of Atsttrin varies among batches from the same expression clone and consequently, variable bioactivity results were observed (157, 158). It is of interest to determine the disulfide bond connectivity in Atsttrin to provide insight into the structure-function relationships of this complex truncated form of human progranulin.

#### ***1.4.2.4 The liver fluke granulin Ov-GRN-1***

The parasitic liver-fluke granulin, *Ov-GRN-1*, isolated from the ES products of the carcinogenic flatworm liver fluke *Opisthorchis viverrini* has significant sequence differences to human granulins (114, 128). The full-length *Ov-GRN-1* structure has not yet been determined due to the difficulty in generating sufficient quantities of recombinant refolded protein (128). However, recent synthesis and characterization of a series of truncated analogues from the N-terminal region of the full-length protein has provided insight into the structure of the full-length *Ov-GRN-1* protein (128).

Three analogues were synthesized from the N-terminal region of the full-length *Ov-GRN-1* protein, comprising four cysteine residues as shown in Figure 1-6A. Cys IV and Cys VI (where present) were replaced with alanine residues. The peptides were synthesized using selective protection of the cysteine residues to form the two native-like disulfide bonds (Cys I-Cys III, Cys II-Cys V) (128).

The activities of the truncated *Ov-GRN-1* peptides were tested in a cell proliferation assay and a mouse wound healing model (128). The most active peptide in the cell assay was the three-disulfide bond-containing peptide. Interestingly, a truncated version of carp granulin-1 was not active in this cell assay, again highlighting the importance of sequence in the bioactivity of granulins (159).

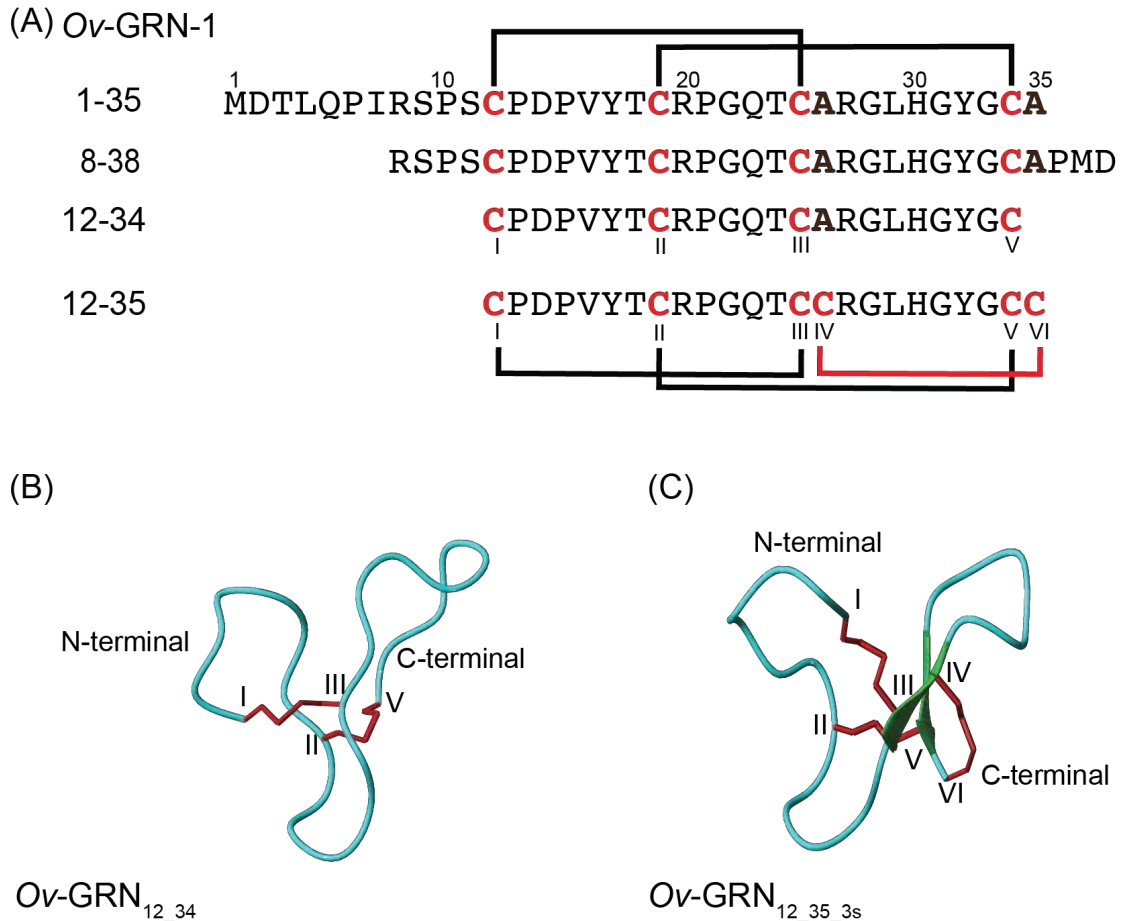


**Figure 1-6 Sequence and three-dimensional structures of the liver fluke *Ov*-GRN-1 truncated analogues.** (A) Sequences show Cys IV and Cys VI were replaced with alanine residues; the cysteines are highlighted in red, and the substitutions are in bold letters. (B) The structures of *Ov*-GRN<sub>12-34</sub> (PDB code 5UJH) and (C) *Ov*-GRN<sub>12-35\_3s</sub> (PDB code 5UJG) in ribbon format showing the secondary structure present in two of the *Ov*-GRN-1 truncated analogues. Figure generated using MOLMOL (152).

All of the *Ov*-GRN-1 peptides were found to significantly improve the rate of wound healing in the mouse wound healing model at similar potency to the full-length protein (128). There was no significant difference in the potency of the peptides in the mouse model (128). Furthermore, the peptides also had similar bioactivity to Regranex, a form of recombinant platelet-derived growth factor currently used in the clinic for treating wounds (160, 161). This finding highlight the potential of the granulin peptides in the development of novel wound healing agents. This potential is based in part on the ease of synthesis of these peptides (compared to recombinant growth factors) and their stability, which is likely to facilitate the delivery methods. The comparable bioactivities of *Ov*-GRN-1 peptides and the full-length protein,

despite the differences in structure, indicates that the precise structure is not critical for the bioactivity.

### **1.4.3 Related proteins – from plants to cone snails**

The  $\beta$ -stack structure present in N-terminal region of granulins has also been found in other proteins including in the C-termini of some plant cysteine proteases (123). The C-terminal region of these plant proteases have a similar cysteine pattern to granulin but otherwise there is limited sequence similarity (123). A peptide derived from rice oryzain  $\beta$  has been synthesized and the structure determined using NMR spectroscopy (123). The region synthesized is similar in size to the truncated carp granulin-1 and has the cysteine residues equivalent to Cys IV and VI in the granulins replaced with serine residues, to prevent formation of a non-native disulfide bond (123). This peptide formed the Cys I-Cys III and Cys II-Cys V connectivity present in the granulins and displayed the  $\beta$ -stack structure as shown in Figure 1-7A. The structural similarity with carp granulin-1 and the independent folding of this structural motif in a plant cysteine protease suggests that this motif could be conserved across a wide range of proteins.

Chemical shift analysis of the two-disulfide bond-containing *Ov*-GRN-1 peptides indicated a lack of  $\beta$ -sheet structure, which was confirmed by determination of the three-dimensional structures as shown for one of the analogues in Figure 1-6B (128). By contrast, the three-dimensional structure of the three-disulfide bond peptide has a  $\beta$ -hairpin similar to that present in the truncated form of carp granulin-1 (Figure 1-4 D-E). In addition to the two native-like disulfide bonds (Cys I-Cys III, Cys II-Cys V), this peptide also contains a non-native bond between Cys IV and Cys VI, which appears to stabilize the  $\beta$ -hairpin structure (128).

In support of the hypothesis that the granulin structure might be wide spread, a peptide was recently found in cone snail venom with structural similarity to the N-terminal region of granulins. The peptide, MiXXVIIA, contains 33 residues, including eight cysteine residues, but does not have the same cysteine framework or any sequence homology as the granulins (162). However, following determination of the structure of MiXXVIIA a database search indicated structural similarity with the

N- terminal region of human granulin-4, as shown in Figure 1-7B. Based on this structural similarity the cell proliferation activity of MiXXVIIA was explored and was found to promote cell proliferation, albeit at lower potency to *Ov*-GRN-1 (128, 162). Cell proliferation effects are unusual for cone snail venom peptides as the majority of these peptides target ion channels or receptors (163). Therefore, the unexpected finding of structural similarity between granulins and a venom peptide led to the discovery of unexpected bioactivity. It should be noted that it appears unlikely that the function of MiXXVIIA in the venom is related to the cell proliferation activity, but no other bioactivity has yet been found for this peptide.

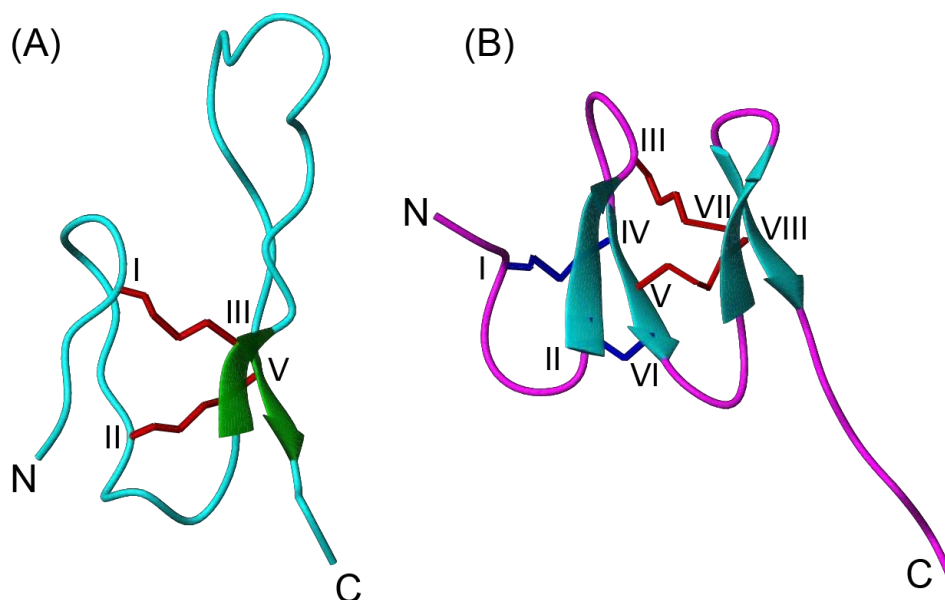


**Figure 1-7 Three-dimensional structures of peptides with granulin-like structures.** (A) A region from the rice oryzain  $\beta$  (PDB code 1FWO). (B) Structure of the conotoxin MiXXVIIA showing the two  $\beta$ -hairpins, which are cross linked by two disulfide bonds shown in red. Figure generated using MOLMOL (152).

#### 1.4.4 Conclusions

The biological functions of granulins are varied and their structure-function relationships are complex. Although only a limited number of granulin structures have been determined, they show significant diversity. The N-terminal region appears to be well defined in several granulins, but the hybrid studies on GRN-4 and carp granulin-1 have shown the important role that the N-terminal residues play in the



formation of structure (128, 153). The differences in the N-terminal sequences might explain, in part, the fact that some of the human granulins did not fold into well-defined structures (147).

To date, only carp granulin-1 displays a well-defined C-terminal region (144). The lack of definition in the C-terminal region of human granulins prevented the definitive elucidation of the disulfide connectivity (147). It should be noted that the carp granulin-1 structure is the only structure that has been determined from native material and it is possible that the recombinant peptides are different to those present in the native protein. Nonetheless, the lack of certainty in the connectivity of human granulins, along with the non-native disulfide bond in *Ov*-GRN-1(128), which apparently stabilizes the  $\beta$ -hairpin structure, poses the intriguing question of whether the disulfide connectivity is conserved throughout the granulin family.

The differences in the activities of the human granulins, even for peptides that displayed similar, well-defined conformations, illustrates that it is not clear what effect (if any) structure has on bioactivity. Further structure-function studies are required to enhance our understanding of the roles that structural elements in granulins play in different functions, and potentially provide insight into their mechanism of action.

## **1.5 Scope of the thesis**

This thesis entitled “Structure-function relationships of disulfide-rich peptides” focused on two peptides: Chlorotoxin and *Ov*-GRN-1. The overall aim was to provide insight into the important features for bioactivity for these interesting disulfide-rich peptides and whether this information could be used to design novel drug leads. The majority of the chapters are based on published manuscripts or manuscripts to be published, therefore each of the experimental chapters comprise all s including a separate introduction and references.

Chapter 1 provides a background to the two major components of this work and highlights the significance of the studies. Section 1.4 from Chapter 1 has been published with the title of “Folding of Granulin Domains” in the Journal of *Peptide Science* (116).

Chapter 2 expands the knowledge of the structure-function relationships of the scorpion venom peptide, chlorotoxin. It is generally believed that disulfide bonds have an important role in both the structure and function of disulfide rich peptides. However, reduced chlorotoxin still has some bioactivity and this chapter explored the hypothesis that a small, unstructured region of chlorotoxin might be contributing to this bioactivity. This study has been published in the *Journal of Frontiers in Pharmacology* (164).

Chapters 3-5 focused on elucidation of the structure function relationships and potential of truncated versions of *Ov*-GRN-1, as the low yield in recombinant expression limits its potential of the full-length protein as a drug lead. Chapter 3 focused on downsizing *Ov*-GRN-1 and investigating the folding, structure and bioactivity features of the minimized analogues. Ultimately, *Ov*-GRN-1 was successfully tailored into a 24-residue peptide, *Ov*-GRN<sub>12-35\_3s</sub>, and the outcome was published in the *Journal of Medicinal Chemistry* (128).

Moving forward to further optimize the truncated *Ov*-GRN-1 peptides, Chapter 4 investigated the role of proline residues in adopting multiple conformations, folding yield and the structure of *Ov*-GRN<sub>12-35\_3s</sub>. This study, published in *Journal of Medicinal Chemistry*, led to identification of a more potent analogue, GRN<sub>P4A</sub>, which surpasses the currently available biologic product in the market for healing diabetic ulcers, Regranex (165).

Chapter 5 focused on expanding the knowledge of structure-function relationships of granulins. In particular, determining whether the folding properties evident for the N-terminal region of *Ov*-GRN-1 are unique to this parasite protein, and whether the C-terminal region can also fold independently and have bioactivity. This study is being prepared for publication.

Chapter 6 provides a summary of the findings from this thesis as well as the gaps in the knowledge in these fields and the future directions that could be taken.

## 1.6 References

1. Bhutia, S.K. and T.K. Maiti. Targeting tumors with peptides from natural sources. *Trends Biotechnol.* 2008; 26(4): 210-7.
2. Edwards, C., M. Cohen, and S. Bloom. Peptides as drugs. *QJM: Int. J. Med.* 1999; 92(1): 1-4.
3. Loffet, A. Peptides as drugs: is there a market? *Peptide Sci.* 2001; 8, DOI: 10.1002/psc.366.
4. Gentilucci, L., A. Tolomelli, and F. Squassabia. Peptides and peptidomimetics in medicine, surgery and biotechnology. *Curr. Med. Chem.* 2006; 13(20): 2449-66.
5. Groner, B. *Peptides as drugs: discovery and development*: Wiley-VCH Verlag GmbH & Co. KGaA: Weinheim, Germany; 2009. 242 p.
6. Sato, A.K., M. Viswanathan, R.B. Kent, and C.R. Wood. Therapeutic peptides: technological advances driving peptides into development. *Curr. Opin. Biotechnol.* 2006; 17(6): 638-42.
7. Vlieghe, P., V. Lisowski, J. Martinez, and M. Khrestchatisky. Synthetic therapeutic peptides: science and market. *Drug Discov. Today.* 2010; 15(1): 40-56.
8. Northfield, S.E., C.K. Wang, C.I. Schroeder, T. Durek, M.-W. Kan, J.E. Swedberg, and D.J. Craik. Disulfide-rich macrocyclic peptides as templates in drug design. *Eur. J. Med. Chem.* 2014; 77: 248-57.
9. Schmidtko, A., J. Lötsch, R. Freynhagen, and G. Geisslinger. Ziconotide for treatment of severe chronic pain. *The Lancet.* 2010; 375(9725): 1569-77.
10. Stein, D., A. Copland, C. Orton, D. McDaniel, and R. Hays. P-115 single dose linaclotide for capsule endoscopy preparation-a pilot study. *Inflamm. Bowel Dis.* 2016; 22, DOI: 10.1097/01.MIB.0000480219.15168.c3.
11. Santibáñez-López, C.E., O.F. Francke, C. Ureta, and L.D. Possani. Scorpions from Mexico: from species diversity to venom complexity. *Toxins (Basel).* 2015; 8, DOI: 10.3390/toxins8010002.
12. Chen, R. and S.-H. Chung. Computational studies of venom peptides targeting potassium channels. *Toxins (Basel).* 2015; 7(12): 5194-211.
13. Kuzmenkov, A., E. Grishin, and A. Vassilevski. Diversity of potassium channel ligands: Focus on scorpion toxins. *Biochemistry (Moscow).* 2015; 80(13): 1764-99.
14. I. Mohanty, K.A., D. Behera, A. Arun Prince Milton, G. Elaiyaraja, G. Rajesh and K. Dhama. Immunomodulatory and therapeutic potential of Zootoxins

- (Venom and Toxins) on the way towards designing and developing novel drugs/medicines: an overview. *Int. J. Pharmacol.* 2016; 12(2): 126-35.
15. Cupo, P. Clinical update on scorpion envenoming. *Rev. Soc. Bras. Med. Trop.* 2015; 48(6): 642-9.
  16. Kujawa, M. *Natural toxins: Characterization, pharmacology and therapeutics*: Oxford: Pergamon Press; 1989. 568 p.
  17. Gwee, M.C., S. Nirathanan, H.E. Khoo, P. Gopalakrishnakone, R.M. Kini, and L.S. Cheah. Autonomic effects of some scorpion venoms and toxins. *Clin. Exp. Pharmacol. Physiol.* 2002; 29(9): 795-801.
  18. Severino, D.N., R.L. Pereira, I. Knysak, D.M. Candido, and F.H. Kwasniewski. Edematogenic activity of scorpion venoms from the Buthidae family and the role of platelet-activating factor and nitric oxide in paw edema induced by Tityus venoms. *Inflammation.* 2009; 32(1): 57-64.
  19. Debin, J.A., J.E. Maggio, and G.R. Strichartz. Purification and characterization of chlorotoxin, a chloride channel ligand from the venom of the scorpion. *Am. J. Physiol. Cell Physiol.* 1993; 264(2): 361-9.
  20. Lippens, G., J. Najib, S. Wodak, and A. Tartar. NMR sequential assignments and solution structure of chlorotoxin, a small scorpion toxin that blocks chloride channels. *Biochemistry.* 1995; 34(1): 13-21.
  21. Ojeda, P.G., C.K. Wang, and D.J. Craik. Chlorotoxin: Structure, activity and potential uses in cancer therapy. *Peptide Sci.* 2016; 106, DOI: 10.1002/bip.22748.
  22. Soroceanu, L., Y. Gillespie, M. Khazaeli, and H. Sontheimer. Use of chlorotoxin for targeting of primary brain tumors. *Cancer Res.* 1998; 58(21): 4871-9.
  23. Lyons, S.A., J. O'Neal, and H. Sontheimer. Chlorotoxin, a scorpion-derived peptide, specifically binds to gliomas and tumors of neuroectodermal origin. *Glia.* 2002; 39(2): 162-73.
  24. Ojeda, P.G., L.Y. Chan, A.G. Poth, C.K. Wang, and D.J. Craik. The role of disulfide bonds in structure and activity of chlorotoxin. *Future Med. Chem.* 2014; 6(15): 1617-28.
  25. Jacoby, D.B., et al. Potent pleiotropic anti-angiogenic effects of TM601, a synthetic chlorotoxin peptide. *Anticancer Res.* 2010; 30(1): 39-46.
  26. Albert, F.K., M. Forsting, K. Sartor, H.-P. Adams, and S. Kunze. Early postoperative magnetic resonance imaging after resection of malignant glioma: Objective evaluation of residual tumor and its influence on regrowth and prognosis. *Neurosurgery.* 1995; 36(4): 873-4.

27. Kieran, M.W., D. Walker, D. Frappaz, and M. Prados. Brain tumors: from childhood through adolescence into adulthood. *J. Clin. Oncol.* 2010; 28(32): 4783-9.
28. Stroud, M.R., S.J. Hansen, and J.M. Olson. In vivo bio-imaging using chlorotoxin-based conjugates. *Curr. Pharm. Des.* 2011; 17(38): 4362-71.
29. Benaron, D.A. The future of cancer imaging. *Cancer Metastasis Rev.* 2002; 21(1): 45-78.
30. Ricci, P.E., J.P. Karis, J.E. Heiserman, E.K. Fram, A.N. Bice, and B.P. Drayer. Differentiating recurrent tumor from radiation necrosis: time for re-evaluation of positron emission tomography? *Am. J. Neuroradiol.* 1998; 19(3): 407-13.
31. Kahn, D., K. Follett, D. Bushnell, M. Nathan, J. Piper, M. Madsen, and P. Kirchner. Diagnosis of recurrent brain tumor: value of 201Tl SPECT vs 18F-fluorodeoxyglucose PET. *AJR Am. J. Roentgenol.* 1994; 163(6): 1459-65.
32. Butzen, J., et al. Discrimination between neoplastic and nonneoplastic brain lesions by use of proton MR spectroscopy: the limits of accuracy with a logistic regression model. *Am. J. Neuroradiol.* 2000; 21(7): 1213-9.
33. Hockaday, D.C., et al. Imaging glioma extent with 131I-TM-601. *J. Nucl. Med.* 2005; 46(4): 580-6.
34. Juratli, T.A., G. Schackert, and D. Krex. Current status of local therapy in malignant gliomas--a clinical review of three selected approaches. *Pharmacol. Ther.* 2013; 139(3): 341-58.
35. Bigner, D.D., et al. Iodine-<sup>131</sup>-labeled antitenascin monoclonal antibody 81C6 treatment of patients with recurrent malignant gliomas: phase I trial results. *J. Clin. Oncol.* 1998; 16(6): 2202-12.
36. Kovar, J.L., E. Curtis, S.F. Othman, M.A. Simpson, and D.M. Olive. Characterization of IRDye 800CW chlorotoxin as a targeting agent for brain tumors. *Anal. Biochem.* 2013; 440(2): 212-9.
37. Veiseh, M., et al. Tumor paint: a chlorotoxin: Cy5. 5 bioconjugate for intraoperative visualization of cancer foci. *Cancer Res.* 2007; 67(14): 6882-8.
38. Wiranowska, M., L.O. Colina, and J.O. Johnson. Clathrin-mediated entry and cellular localization of chlorotoxin in human glioma. *Cancer Cell Int.* 2011; 11, DOI: 10.1186/1475-2867-11-27.
39. Kesavan, K., et al. Annexin A2 is a molecular target for TM601, a peptide with tumor-targeting and anti-angiogenic effects. *J. Biol. Chem.* 2010; 285(7): 4366-74.
40. Gribbin, T.E., N. Senzer, J.J. Raizer, S. Shen, L.B. Nabors, M. Wiranowska, and J.B. Fiveash. A phase I evaluation of intravenous (IV) 131I-chlorotoxin

- delivery to solid peripheral and intracranial tumors. *J. Clin. Oncol.* 2009; 27, DOI: 10.1200/jco.2009.27.15s.e14507.
41. Mamelak, A.N., et al. Phase I single-dose study of intracavitary-administered iodine-131-TM-601 in adults with recurrent high-grade glioma. *J. Clin. Oncol.* 2006; 24(22): 3644-50.
  42. Mamelak, A.N. and D.B. Jacoby. Targeted delivery of antitumoral therapy to glioma and other malignancies with synthetic chlorotoxin (TM-601). *Expert Opin. Drug. Deliv.* 2007; 4, DOI: 10.1517/17425247.4.2.175.
  43. Akcan, M., M.R. Stroud, S.J. Hansen, R.J. Clark, N.L. Daly, D.J. Craik, and J.M. Olson. Chemical re-engineering of chlorotoxin improves bioconjugation properties for tumor imaging and targeted therapy. *J. Med. Chem.* 2011; 54(3): 782-7.
  44. Sun, C., et al. Tumor-targeted drug delivery and MRI contrast enhancement by chlorotoxin-conjugated iron oxide nanoparticles. *Nanomedicine (London, England)*. 2008; 3, DOI: 10.2217/17435889.3.4.495.
  45. Wang, X. and Z. Guo. Anti-gliomas effect of chlorotoxin-conjugated onconase at high dose. *Cell Biochem. Biophys.* 2015: 1-4.
  46. Wang, X. and Z. Guo. Chlorotoxin-conjugated onconase as a potential anti-glioma drug. *Oncol. Lett.* 2015; 9(3): 1337-42.
  47. Pourgholi, F., J.-N. Farhad, H.S. Kafil, and M. Yousefi. Nanoparticles: Novel vehicles in treatment of Glioblastoma. *Biomed. Pharmacother.* 2016; 77: 98-107.
  48. Mu, Q., M. Jeon, M.H. Hsiao, V.K. Patton, K. Wang, O.W. Press, and M. Zhang. Stable and efficient paclitaxel nanoparticles for targeted glioblastoma therapy. *Adv. Healthc. Mater.* 2015; 4(8): 1236-45.
  49. Wu, C., et al. Design of highly emissive polymer dot bioconjugates for in vivo tumor targeting. *Angew. Chem. Int. Ed. Engl.* 2011; 50(15): 3430-4.
  50. Costa, P.M., et al. Tumor-targeted chlorotoxin-coupled nanoparticles for nucleic acid delivery to glioblastoma cells: a promising system for glioblastoma treatment. *Mol. Ther. Nucleic Acids.* 2013; 2, DOI: 10.1038/mtna.2013.30.
  51. Graf, N., T.E. Mokhtari, I.A. Papayannopoulos, and S.J. Lippard. Platinum(IV)-chlorotoxin (CTX) conjugates for targeting cancer cells. *J. Inorg. Biochem.* 2012; 110: 58-63.
  52. Cheng, Y., J. Zhao, W. Qiao, and K. Chen. Recent advances in diagnosis and treatment of gliomas using chlorotoxin-based bioconjugates. *Am. J. Nucl. Med. Mol. Imaging.* 2014; 4(5): 385-405.

53. Xiang, Y., L. Liang, X. Wang, J. Wang, X. Zhang, and Q. Zhang. Chloride channel-mediated brain glioma targeting of chlorotoxin-modified doxorubicine-loaded liposomes. *J. Controlled Release*. 2011; 152(3): 402-10.
54. Ullrich, N., G.Y. Gillespie, and H. Sontheimer. Human astrocytoma cells express a unique chloride current. *Neuroreport*. 1996; 7(5): 1020-4.
55. Deshane, J., C.C. Garner, and H. Sontheimer. Chlorotoxin inhibits glioma cell invasion via matrix metalloproteinase-2. *J. Biol. Chem*. 2003; 278(6): 4135-44.
56. Ullrich, N. and H. Sontheimer. Biophysical and pharmacological characterization of chloride currents in human astrocytoma cells. *Am. J. Physiol. Cell Physiol*. 1996; 270(5): 1511-21.
57. Olsen, M., S. Schade, S. Lyons, M. Amaral, and H. Sontheimer. Expression of voltage-gated chloride channels in human glioma cells. *J. Neurosci*. 2003; 23(13): 5572-82.
58. Jentsch, T.J. CLC chloride channels and transporters: from genes to protein structure, pathology and physiology. *Crit. Rev. Biochem. Mol. Biol*. 2008; 43(1): 3-36.
59. Ullrich, N., A. Bordey, G. Gillespie, and H. Sontheimer. Expression of voltage-activated chloride currents in acute slices of human gliomas. *Neuroscience*. 1998; 83(4): 1161-73.
60. McFerrin, M.B. and H. Sontheimer. A role for ion channels in glioma cell invasion. *Neuron Glia Biol*. 2006; 2(01): 39-49.
61. Soroceanu, L., T.J. Manning, and H. Sontheimer. Modulation of glioma cell migration and invasion using Cl<sup>-</sup> and K<sup>+</sup> ion channel blockers. *J. Neurosci*. 1999; 19(14): 5942-54.
62. DeBin, J. and G. Strichartz. Chloride channel inhibition by the venom of the scorpion *Leiurus quinquestriatus*. *Toxicon*. 1991; 29(11): 1403-8.
63. Nakagawa, T., T. Kubota, M. Kabuto, K. Sato, H. Kawano, T. Hayakawa, and Y. Okada. Production of matrix metalloproteinases and tissue inhibitor of metalloproteinases-1 by human brain tumors. *J. Neurosurg*. 1994; 81(1): 69-77.
64. Qin, C., et al. The impact of a chlorotoxin-modified liposome system on receptor MMP-2 and the receptor-associated protein CIC-3. *Biomaterials*. 2014; 35(22): 5908-20.
65. Kähäri, V.-M. and U. Saarialho-Kere. Trends in Molecular Medicine: Matrix metalloproteinases and their inhibitors in tumour growth and invasion. *Ann. Med*. 1999; 31(1): 34-45.
66. Hofmann, U.B., J.R. Westphal, E.T. Waas, J.C. Becker, D.J. Ruitter, and G.N. van Muijen. Coexpression of integrin  $\alpha\beta3$  and matrix metalloproteinase-2

- (MMP-2) coincides with MMP-2 activation: correlation with melanoma progression. *J. Invest. Dermatol.* 2000; 115(4): 625-32.
67. Sato, H. and M. Seiki. Membrane-type matrix metalloproteinases (MT-MMPs) in tumor metastasis. *J. Biochem.* 1996; 119(2): 209-15.
  68. Strongin, A.Y., I. Collier, G. Bannikov, B.L. Marmer, G.A. Grant, and G.I. Goldberg. Mechanism of cell surface activation of 72-kDa type IV collagenase isolation of the activated form of the membrane metalloprotease. *J. Biol. Chem.* 1995; 270(10): 5331-8.
  69. Nakahara, H., L. Howard, E.W. Thompson, H. Sato, M. Seiki, Y. Yeh, and W.-T. Chen. Transmembrane/cytoplasmic domain-mediated membrane type 1-matrix metalloprotease docking to invadopodia is required for cell invasion. *Proc. Natl. Acad. Sci. U.S.A.* 1997; 94(15): 7959-64.
  70. Kasai, T., et al. Chlorotoxin fused to IgG-Fc inhibits glioblastoma cell motility via receptor-mediated endocytosis. *J. Drug Deliv.* 2012; 2012, DOI: 10.1155/2012/975763.
  71. Ellerbroek, S.M. and M.S. Stack. Membrane associated matrix metalloproteinases in metastasis. *Bioessays.* 1999; 21(11): 940-9.
  72. Friedberg, M.H., M.J. Glantz, M.S. Klempner, B.F. Cole, and G. Perides. Specific matrix metalloproteinase profiles in the cerebrospinal fluid correlated with the presence of malignant astrocytomas, brain metastases, and carcinomatous meningitis. *Cancer.* 1998; 82(5): 923-30.
  73. Sawaya, R.E., et al. Expression and localization of 72 kDa type IV collagenase (MMP-2) in human malignant gliomas in vivo. *Clin. Exp. Metastasis.* 1996; 14(1): 35-42.
  74. Deryugina, E.I., M.A. Bourdon, G.-X. Luo, R.A. Reisfeld, and A. Strongin. Matrix metalloproteinase-2 activation modulates glioma cell migration. *J. Cell Sci.* 1997; 110(19): 2473-82.
  75. El-Ghlban, S., et al. Chlorotoxin-Fc fusion inhibits release of MMP-2 from pancreatic cancer cells. *J. Biomed. Biotechnol.* 2014; 2014, DOI: 10.1155/2014/152659.
  76. Rand, J.H. "Annexinopathies"—a new class of diseases. *New Engl. J. Med.* 1999; 340(13): 1035-6.
  77. Bandorowicz-Pikula, J. Annexins: biological importance and annexin-related pathologies: Kluwer Academic/Plenum; 2003. 300 p.
  78. Benz, J. and A. Hofmann. Annexins: from structure to function. *Biol. Chem.* 1997; 378(3-4): 177-83.
  79. Grewal, T. and C. Enrich. Annexins--modulators of EGF receptor signalling and trafficking. *Cell. Signal.* 2009; 21(6): 847-58.



80. Siever, D.A. and H.P. Erickson. Extracellular annexin II. *Int. J. Biochem. Cell. Biol.* 1997; 29(11): 1219-23.
81. Turpin, E., F. Russo-Marie, T. Dubois, C. de Paillerets, A. Alfsen, and M. Bomsel. In adrenocortical tissue, annexins II and VI are attached to clathrin coated vesicles in a calcium-independent manner. *Biochim. Biophys. Acta.* 1998; 1402(2): 115-30.
82. Burger, A., et al. The crystal structure and ion channel activity of human annexin II, a peripheral membrane protein. *J. Mol. Biol.* 1996; 257(4): 839-47.
83. Réty, S., et al. The crystal structure of a complex of p11 with the annexin II N-terminal peptide. *Nat. Struct. Mol. Biol.* 1999; 6(1): 89-95.
84. Creutz, C.E. The annexins and exocytosis. *Science (New York, N.Y.)*. 1992; 258(5084): 924-31.
85. Bieri, M., A.H. Kwan, M. Mobli, G.F. King, J.P. Mackay, and P.R. Gooley. Macromolecular NMR spectroscopy for the non-spectroscopist: beyond macromolecular solution structure determination. *FEBS J.* 2011; 278(5): 704-15.
86. Kwan, A.H., M. Mobli, P.R. Gooley, G.F. King, and J.P. Mackay. Macromolecular NMR spectroscopy for the non-spectroscopist. *FEBS J.* 2011; 278(5): 687-703.
87. Marx, U.C., N.L. Daly, and D.J. Craik. NMR of conotoxins: structural features and an analysis of chemical shifts of post-translationally modified amino acids. *Magn. Reson. Chem.* 2006; 44 Spec No: S41-50.
88. Zhang, H., et al. Structure-activity relationship and conformational studies of the natural product cyclic depsipeptides YM-254890 and FR900359. *Eur. J. Med. Chem.* 2018; 156: 847-60.
89. Rjeibi, I., et al. Purification, synthesis and characterization of AaCtx, the first chlorotoxin-like peptide from *Androctonus australis* scorpion venom. *Peptides.* 2011; 32(4): 656-63.
90. Fuller, M.D., et al. State-dependent inhibition of cystic fibrosis transmembrane conductance regulator chloride channels by a novel peptide toxin. *J. Biol. Chem.* 2007; 282(52): 37545-55.
91. Smout, M.J., et al. Infection with the carcinogenic human liver fluke, *Opisthorchis viverrini*. *Mol. Biosyst.* 2011; 7(5): 1367-75.
92. Cancer, I.A.f.R.o. Infection with liver flukes (*Opisthorchis viverrini*, *Opisthorchis felinus* and *Clonorchis sinensis*). *IARC Monogr. Eval. Carcinog. Risks Hum.* 1994; 61: 121-75.
93. Sripa, B. Global burden of food-borne trematodiasis. *Lancet Infect. Dis.* 2012; 12(3): 171-2.

94. Sripa, B., et al. Liver fluke induces cholangiocarcinoma. *PLoS Med.* 2007; 4, DOI: 10.1371/journal.pmed.0040201.
95. Thuwajit, C., P. Thuwajit, S. Kaewkes, B. Sripa, K. Uchida, M. Miwa, and S. Wongkham. Increased cell proliferation of mouse fibroblast NIH-3T3 in vitro induced by excretory/secretory product (s) from *Opisthorchis viverrini*. *Parasitology.* 2004; 129(04): 455-64.
96. Blechacz, B., M. Komuta, T. Roskams, and G.J. Gores. Clinical diagnosis and staging of cholangiocarcinoma. *Nat. Rev. Gastroenterol. Hepatol.* 2011; 8(9): 512-22.
97. Hou, P. and S. Pang. Chorionepithelioma: an analytical study of 28 necropsied cases, with special reference to the possibility of spontaneous retrogression. *J. Pathol. Bacteriol.* 1956; 72(1): 95-104.
98. Sripa, B. and C. Pairojkul. Cholangiocarcinoma: lessons from Thailand. *Curr. Opin. Gastroenterol.* 2008; 24(3): 349-56.
99. Mulvenna, J., et al. The secreted and surface proteomes of the adult stage of the carcinogenic human liver fluke *Opisthorchis viverrini*. *Proteomics.* 2010; 10(5): 1063-78.
100. Laha, T., et al. Gene discovery for the carcinogenic human liver fluke, *Opisthorchis viverrini*. *BMC Genomics.* 2007; 8(1): 189-204.
101. Smout, M.J., et al. A granulins-like growth factor secreted by the carcinogenic liver fluke, *Opisthorchis viverrini*, promotes proliferation of host cells. *PLoS Pathog.* 2009; 5, DOI: 10.1371/journal.ppat.1000611.
102. Smout, M.J., et al. Carcinogenic parasite secretes growth factor that accelerates wound healing and potentially promotes neoplasia. *PLoS Pathog.* 2015; 11, DOI: 10.1371/journal.ppat.1005209.
103. Clancy, S. RNA splicing: introns, exons and spliceosome. *Nature Ed.* 2008; 1(1): 31.
104. Kalluri, R. and R.A. Weinberg. The basics of epithelial-mesenchymal transition. *J. Clin. Invest.* 2009; 119(6): 1420-8.
105. Zaja-Milatovic, S. and A. Richmond. CXC chemokines and their receptors: a case for a significant biological role in cutaneous wound healing. *Histol. Histopathol.* 2008; 23(11): 1399-407.
106. Strieter, R.M., M.D. Burdick, J. Mestas, B. Gomperts, M.P. Keane, and J.A. Belperio. Cancer CXC chemokine networks and tumour angiogenesis. *Eur. J. Cancer.* 2006; 42(6): 768-78.
107. Bolitho, C., M.A. Hahn, R.C. Baxter, and D.J. Marsh. The chemokine CXCL1 induces proliferation in epithelial ovarian cancer cells by transactivation of the epidermal growth factor receptor. *Endocr. Relat. Cancer.* 2010; 17(4): 929-40.

108. Raghuwanshi, S.K., Y. Su, V. Singh, K. Haynes, A. Richmond, and R.M. Richardson. The chemokine receptors CXCR1 and CXCR2 couple to distinct G protein-coupled receptor kinases to mediate and regulate leukocyte functions. *J. Immunol.* 2012; 189(6): 2824-32.
109. Tangkeangsirisin, W. and G. Serrero. PC cell-derived growth factor (PCDGF/GP88, progranulin) stimulates migration, invasiveness and VEGF expression in breast cancer cells. *Carcinogenesis.* 2004; 25(9): 1587-92.
110. Thuwajit, C., P. Thuwajit, K. Uchida, D. Daorueang, S. Kaewkes, S. Wongkham, and M. Miwa. Gene expression profiling defined pathways correlated with fibroblast cell proliferation induced by *Opisthorchis viverrini* excretory/secretory product. *World J. Gastroenterol.* 2006; 12(22): 3585-92.
111. Danen, E.H. Ignoring matrix boundaries when the LKB1 master kinase is gone. *J. Cell Biol.* 2014; 207(2): 167-9.
112. Ringwood, L. and L. Li. The involvement of the interleukin-1 receptor-associated kinases (IRAKs) in cellular signaling networks controlling inflammation. *Cytokine.* 2008; 42(1): 1-7.
113. Vos, T., J. Goss, S. Begg, and N. Mann. Projection of health care expenditure by disease: a case study from Australia, 2003 to 2033. Canberra: AIHW; 2008. Report No.: HWE 43.
114. Smout, M.J., J.P. Mulvenna, M.K. Jones, and A. Loukas. Expression, refolding and purification of *Ov*-GRN-1, a granulin-like growth factor from the carcinogenic liver fluke, that causes proliferation of mammalian host cells. *Protein Expr. Purif.* 2011; 79(2): 263-70.
115. Wuerth, K.C., A.L. Hilchie, K.L. Brown, and R.E. Hancock. Host defence (antimicrobial) peptides and proteins. In *eLS*, (Ed.). 2013, DOI: doi:10.1002/9780470015902.a0001212.pub3.
116. Dastpeyman, M., M.J. Smout, D. Wilson, A. Loukas, and N.L. Daly. Folding of granulin domains. *Peptide Sci.* 2018: 10.1002/pep2.24062.
117. Bateman, A., D. Belcourt, H. Bennett, C. Lazure, and S. Solomon. Granulins, a novel class of peptide from leukocytes. *Biochem. Biophys. Res. Commun.* 1990; 173(3): 1161-8.
118. Palfree, R.G., H.P. Bennett, and A. Bateman. The evolution of the secreted regulatory protein progranulin. *PloS one.* 2015; 10, DOI: 10.1371/journal.pone.0133749.
119. Zhao, M., M. He, X. Huang, Q. Wang, and Y. Shi. Functional characterization and molecular mechanism exploration of three granulin epithelin precursor splice variants in biomineralization of the pearl oyster *Pinctada fucata*. *Mol. Genet. Genomics.* 2016; 291(1): 399-409.

120. Hanington, P.C., L.J. Brennan, M. Belosevic, and B. Andrew Keddie. Molecular and functional characterization of granulin-like molecules of insects. *Insect Biochem. Mol. Biol.* 2008; 38(5): 596-603.
121. Zhao, J., et al. Cloning, characterization and expression of a cDNA encoding a granulin-like polypeptide in *Ciona savignyi*. *Biochimie*. 2013; 95(8): 1611-9.
122. Nara, K., H. Matsue, and T. Naraoka. Granulin-like peptide in the mid-gut gland of the bivalve mollusk, *Patinopecten yessoensis*. *Biochim. Biophys. Acta*. 2004; 1675(1-3): 147-54.
123. Tolkatchev, D., P. Xu, and F. Ni. A peptide derived from the C-terminal part of a plant cysteine protease folds into a stack of two  $\beta$ -hairpins, a scaffold present in the emerging family of granulin-like growth factors. *J. Pept. Res.* 2001; 57(3): 227-33.
124. Borroni, B., et al. Granulin mutation drives brain damage and reorganization from preclinical to symptomatic FTL. *Neurobiol. Aging*. 2012; 33(10): 2506-20.
125. Kleinberger, G., A. Capell, C. Haass, and C. Van Broeckhoven. Mechanisms of granulin deficiency: lessons from cellular and animal models. *Mol. Neurobiol.* 2013; 47(1): 337-60.
126. Plowman, G.D., J.M. Green, M.G. Neubauer, S.D. Buckley, V.L. McDonald, G.J. Todaro, and M. Shoyab. The epithelin precursor encodes two proteins with opposing activities on epithelial cell growth. *J. Biol. Chem.* 1992; 267(18): 13073-8.
127. Halper, J. Growth factors as active participants in carcinogenesis: a perspective. *Vet. Pathol.* 2010; 47(1): 77-97.
128. Bansal, P.S., et al. Development of a potent wound healing agent based on the liver fluke granulin structural fold. *J. Med. Chem.* 2017; 60(10): 4258-66.
129. Toh, H., B.P. Chitramuthu, H.P. Bennett, and A. Bateman. Structure, function, and mechanism of progranulin; the brain and beyond. *J. Mol. Neurosci.* 2011; 45, DOI: 10.1007/s12031-011-9569-4.
130. Wang, X., H. Xu, X. Chen, Y. Tian, F. Wang, and X. Lin. Cloning, expression and cytotoxicity of granulin A, a novel polypeptide contained in human progranulin. *Biosci. Trends*. 2016; 10(3): 181-7.
131. Bateman, A. and H.P. Bennett. The granulin gene family: from cancer to dementia. *Bioessays*. 2009; 31(11): 1245-54.
132. Chen, X., et al. Interaction between granulin A and enolase 1 attenuates the migration and invasion of human hepatoma cells. *Oncotarget*. 2017; 8(18): 30305-16.

133. Bhandari, V., R. Palfree, and A. Bateman. Isolation and sequence of the granulin precursor cDNA from human bone marrow reveals tandem cysteine-rich granulin domains. *Proc. Natl. Acad. Sci. U.S.A.* 1992; 89(5): 1715-9.
134. Ong, C. and A. Bateman. Progranulin (granulin-epithelin precursor, PC-cell derived growth factor, acrogranin) in proliferation and tumorigenesis. *Histol. Histopathol.* 2003; 18(4): 1275-88.
135. Lu, R. and G. Serrero. Inhibition of PC cell-derived growth factor (PCDGF, epithelin/granulin precursor) expression by antisense PCDGF cDNA transfection inhibits tumorigenicity of the human breast carcinoma cell line MDA-MB-468. *Proc. Natl. Acad. Sci. U.S.A.* 2000; 97(8): 3993-8.
136. Baba, T., H.B. Hoff, 3rd, H. Nemoto, H. Lee, J. Orth, Y. Arai, and G.L. Gerton. Acrogranin, an acrosomal cysteine-rich glycoprotein, is the precursor of the growth-modulating peptides, granulins, and epithelins, and is expressed in somatic as well as male germ cells. *Mol. Reprod. Dev.* 1993; 34(3): 233-43.
137. Cenik, B., C.F. Sephton, B.K. Cenik, J. Herz, and G. Yu. Progranulin: a proteolytically processed protein at the crossroads of inflammation and neurodegeneration. *J. Biol. Chem.* 2012; 287(39): 32298-306.
138. Bateman, A. and H. Bennett. Granulins: the structure and function of an emerging family of growth factors. *J. Endocrinol.* 1998; 158(2): 145-51.
139. Díaz-Cueto, L., P. Stein, A. Jacobs, R.M. Schultz, and G.L. Gerton. Modulation of mouse preimplantation embryo development by acrogranin (epithelin/granulin precursor). *Dev. Biol.* 2000; 217(2): 406-18.
140. He, Z., C.H. Ong, J. Halper, and A. Bateman. Progranulin is a mediator of the wound response. *Nat. Med.* 2003; 9(2): 225-9.
141. Yip, C.W., et al. Granulin-epithelin precursor interacts with 78-kDa glucose-regulated protein in hepatocellular carcinoma. *BMC cancer.* 2017; 17, DOI: 10.1186/s12885-017-3399-x.
142. Arechavaleta-Velasco, F., C.E. Perez-Juarez, G.L. Gerton, and L. Diaz-Cueto. Progranulin and its biological effects in cancer. *Med. Oncol.* 2017; 34, DOI: 10.1007/s12032-017-1054-7.
143. Wei, J., A. Hettinghouse, and C. Liu. The role of progranulin in arthritis. *Ann. N. Y. Acad. Sci.* 2016; 1383, DOI: 10.1111/nyas.13191.
144. Hrabal, R., Z. Chen, S. James, H. Bennett, and F. Ni. The hairpin stack fold, a novel protein architecture for a new family of protein growth factors. *Nat. Struct. Biol.* 1996; 3(9): 747-52.
145. Belcourt, D.R., C. Lazure, and H.P. Bennett. Isolation and primary structure of the three major forms of granulin-like peptides from hematopoietic tissues of a teleost fish (*Cyprinus carpio*). *J. Biol. Chem.* 1993; 268(13): 9230-7.

146. Vranken, W., Z. Chen, P. Xu, S. James, H. Bennett, and F. Ni. A 30-residue fragment of the carp granulin-1 protein folds into a stack of two  $\beta$ -hairpins similar to that found in the native protein. *J. Pept. Res.* 1999; 53(5): 590-7.
147. Tolkatchev, D., et al. Structure dissection of human progranulin identifies well-folded granulin/epithelin modules with unique functional activities. *Protein Sci.* 2008; 17(4): 711-24.
148. Ghag, G., C.J. Holler, G. Taylor, T.L. Kukar, V.N. Uversky, and V. Rangachari. Disulfide Bonds and Disorder in Granulin-3: an Unusual Handshake between Structural Stability and Plasticity. *Protein Sci.* 2017; 26, DOI: 10.1002/pro.3212.
149. Ghag, G., L.M. Wolf, R.G. Reed, N.P. Van Der Munnik, C. Mundoma, M.A. Moss, and V. Rangachari. Fully reduced granulin-B is intrinsically disordered and displays concentration-dependent dynamics. *Protein Eng. Des. Sel.* 2016; 29(5): 177-86.
150. Harrison, P.M. and M.J. Sternberg. The disulphide  $\beta$ -cross: from cystine geometry and clustering to classification of small disulphide-rich protein folds. *J. Mol. Biol.* 1996; 264(3): 603-23.
151. Vranken, W.F., S. James, H.P. Bennett, and F. Ni. Solution structures of a 30-residue amino-terminal domain of the carp granulin-1 protein and its amino-terminally truncated 3-30 subfragment: Implications for the conformational stability of the stack of two  $\beta$ -hairpins. *Proteins.* 2002; 47(1): 14-24.
152. Koradi, R., M. Billeter, and K. Wüthrich. MOLMOL: a program for display and analysis of macromolecular structures. *J. Mol. Graph.* 1996; 14(1): 51-5.
153. Tolkatchev, D., A. Ng, W. Vranken, and F. Ni. Design and solution structure of a well-folded stack of two  $\beta$ -hairpins based on the amino-terminal fragment of human granulin A. *Biochemistry.* 2000; 39(11): 2878-86.
154. Tang, W., et al. The growth factor progranulin binds to TNF receptors and is therapeutic against inflammatory arthritis in mice. *Science (New York, N.Y.).* 2011; 332(6028): 478-84.
155. Wang, B.C., H. Liu, A. Talwar, and J. Jian. New discovery rarely runs smooth: an update on progranulin/TNFR interactions. *Protein & cell.* 2015; 6(11): 792-803.
156. Zhao, Y.P., Q.Y. Tian, and C.J. Liu. Progranulin deficiency exaggerates, whereas progranulin-derived Atsttrin attenuates, severity of dermatitis in mice. *FEBS letters.* 2013; 587(12): 1805-10.
157. Jian, J., et al. Progranulin directly binds to the CRD2 and CRD3 of TNFR extracellular domains. *FEBS letters.* 2013; 587(21): 3428-36.
158. Tian, Q., Y. Zhao, J.J. Mundra, E. Gonzalez-Gugel, J. Jian, S.M. Uddin, and C. Liu. Three TNFR-binding domains of PGRN act independently in

- inhibition of TNF-alpha binding and activity. *Front. Biosci.* 2014; 19: 1176-85.
159. Smout, M.J., et al. Carcinogenic parasite secretes growth factor that accelerates wound healing and potentially promotes neoplasia. *PLoS Pathog.* 2015; 11, DOI: 10.1371/journal.ppat.1005209.
  160. Niezgoda, J.A., C.C. Van Gils, R.G. Frykberg, J.P. Hodde, and O.D.U.S. Group. Randomized clinical trial comparing OASIS Wound Matrix to Regranex Gel for diabetic ulcers. *Adv. Skin Wound Care.* 2005; 18(5): 258-66.
  161. Chan, R.K., P.H. Liu, G. Pietramaggiore, S.I. Ibrahim, H.B. Hechtman, and D.P. Orgill. Effect of recombinant platelet-derived growth factor (Regranex) on wound closure in genetically diabetic mice. *J. Burn Care Res.* 2006; 27(2): 202-5.
  162. Jin, A.H., et al. Conotoxin  $\Phi$ -MiXXVIIA from the superfamily G2 employs a novel cysteine framework that mimics granulin and displays anti-apoptotic activity. *Angew. Chem. Int. Ed. Engl.* 2017; 56, DOI: 10.1002/anie.201708927.
  163. Lewis, R.J. and M.L. Garcia. Therapeutic potential of venom peptides. *Nat. Rev. Drug Discov.* 2003; 2(10): 790-802.
  164. Dastpeyman, M., P.R. Giacomini, D. Wilson, M.J. Nolan, P.S. Bansal, and N.L. Daly. A C-terminal fragment of chlorotoxin retains bioactivity and inhibits cell migration. *Front. Pharmacol.* 2019, DOI: 10.3389/fphar.2019.00250.
  165. Dastpeyman, M., et al. Structural Variants of a Liver Fluke Derived Granulin Peptide Potently Stimulate Wound Healing. *J. Med. Chem.* 2018; 61(19): 8746-53.

**Chapter 2. A C-terminal Fragment of  
Chlorotoxin Retains Bioactivity and  
Inhibits Cell Migration**

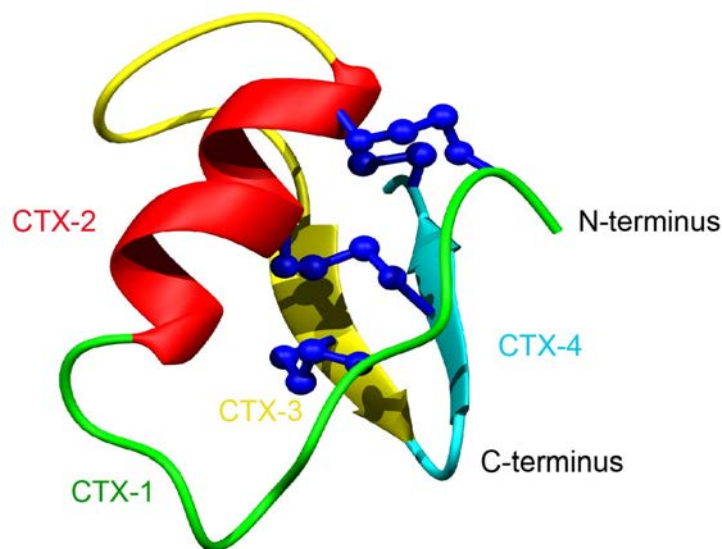


## 2.1 Abstract

Chlorotoxin was originally isolated from the venom of the Israeli scorpion *Leiurus quinquestriatus*, and has potential as a tumour imaging agent based on its selective binding to tumour cells. Several targets have been suggested for chlorotoxin including voltage-gated chloride channels, and it has been shown to have anti-angiogenic activity and inhibit cell migration. The structure of chlorotoxin is stabilized by four disulfide bonds and contains  $\beta$ -sheet and helical structure. Interestingly, the reduced form has previously been shown to inhibit cell migration to the same extent as the wild type, but structural analysis indicates that the reduced form of the peptide does not maintain the native secondary structure and appears unstructured in solution. This lack of structure suggests that a short stretch of amino acids might be responsible for the bioactivity. To explore this hypothesis we have synthesised fragments of chlorotoxin without disulfide bonds. As expected for such small peptides, NMR analysis indicated that the peptides were unstructured in solution. However, the peptide corresponding to the eight C-terminal residues, inhibited cell migration, in contrast to the other fragments. Our results suggest that the C-terminal region plays a critical role in the bioactivity of chlorotoxin.

## 2.2 Introduction

One of the most well studied scorpion venom peptides is chlorotoxin (CTX), which was originally purified from the venom of the Israeli scorpion *Leiurus quinquestriatus* (1). Chlorotoxin contains 36 amino acids with four disulfide bonds at the core of its well-defined structure. The tertiary structure, as shown in Figure 2-1, comprises a  $\beta$ -hairpin and an  $\alpha$ -helix (2, 3). The disulfide connectivity is C<sub>I</sub>-C<sub>IV</sub>, C<sub>II</sub>-C<sub>VI</sub>, C<sub>III</sub>-C<sub>VII</sub> and C<sub>V</sub>-C<sub>VIII</sub> (Figure 2- 1).



Peptide	Sequence
Chlorotoxin	1 10 20 30 MCMPCTTDHQM ARKCDDCCGKGRGKCYGPQCLCR
CTX-1	MAMPAFTTDH
CTX-2	QMARKADDAAG
CTX-3	GKGRGKA
CTX-4	YGPQALAR

**Figure 2-1 Schematic three-dimensional structure of chlorotoxin (PDB code 5L1C).** Each structural element represents the four fragments and are color coded. The sequences for the fragments are given below the structure.

Chlorotoxin selectively binds to glioma cells and other embryologically related cells and derived tumors of neuroectodermal origin (4, 5). In contrast, more than fifteen

normal human tissues have been shown to be negative for chlorotoxin binding (5). The selective binding of chlorotoxin to tumor cells bodes well for its application in cancer therapy as a tumor optical imaging contrast agent, particularly for brain cancer (6-10). Radiolabeled chlorotoxin successfully passed human clinical trial phases I and II (11-13) and FDA approval has been granted to progress to phase III, under the name TM-601 (14).

Chlorotoxin is known to inhibit migration and invasion of tumor cells through mechanisms that potentially involve multiple pathways (4, 5, 8, 15). The molecular targets identified for chlorotoxin are all involved in malignant cell migration and invasion, including voltage-gated chloride channels (ClC-3), annexin-2 and matrix metalloproteinase-2 (MMP-2) (16-19). It has been shown chlorotoxin can effectively block the ClC-3 voltage-gated chloride channel (1, 20), which is selectively expressed in glioma cells, (17, 21, 22). ClC-3 is involved in cell cytoskeleton rearrangements and consequently cell shape and movements during cell migration (4, 23, 24). Furthermore, it has been shown that chlorotoxin also interacts with a cell surface protein complex composed of MMP-2, membrane type-I MMP (MT1-MMP), a transmembrane inhibitor of metalloproteinase-2,  $\alpha_v\beta_3$  integrin, and other proteins (18, 25, 26).

Direct binding of chlorotoxin with molecular targets has not been experimentally characterized but a recent computational study predicted the binding of chlorotoxin with MMP-2 (27). The model proposed in this study suggests that the  $\beta$ -sheet of chlorotoxin interacts in a region between the collagen binding domain and catalytic domain of the MMP-2, whereas the  $\alpha$ -helix of chlorotoxin does not appear to be involved in the interaction (27).

The three-dimensional structure of disulfide-rich toxins, such as the scorpion venom peptides leiurotoxin-I and charybdotoxin (28, 29), is generally critical for bioactivity. However, a recent study suggests this is not the case for chlorotoxin. A reduced form of chlorotoxin, with the cysteine residues mutated to aminobutyric acid, maintains inhibitory effects on HUVEC cell migration compared to the wild-type peptide, but does not have regular secondary structure (8). This lack of structure suggests that a

short stretch of amino acids might be responsible for the bioactivity. Determining the minimal sequence of chlorotoxin with bioactivity is likely to enhance the understanding of the structure-function relationships. We have synthesised four fragments of chlorotoxin, containing 7-11 residues, with the cysteine residues replaced with alanine residues to prevent disulfide bond formation, and analysed the structure, *in vitro* binding and bioactivity.

## 2.3 Experimental section

### 2.3.1 Peptide synthesis, purification and characterization

Chlorotoxin (CTX) was purchased from Iris Biotech GmbH (Marktredwitz, Germany). Chlorotoxin fragments were chemically synthesised using standard stepwise Fmoc solid-phase peptide synthesis methods on the rink amide resin (Anaspec, Fremont, CA, USA) using an automated PS3 bench top peptide synthesiser (Protein Technologies, Tuscon, AZ, USA). Peptides were deprotected and cleaved from the resin using the following cleavage cocktail: 95% TFA:2.5% TIPS:2.5% H<sub>2</sub>O (v/v/v). The peptide was then precipitated and washed several times with cold diethyl ether, dissolved in 50% acetonitrile:50% H<sub>2</sub>O, lyophilised and stored as lyophilized powder. Crude peptide mixtures were purified by reversed-phase HPLC (RP-HPLC) on a C<sub>18</sub> preparative column (Phenomenex Jupiter 250 x 21.2 mm, 10 μm, 300 Å). The peptides were eluted with a 1% gradient from 1% to 60% of solvent B in solvent A over 60 min at the flow rate of 5 ml/min (Solvent A: 0.05% TFA/water, Solvent B: 0.05% TFA in 90% acetonitrile/water). The purified fractions were characterised by a SCIEX 5800 MALDI TOF/TOF mass spectrometer (SCIEX, Foster city, CA, USA).

### 2.3.2 NMR spectroscopy and structure analysis

Samples were prepared from lyophilised peptides at a concentration of 0.2 mM in 90% H<sub>2</sub>O:10% D<sub>2</sub>O with 4,4-dimethyl-4-silapentane-1-sulfonic acid (DSS) as a reference. All NMR spectra were recorded on a 600 MHz AVANCE III NMR spectrometer (Bruker, Karlsruhe, Germany). 2D <sup>1</sup>H-<sup>1</sup>H TOCSY, <sup>1</sup>H-<sup>1</sup>H NOESY, <sup>1</sup>H-<sup>15</sup>N HSQC, and <sup>1</sup>H-<sup>13</sup>C HSQC spectra were collected at 290 K and used for amino acid assignment. All spectra were recorded with an interscan delay of 1 s. NOESY spectra were acquired with mixing times of 200 ms, and TOCSY spectra were acquired with isotropic mixing periods of 80 ms. All spectra were assigned using CCPNMR (30) based on the approach described by Wüthrich (31).

### 2.3.3 Serum stability assay

The serum stability of the peptides was tested using human male serum (Sigma, USA), as previously described (32). All peptides were tested at a final concentration of 6.6 μM after dilution from a stock solution at 200 μM. The serum was centrifuged

at 17000 *g* for 10 min to remove the lipid component, and the supernatant was incubated at 37°C for 15 min before the assay. Each peptide was incubated in serum or phosphate-buffered saline (PBS) at 37°C, and 40 µL triplicate aliquots were taken at 0 h, 3 h, 8 h, and 24 h. The aliquots of serum were quenched with 40 µL of 6 M urea and incubated for 10 min at 4°C. Then, each aliquot was quenched with 40 µL of 20% trichloroacetic acid (TCA) and incubated for another 10 min at 4°C to precipitate serum proteins. Finally, samples were centrifuged at 17000 *g* for 10 min, and 90 µL of the supernatant was analysed on Reverse Phase HPLC using a Phenomenex Jupiter Proteo C<sub>12</sub> analytical column (150 x 2.00 mm, 4 µm, 90 Å; Phenomenex, Torrance, CA, USA) and a linear gradient of solvent B (90% acetonitrile/10% H<sub>2</sub>O, 0.045% trifluoroacetic acid (TFA)) at a flow rate of 0.4 mL/min using an Agilent 1260 Infinity system (Agilent Technologies, Hanover, Germany). The control samples contained equivalent amounts of the peptides in PBS and subjected to the same treatment procedure. The percentage recovery of peptides was detected by a wavelength UV detector set to 214 nm.

The stability at each time point was calculated as the area of the serum-treated peptide peak on the RP-HPLC at 214 nm as a percentage of the area of zero hour serum-treated peptides (33).

#### **2.3.4 Mammalian cell culture**

The U-87 MG (ATCC<sup>®</sup> HTB-14), human primary glioblastoma astrocytoma cell line was grown and maintained in modified Minimum Essential Medium (MEM) (Life Technologies) at 37°C and 5% CO<sub>2</sub>. The growth medium was supplemented to a final concentration of 10% fetal bovine serum (FBS) (Gibco, Scotland), 15 mM HEPES, 1x penicillin-streptomycin solution, 1 mM sodium pyruvate and 2 mM L-glutamine.

The 1BR.3.GN (ECACC 90020509), human skin normal fibroblast cell line was purchased from the European Collection of Authenticated Cell Cultures (ECACC). 1BR.3.GN cells were grown and maintained in DMEM/F12 (Life Technologies, Australia) containing 1× GlutaMAX, 1x penicillin-streptomycin solution, and supplemented with FBS at 37°C and 5% CO<sub>2</sub>.

### 2.3.5 Cytotoxicity assay

The 2,3-bis-(2-methoxy-4-nitro-5-sulphophenyl)2*H*-tetrazolium-5-carboxanilide (XTT) colorimetry assay was performed to determine whether chlorotoxin at the applied concentration was toxic to the U-87 cell line (34). Cells were seeded in 96-well microplates ( $7.5 \times 10^3$  cells/well) and incubated at 37°C for 24 h. The culture media were then replaced with 150 µL of treatment at two final concentrations of 5 and 60 µM. The treatment were in either media supplemented with 10% FBS or media supplemented with 0.5% FBS, 1x ITS-G and 1% BSA. DMSO (50% v/v) was used as a control for cell death (35). Cells then were incubated at 37°C for 24 h. The media was removed after 24 hours and the cells were incubated with 50 µL XTT (1.0 mg/ml in media without phenol red and 0.025 mM phenazine methosulfate (Sigma, USA)) for 3.5 hour. Absorbance (A) was measured at 450 nm wavelength, 650 nm used as reference wavelength in a plate reader (Polarstar Optima, Germany). Cell viability was calculated as percentage of control cells using the equation:  $(A_{450} - A_{650})$  of treated cells  $\times 100 / (A_{450} - A_{650})$  of control cells.

The experiments were repeated three times in pentaplicates and statistical significance of the observed difference was determined using one-way ANOVA with Dunnett's multiple comparison tests using the GraphPad Prism v7 software (GraphPad Software Inc., USA).

### 2.3.6 Peptide biotinylation

Chlorotoxin fragments were biotinylated on the resin to be detected by streptavidin-APC for the binding assay according to the following protocol. The assembled peptide on the resin (0.1 mmol) was washed with DMF. Biotin (Sigma, USA) was coupled to the N-terminal amide using HCTU/DIPEA activation in DMSO:DMF (1:1), overnight. The resin was washed with DMSO:DMF (1:1) twice to remove excess biotin and washed further with DMF (2x) and DCM (2x) and allowed to dry before proceeding to cleavage step. The biotinylated peptide was cleaved from the resin as previously mentioned. The mono-labelled peptides were then purified using preparative RP-HPLC and characterised using a SCIEX 5800 MALDI TOF/TOF mass spectrometer (SCIEX, Foster City, CA, USA) and analytical RP-HPLC.

The chlorotoxin biotinylation was performed as described previously (36). Briefly, 1mg/ml chlorotoxin (Iris, Germany) solution was prepared in phosphate buffer (pH 8.0) and incubated with 27.5  $\mu$ l of 10 mM NHS-Biotin (Sigma, USA) in DMSO (10 molar excess). The final concentration of the organic solvent was kept <20% in the reaction buffer. After 6 h incubation at room temperature, excess biotin was removed by passing the reaction solution through Phenomenex Strata C<sub>8</sub> unit (55  $\mu$ m, 70 Å). The collected sample was characterized using TripleTOF<sup>®</sup> 6600 Quadrupole Time-Of-Flight (QTOF) mass analyser (SCIEX, Foster City, CA, USA) and analytical RP-HPLC.

### **2.3.7 Cell surface binding and internalization assay**

Flow cytometric analysis was performed to investigate binding of chlorotoxin and fragments to U-87 MG and 1BR.3.GN cells. For cell surface binding analysis, cells were detached from adherent culture using StemPro<sup>™</sup> Accutase<sup>™</sup> Cell Dissociation reagents (Gibco, USA), washed and resuspended in media supplemented with 0.5% FBS, 1x ITS-G and 0.1% BSA. After adjusting the cell density to 10<sup>6</sup> cells per mL, 100  $\mu$ L of the cell suspension was placed in round-bottom 96-well plate. For each concentration of chlorotoxin and fragments duplicate wells received treatments of either 5 or 50  $\mu$ M chlorotoxin or chlorotoxin fragments for 30 min at 4°C. Biotinylated anti-mouse/human CD44 antibody (BioLegend) was used as control positive in all sets of experiments (37).

Following the incubation cells were washed three times with PBS and centrifuged at 400 g for 3 min to remove the unbound peptides. APC-conjugated streptavidin (BD Pharmingen, USA) was added at a concentration of 6.5  $\mu$ g/mL to each well and incubated for further 30 min on ice. Incubation was followed by two further washes in PBS and stained cells were then analysed on a BD FACS Canto II flow cytometer (BD Bioscience, USA). Data analysis was performed using FlowJo software (Tree Star, v. 8.8.4.).

To investigate whether chlorotoxin fragments internalize into cells via the same thermodynamic pathway as chlorotoxin, cells were incubated with chlorotoxin fragments at a concentration of 50  $\mu$ M in 0.5% media supplemented with 1x ITS-G



and 0.1% BSA for 30 min at 37°C, with 5% CO<sub>2</sub>. Then cells were washed with PBS and fixed using 1x fixation/permeabilization buffer (eBioscience, USA). Cells were washed and permeabilized using 1x permeabilization buffer (eBioscience, USA) for 10 min. Cells then were stained with APC-streptavidin at 4°C for 30 min. Samples were washed twice with PBS and subsequently analysed on BD FACS Canto II flow cytometer (BD Bioscience, USA) and data were analysed as described above.

### **2.3.8 Cell migration/invasion assay**

Migration assays were performed using CytoSelect cell migration assay kit (8 µm, Fluorometric format, Cell Biolabs, USA) according to the manufacturer's instructions. Briefly, cells were serum-starved overnight, then harvested using StemPro™ Accutase™ Cell Dissociation reagents and resuspended in media supplemented with 1x ITS-G and 1% BSA at 10<sup>6</sup> cells/ml. Aliquots of 100 µL of cells were then pre-incubated with chlorotoxin or fragments (at two concentrations of 5 and 50 µM) for 30 min at room temperature. Then cells were added to the each insert (upper chamber), and 150 µL media supplemented with or without 10% FBS (chemoattractants) was added to each well (lower chamber). The plate was incubated at 37°C for 16 h to allow cell migration through the polycarbonate membrane pores in response to chemoattractant (10% FBS) and subsequently lysed and detected by CyQuant® GR dye. Fluorescence measurement was performed using a fluorescence plate reader (Polarstar Optima, Germany) with a 485/520 nm filter (at an extinction of 480 nm and an emission of 520 nm). The percentage inhibition of migration in each treatment was calculated relative to that of the untreated cells. Statistical analyses using one-way ANOVA were performed for comparing treatments against control cells followed by Dunnett's using the GraphPad Prism software.

The invasion assay was performed using CytoSelect cell invasion assay kit (8 µm, Fluorometric format, Cell Biolabs, USA) using the same protocol. The cells were allowed to pass through a polycarbonate membrane bearing 8 µm sized pores with a thin layer of basement membrane for 24 h. Cells that had invaded to the other side of the inserts were lysed and detected by CyQuant® GR dye. The percentage inhibition of invasion in each treatment was calculated relative to that of the untreated cells.

Statistical analyses using one-way ANOVA were performed for comparing treatments against control cells followed by Dunnett's using the GraphPad Prism software.

### **2.3.9 Protein array analysis of chlorotoxin**

Chlorotoxin used for the protein array analysis was chemically synthesised using Fmoc chemistry with 2-chlorotrityl resin and oxidised using 0.1 M ammonium bicarbonate pH 8 and 1mM reduced glutathione, with stirring overnight at room temperature. The peptide was biotinylated using a 20-fold excess of EZ-Link<sup>®</sup> Sulfo-NHS-LC-biotin (ThermoFisher Scientific), according to the manufacturer's instructions. To ensure that successful labelling of chlorotoxin was achieved, the sample was analysed utilising an SCIEX 5800 MALDI TOF/TOF mass spectrometer (SCIEX, Foster city, CA, USA), followed by purification of labelled chlorotoxin (to remove excess non-reacted and hydrolyzed biotin reagent from the solution) via HPLC. The purified sample was dried and resuspended in 100  $\mu$ L of 1.0% PBS (pH 7.2) in order to achieve a required final concentration of 10  $\mu$ g. Protein-protein interactions among biotinylated chlorotoxin and more than 9000 human proteins were then investigated employing a ProtoArray<sup>®</sup> Human Protein Microarray v5.0 Protein-Protein Interaction (PPI) kit (Invitrogen<sup>™</sup>) and significant interactions detected employing a GenePix<sup>®</sup> microarray scanner (Molecular Devices), according to the manufacturer's instructions.

## 2.4 Results

### 2.4.1 Design and synthesis of chlorotoxin fragments

To determine the minimal sequence requirements of chlorotoxin to elicit cellular effects, four chlorotoxin fragments (CTX-1, -2, -3, -4) were chemically synthesised using Fmoc solid-phase peptide synthesis. The sequences of the full-length chlorotoxin and synthetic fragments, and the location of the fragments in the chlorotoxin structure are shown in Figure 2-1. The crude peptides were purified using RP-HPLC and mass analysis carried out using MALDI TOF/TOF mass spectrometry.

### 2.4.2 Structural analysis with NMR spectroscopy

The structures of the purified peptides were analysed using NMR spectroscopy. The one-dimensional spectra of the chlorotoxin fragments did not have significant dispersion in the amide region. Further analysis of the TOCSY and NOESY spectra for the individual fragments allowed assignment of the resonances and analysis of the secondary shifts, which indicated that the peptides had shifts close to random coil, consistent with the peptides being unstructured in solution (Figure 2-2).

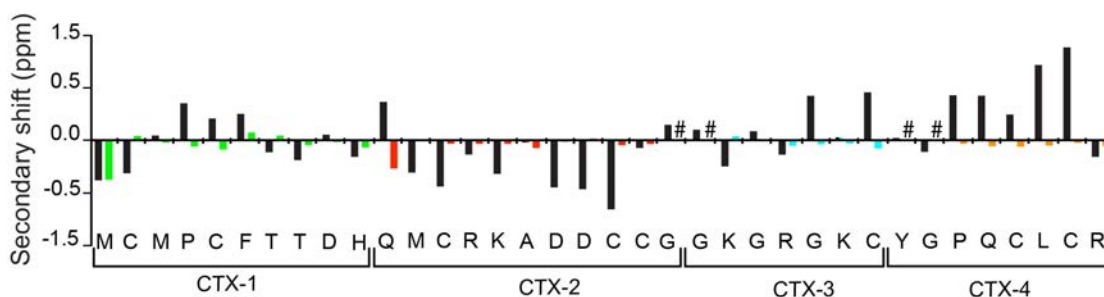


**Figure 2-2 Secondary shifts of chlorotoxin and chlorotoxin fragments.** The secondary shifts were obtained by subtracting random coil shifts from the  $\alpha$ H shifts (38). Secondary shifts for chlorotoxin residues are shown in black (39). The secondary shifts for CTX-1, 2, 3 and 4 are shown in green, red, blue and orange respectively. The sequence for chlorotoxin is given below the graph. The cysteine residues were replaced with alanine residues in the chlorotoxin fragments. (#: could not be assigned).

#### 2.4.2.1 Serum stability assay

The stability of the chlorotoxin peptide fragments in human serum was assessed using RP-HPLC, and the degradation profiles are shown in Figure 2-3. CTX-1 and -2

degraded more slowly than CTX-4. The latter peptide had less than 10% peptide remaining after 3 hours, whereas CTX-1 had more than 18% remaining at the 8 h time point and could be detected up to 24 hours. The serum stability could not be measured accurately for CTX-3 peptide, using the same column as that used for the other fragments, because of the hydrophilic nature of this peptide. Chlorotoxin has been previously shown to be highly stable in serum with only 10% degradation after 24 hour incubation with human serum at 37°C using the same protocol (35, 39).

Due to low serum stability of chlorotoxin fragments, the cell assays were designed to minimize the exposure of the peptides to serum media (FBS). Prior to the cell assays, cells were pre-treated with chlorotoxin or chlorotoxin fragments in 0.5-1% media supplemented with 1x ITS-G and 0.1% BSA which were used to ensure cells remain healthy and viable over the course of the 30 min treatment (40). It has been previously shown that, chlorotoxin achieves the maximum cellular level at a concentration of 10  $\mu$ M within 30 min of incubation with cells under physiological conditions (37°C, 5% CO<sub>2</sub>) (7). Chlorotoxin has been shown to significantly label cells (19), block chloride channel (23), inhibit endothelial cell migration (8), and induce biochemical changes in U87-MG cells (41) over 30 min incubation with cells. Thus, 30 minutes pre-treatment appears to be the optimum treatment time for chlorotoxin and fragments, in this study.

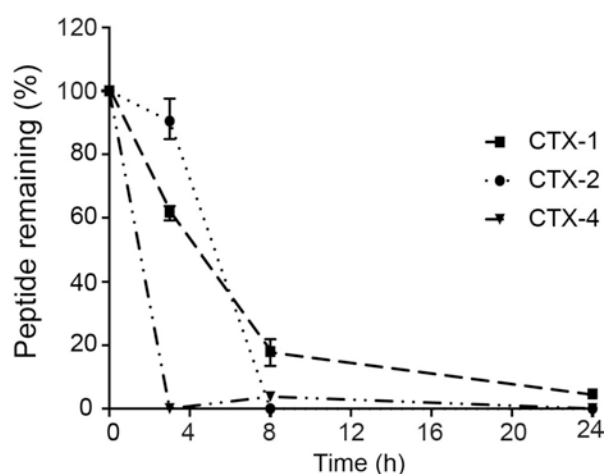


**Figure 2-3 Stability of the peptides in human serum.** The amount of peptide remaining was calculated by comparing the area of the elution peak of peptides incubated in human serum and that of peptides that had not been incubated. The experiments were performed in triplicates. All data are represented as mean  $\pm$  SEM. Chlorotoxin has been previously shown to be highly stable in serum with only 10% degradation after 24 hour incubation with human serum, using the same protocol (35, 39).

### 2.4.2.2 Cytotoxicity assay

The cytotoxicity of chlorotoxin and the chlorotoxin fragments was investigated using an XTT assay on the U-87 MG cell line. Cells were incubated with either 5 or 60  $\mu\text{M}$  peptide. These concentrations are comparable to those used in the subsequent cell assays. The XTT assays were carried out in media (10%), and also in media supplemented with 0.5% FBS, 1x ITS-G and 1% BSA. The chlorotoxin fragments were not cytotoxic to U87-MG cells under either media condition or peptide concentration, with cell viability after a 24 h incubation period higher than 90% for all peptides tested (Figure 2-4).

These results are consistent with previous study that showed chlorotoxin is not toxic on U87-MG and HUVECs cells at concentrations up to 10  $\mu\text{M}$  and 200  $\mu\text{M}$ , respectively (8, 42).

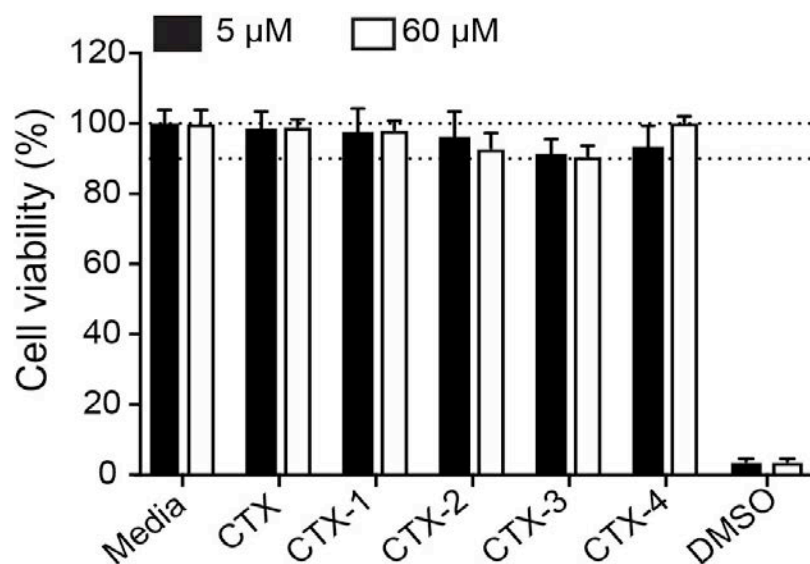


**Figure 2-4 Cell viability assay of chlorotoxin and fragments treated U87-MG cells for 24 hours.** Chlorotoxin and fragments were added in media supplemented with 0.5% FBS, 1x ITS-G and 1% BSA. Cell viability was determined by XTT assay. Controls with media and DMSO at 50% (v/v) were used to establish 100 and 0% of cell survival, respectively. The experiments were repeated three times in pentaplicates. Data are shown as mean  $\pm$  SEM.

#### **2.4.2.3 Peptide biotinylation**

Peptides were labelled with biotin to allow detection using flow cytometry. The chlorotoxin fragments were biotinylated on resin, resulting in a single biotin moiety attached to the N-terminus. Following incubation with biotin, the peptides were purified using RP-HPLC to remove excess biotin. By contrast, chlorotoxin was biotinylated in solution. The mass spectrometry analysis indicated the presence of chlorotoxin species with one, two, three and four biotin moieties attached, consistent with the four biotinylation sites. Excess biotin was removed from the sample using RP-HPLC but it was not possible to purify the individual species and therefore the mixture was used in the subsequent experiments.

#### **2.4.2.4 Cell surface binding/endocytosis assay**

To evaluate the interaction of chlorotoxin fragments with U87-MG cells, a cell line previously shown to bind to chlorotoxin, *in vitro* binding assays were carried out with the biotinylated peptides and binding detected by flow cytometry using APC-conjugated streptavidin as shown in Figure 2-5A. As expected, native chlorotoxin demonstrated a significant level of APC fluorescence and surface binding to cells when compared to control-treated cells (Figure 2-5A). Further analysis of the relative binding efficiency of the four fragments revealed that while CTX-1, CTX-2 and CTX-4 did not display any significant binding to the surface of cells, CTX-3 did significantly bind to the surface of both U87-MG and 1BR.3.GN cell lines in a dose dependent manner (Figure 2-5A and B).

These studies were done at 4°C. A direct comparison of the peptides with chlorotoxin is difficult, given the differences in the number of biotin moieties present in the full-length peptide and the fragments, which will affect the signal intensity.

We next assessed whether the peptide fragments were being internalized and interacting with a target within the cell. Analysis of the internalization of the fragments into the U87-MG cells at 37°C, indicated that while CTX-1 and CTX-2 do not appear to be internalized into either the tumor cell line (U87-MG) or normal cell line (1BR.3.GN), CTX-3 and CTX-4 appeared to be binding internally to U87-MG cells (Figure 2-6A and B).

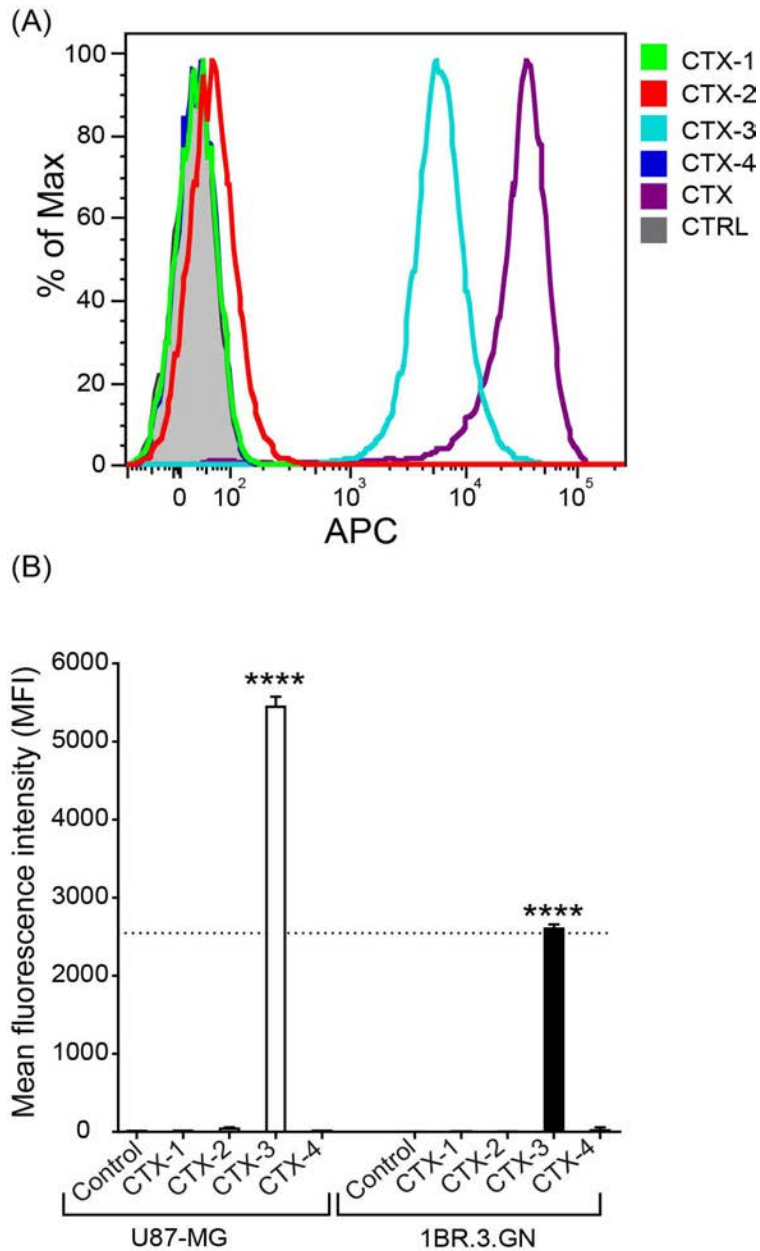


**Figure 2-5 *In vitro* cell surface binding of chlorotoxin fragments.** (A) Representative flow cytometric histogram of *in vitro* U87-MG cell surface binding of biotinylated chlorotoxin fragments detected by APC labelled streptavidin. Cells were treated with 50  $\mu$ M chlorotoxin or fragments at 4°C for 30 min. Grey shaded histograms represent cells treated with APC-streptavidin alone. (B) Mean fluorescence intensity (MFI) of *in vitro* cell surface binding of chlorotoxin fragments (50  $\mu$ M) to U87-MG and 1BR.3.GN cell line. The experiments were performed three times in duplicates. Data are presented as mean  $\pm$  SEM. The statistical analysis was performed using an ANOVA Dunnett's multiple comparison test by comparison of chlorotoxin fragments with control cells (\*\*\*\* $P$ <0.0001.). The data was normalised to account for differences in cell number and expressed as percent of maximum cell number for each sample (% of Max).

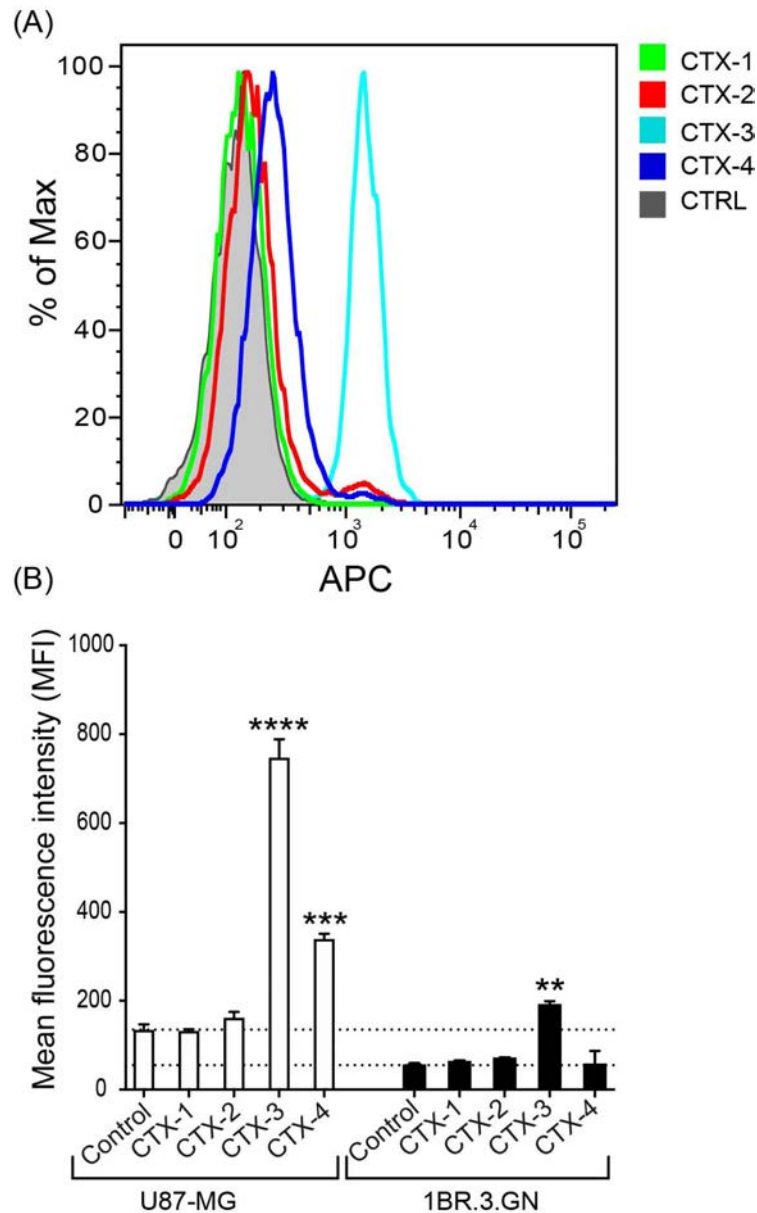


**Figure 2-6 *In vitro* cell internalization of chlorotoxin fragments.** (A) Representative flow cytometric histogram of *in vitro* U87-MG cell internalization of biotinylated chlorotoxin fragments detected by APC labelled streptavidin. Cells were treated with 50  $\mu$ M chlorotoxin fragments at 37°C for 30 min. Grey shaded histograms represent cells treated with APC-streptavidin alone. (B) Mean fluorescence intensity (MFI) of *in vitro* cell internalization of chlorotoxin fragments (50  $\mu$ M) to U87-MG and 1BR.3.GN cell line. The experiments were performed two times in quadruplicates. Data are presented as mean  $\pm$  SEM. The statistical analysis was performed using an ANOVA Dunnett's multiple comparison test by comparison of chlorotoxin fragments with control cells (\*\*  $P < 0.01$ , \*\*\*  $P < 0.001$  \*\*\*\*  $P < 0.0001$ ).



Interestingly, only CTX-3 showed any evidence of fluorescence signal when exposed to 1BR.3.GN cells, however it is not clear whether this binding was on the surface of the cell or internal (Figure 2-6B). Given that CTX-4 appeared to bind internally to U87-MG cells, but not 1BR.3.GN cells suggests that this intracellular interaction may be specific to the glioblastoma cell line. Chlorotoxin has been previously shown not to bind to human fibroblasts. (5).

#### **2.4.2.5 Migration and invasion assay**

The inhibitory effects of chlorotoxin and the chlorotoxin fragments on migration and invasion of U87-MG cells were analysed and the results summarised in Figure 2-7. chlorotoxin significantly inhibited U87-MG cell migration with inhibitory effects of 32.9% ( $P<0.01$ ) and 34.6% ( $P<0.001$ ) compared to control cells at 5 and 50  $\mu\text{M}$ , respectively (Figure 2-7A). Only CTX-4 inhibited U87-MG cell migration at a concentration of 50  $\mu\text{M}$  (20.4%,  $P<0.05$ ).

Chlorotoxin also significantly inhibited U87-MG cell invasion by 37% ( $P<0.05$ ) and 36.7% ( $P<0.05$ ) at 5 and 50  $\mu\text{M}$  (Figure 2-7B), respectively, consistent with previous studies (18, 19, 23). None of the chlorotoxin fragments significantly inhibited U87-MG cells invasion even at the highest concentration tested (50  $\mu\text{M}$ ).

#### **2.4.2.6 Protein array analysis of chlorotoxin**

Protein-protein interactions among biotinylated chlorotoxin and more than 9000 human proteins were investigated employing a ProtoArray® Human Protein Microarray v5.0 Protein-Protein Interaction (PPI) kit (Invitrogen™) and monitored with a GenePix® microarray scanner (Molecular Devices). Of the more than 9000 possible interactions tested herein, 104 (ca. 1.0%) were significant (Z-score of  $> 3$ ), while four of the top nine, including interactions between chlorotoxin and cortactin (CTTN; Z-score 32.27), polo-like kinase 1 (PLK1; Z-score 11.20), homeobox protein HOXB6 (Z-score 10.47) and XTP3-transactivated protein A (XTP3TPA; Z-score 6.21825), are relevant to the present investigation as these proteins have been shown to be involved in cancer.

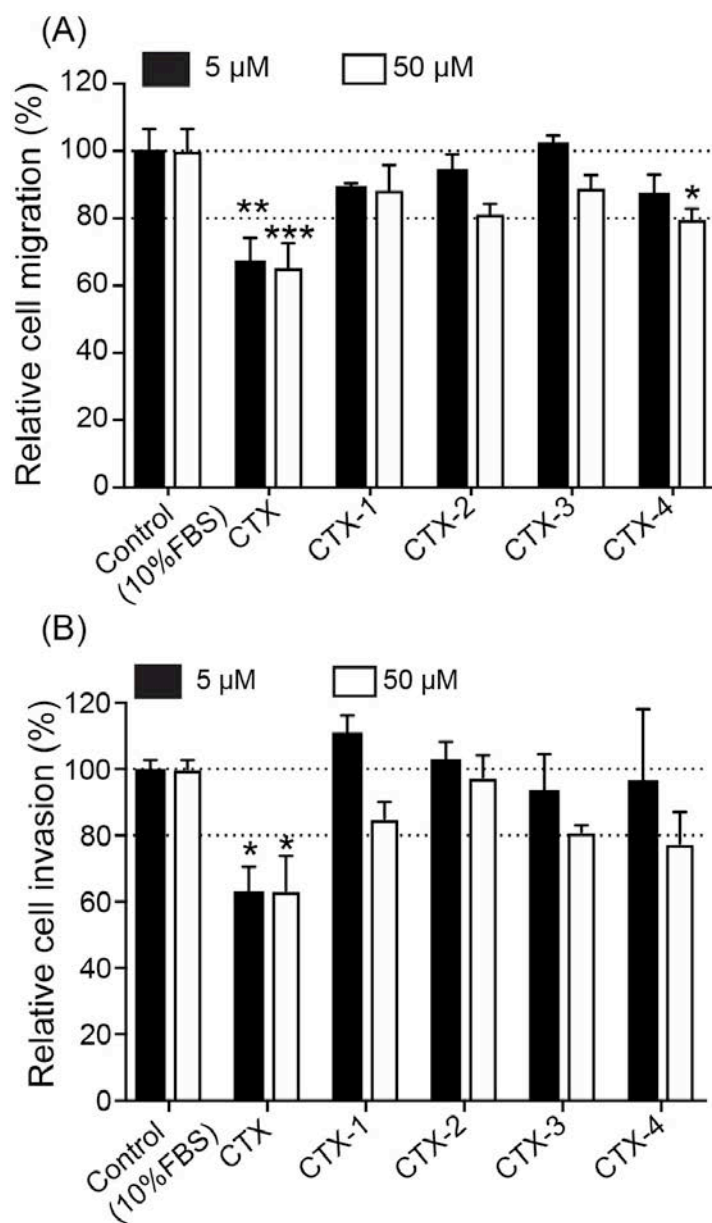


**Figure 2-7 The migration and invasion assay.** Cells were pre-incubated with chlorotoxin and fragments at 5 and 50  $\mu\text{M}$  and then were used for migration/invasion assay. (A) The effect of chlorotoxin and fragments on U87-MG cell migration. (B) The effect of chlorotoxin and fragments on U87-MG cell invasion. The percentage inhibition of migration/invasion in each treatment was calculated relative to that of the untreated well. The data was expressed as mean  $\pm$  SEM. Data were analyzed by one-way ANOVA against peptide control. \*  $P < 0.05$ , \*\*  $P < 0.01$ .

## 2.5 Discussion

Given the potential of chlorotoxin as a therapeutic it is of significant interest to understand the structural features important for function, as this information is likely to facilitate the development of chlorotoxin as a therapeutic. Numerous studies have analyzed the binding of chlorotoxin and conjugates to cells but there is still limited information on the structure-function relationships and target interaction.

The chlorotoxin fragments synthesized in the current study showed limited stability in human serum and did not display regular secondary structure in solution. Interestingly, CTX-2 was the most stable of the peptides tested in human serum and is also the longest peptide, which might explain the enhanced stability. The lack of structure in solution is expected for such small peptides and is consistent with the previous study, which showed that the disulfide bonds in chlorotoxin are critical for the three-dimensional structure (8).

The C-terminal fragments of chlorotoxin (CTX-3 and CTX-4) displayed interesting properties in the cellular assays. CTX-3 showed cell surface binding and cell internalization, whereas CTX-4 was internalized into cells and was the only fragment to inhibit U87-MG cell migration at the highest concentration tested (50  $\mu$ M). Despite the effect of CTX-4 on cell migration it did not inhibit cell invasion.

The cell surface binding and internalization of chlorotoxin is critical to its potential as a tumor imaging agent and our current results suggest that residues 22 to 28, present in CTX-3, might be involved with this process. However, given that CTX-3 binds to both a tumor cell line and a normal cell line, in contrast to previous studies on chlorotoxin, it appears likely that this region is not sufficient by itself to account for the selective binding to tumor cells. It is possible the cell surface binding observed for CTX-3 is non-specific membrane binding mediated by the presence of the high proportion of positively charged (2 lysine and 1 arginine) residues within a seven-residue peptide as reported for other highly charged peptides (43, 44). Although no cell surface binding was observed for CTX-4, it was the only fragment that appeared to be specifically internalized into the glioma cells at 37°C. The differences between CTX-3 and CTX-4 suggest they might have different internalization mechanisms.

Our results, whereby CTX-4 only inhibits migration and not invasion, indicates that it might inhibit the ClC-3 channel, which is involved in cell migration, independently from the MMP2 macromolecular complex, which is involved in cell invasion. The other possibility is that CTX-4 inhibits U87-MG cell migration through another pathway, which does not necessarily involve the macromolecular complex. Annexin A2, which is identified as another chlorotoxin target, is involved in cell migration in a series of glioma cells including U87-MG cells (19, 45). Therefore, it is possible that CTX-4 inhibits U87-MG cell migration through an annexin A2 interaction. However, more research, including mutagenesis studies, are required to investigate CTX-4 binding to the targets previously suggested for chlorotoxin. Additional studies involving the synthesis of over-lapping peptide fragments might also provide further insight into the structure-function relationships.

The recently proposed model of MMP-2 interacting with chlorotoxin (27) shows that residues 29-36 (which correspond to CTX-4) are directly involved in the interaction with MMP-2 (27). Neither of the cysteine residues (C33 and C35) in this region interact with MMP-2, therefore it is highly likely that replacing cysteines with alanine in our study would not make a significant difference in CTX-4 binding and bioactivity. Furthermore, a recent study has used chlorotoxin as inspiration to design blood-brain barrier shuttles. MiniCTX3, contains residues 28-32 of chlorotoxin and a lactam bridge, and was able to transport nanoparticles across endothelial cell (35). These studies highlight the potential importance of the C-terminal region of chlorotoxin in cellular interactions and support our current findings.

Although several biological targets for chlorotoxin have been proposed, direct binding has not been reported. Here we used protein array technology to identify another possible target for chlorotoxin. Chlorotoxin bound most strongly to cortactin, which was initially identified as a substrate of the Src nonreceptor tyrosine kinase but its overexpression has now been linked to invasive cancers, including melanoma, colorectal cancer and glioblastoma, making it an important biomarker for invasive cancers (46). Cortactin localizes to invasive protrusions in cells including invadopodia and has been shown to associate with MMP-2 using co-immunoprecipitation studies (47). Similarly to annexin A2, it has been suggested that a transient interaction between cortactin and complexes containing MMPs might exist (47). Given

chlorotoxin can penetrate cells via clathrin-mediated endocytosis, it is possible that it can interact with cortactin intracellularly, or alternatively as part of a MMP-2 complex that is subsequently internalised (7). The importance of intracellular targeting of cortactin has been shown with a cell permeable peptide that binds cortactin, and inhibits the invasion of a range of cancers including glioblastomas (48). Our cell internalization assay provides supports for the possibility that CTX-4 can bind an intracellular target that is specific to tumor cells compared to normal cells. It would be of interest to determine if CTX-4 can also bind to cortactin.

Overall, this study provides insight into understanding the important sequence requirements for chlorotoxin bioactivity, and indicates that a small region of chlorotoxin, which is not structured in solution, can have an influence on cell migration, albeit at relatively high concentrations. This result might explain the bioactivity previously observed for the reduced form of chlorotoxin (8). We also provide evidence that fragments of chlorotoxin are involved in cell binding and/or internalisation. Further study is required to determine if these fragments can bind to the biological targets previously suggested for chlorotoxin.

## 2.6 Acknowledgements

MD would like to thank James Cook University for a PhD scholarship. The authors would like to thank Dr Roland Ruscher for his valuable comments on analysing the flow cytometry data. This work was supported by a Future Fellowship to NLD (110100226). PG is supported by an Advance Queensland Mid-Career Fellowship. The James Cook University NMR facility was partially funded by the Australian Research Council (LE120100015, LE160100218).

## 2.7 Non-standard abbreviations

Human Umbilical Vein Endothelial Cells (HUVEC); Minimum Essential Medium (MEM); Fetal Bovine Serum (FBS); 4-(2-hydroxyethyl)-1-piperazineethanesulfonic acid (HEPES); Reversed-phase HPLC (RP-HPLC); Matrix assisted laser desorption/ionisation - time of flight mass spectrometry (MALDI TOF/TOF MS); Nuclear Magnetic Resonance (NMR); Total Correlated Spectroscopy (TOCSY); Nuclear Overhauser Spectroscopy (NOESY); heteronuclear single quantum correlation experiment (HSQC); trichloroacetic acid (TCA); 2,3-Bis(2-methoxy-4-nitro-5-sulphophenyl)-2H-tetrazolium-5-carboxanilide inner salt (XTT); Insulin-Transferrin-Selenium (ITS-G); Dimethyl sulfoxide (DMSO); 2-(6-Chloro-1-H-benzotriazole-1-yl)-1,1,3,3-tetramethylammonium hexafluorophosphate (HCTU); Ethyldiisopropylamine (DIPEA); Time-of-flight mass spectrometry (QTOF); Bovine serum albumin (BSA); allophycocyanin (APC); Phosphate-buffered saline (PBS); chlorotxin (CTX); trifluoroacetic acid (TFA); N-hydroxy-succinimide (NHS); MMP matrix metalloproteinase-2(MMP-2); 4,4-dimethyl-4-silapentane-1-sulfonic acid (DSS); Analysis Of Variance (ANOVA); European Collection of Authenticated Cell Cultures (ECACC).

## 2.8 References

1. DeBin, J.A., J.E. Maggio, and G.R. Strichartz. Purification and characterization of chlorotoxin, a chloride channel ligand from the venom of the scorpion. *Am. J. Physiol.* 1993; 264(2 Pt 1): 361-9.
2. Lippens, G., J. Najib, S.J. Wodak, and A. Tartar. NMR sequential assignments and solution structure of chlorotoxin, a small scorpion toxin that blocks chloride channels. *Biochemistry.* 1995; 34(1): 13-21.
3. Correnti, C.E., et al. Nature structural and molecular biology. *Nat. Struct. Mol. Biol.* 2018; 25(3): 270-8.
4. Soroceanu, L., Y. Gillespie, M. Khazaeli, and H. Sontheimer. Use of chlorotoxin for targeting of primary brain tumors. *Cancer Res.* 1998; 58(21): 4871-9.
5. Lyons, S.A., J. O'Neal, and H. Sontheimer. Chlorotoxin, a scorpion-derived peptide, specifically binds to gliomas and tumors of neuroectodermal origin. *Glia.* 2002; 39(2): 162-73.
6. Kovar, J.L., E. Curtis, S.F. Othman, M.A. Simpson, and D.M. Olive. Characterization of IRDye 800CW chlorotoxin as a targeting agent for brain tumors. *Anal. Biochem.* 2013; 440(2): 212-9.
7. Wiranowska, M., L.O. Colina, and J.O. Johnson. Clathrin-mediated entry and cellular localization of chlorotoxin in human glioma. *Cancer Cell Int.* 2011; 11, DOI: 10.1186/1475-2867-11-27.
8. Ojeda, P.G., L.Y. Chan, A.G. Poth, C.K. Wang, and D.J. Craik. The role of disulfide bonds in structure and activity of chlorotoxin. *Future Med. Chem.* 2014; 6(15): 1617-28.
9. Albert, F.K., M. Forsting, K. Sartor, H.P. Adams, and S. Kunze. Early postoperative magnetic resonance imaging after resection of malignant glioma: objective evaluation of residual tumor and its influence on regrowth and prognosis. *Neurosurgery.* 1994; 34(1): 45-60; discussion -1.
10. Kieran, M.W., D. Walker, D. Frappaz, and M. Prados. Brain tumors: from childhood through adolescence into adulthood. *J. Clin. Oncol.* 2010; 28(32): 4783-9.
11. Mamelak, A.N., et al. Phase I single-dose study of intracavitary-administered iodine-131-TM-601 in adults with recurrent high-grade glioma. *J. Clin. Oncol.* 2006; 24(22): 3644-50.
12. Mamelak, A.N. and D.B. Jacoby. Targeted delivery of antitumoral therapy to glioma and other malignancies with synthetic chlorotoxin (TM-601). *Expert Opin. Drug. Deliv.* 2007; 4: 175-86.

13. Gribbin, T.E., N. Senzer, J.J. Raizer, S. Shen, L.B. Nabors, M. Wiranowska, and J.B. Fiveash. A phase I evaluation of intravenous (IV) <sup>131</sup>I-chlorotoxin delivery to solid peripheral and intracranial tumors. *J. Clin. Oncol.* 2009; 27, DOI: 10.1200/jco.2009.27.15s.e14507.
14. Lefranc, F., E. Le Rhun, R. Kiss, and M. Weller. Glioblastoma quo vadis: Will migration and invasiveness reemerge as therapeutic targets? *Cancer Treat. Rev.* 2018; 68: 145-54.
15. Dardevet, L., et al. Chlorotoxin: a helpful natural scorpion peptide to diagnose glioma and fight tumor invasion. *Toxins.* 2015; 7(4): 1079-101.
16. Ullrich, N. and H. Sontheimer. Biophysical and pharmacological characterization of chloride currents in human astrocytoma cells. *Am. J. Physiol. Cell Physiol.* 1996; 270(5): 1511-21.
17. Olsen, M., S. Schade, S. Lyons, M. Amaral, and H. Sontheimer. Expression of voltage-gated chloride channels in human glioma cells. *J. Neurosci.* 2003; 23(13): 5572-82.
18. Deshane, J., C.C. Garner, and H. Sontheimer. Chlorotoxin inhibits glioma cell invasion via matrix metalloproteinase-2. *J. Biol. Chem.* 2003; 278(6): 4135-44.
19. Kesavan, K., et al. Annexin A2 is a molecular target for TM601, a peptide with tumor-targeting and anti-angiogenic effects. *J. Biol. Chem.* 2010; 285(7): 4366-74.
20. DeBin, J. and G. Strichartz. Chloride channel inhibition by the venom of the scorpion *Leiurus quinquestriatus*. *Toxicon.* 1991; 29(11): 1403-8.
21. Ullrich, N., A. Bordey, G. Gillespie, and H. Sontheimer. Expression of voltage-activated chloride currents in acute slices of human gliomas. *Neuroscience.* 1998; 83(4): 1161-73.
22. Jentsch, T.J. CLC chloride channels and transporters: from genes to protein structure, pathology and physiology. *Crit. Rev. Biochem. Mol. Biol.* 2008; 43(1): 3-36.
23. McFerrin, M.B. and H. Sontheimer. A role for ion channels in glioma cell invasion. *Neuron Glia Biol.* 2006; 2(01): 39-49.
24. Soroceanu, L., T.J. Manning, and H. Sontheimer. Modulation of glioma cell migration and invasion using Cl<sup>-</sup> and K<sup>+</sup> ion channel blockers. *J. Neurosci.* 1999; 19(14): 5942-54.
25. Hofmann, U.B., J.R. Westphal, E.T. Waas, J.C. Becker, D.J. Ruiter, and G.N. van Muijen. Coexpression of integrin  $\alpha_v\beta_3$  and matrix metalloproteinase-2 (MMP-2) coincides with MMP-2 activation: correlation with melanoma progression. *J. Invest. Dermatol.* 2000; 115(4): 625-32.



26. Jacoby, D.B., et al. Potent pleiotropic anti-angiogenic effects of TM601, a synthetic chlorotoxin peptide. *Anticancer Res.* 2010; 30(1): 39-46.
27. Othman, H., S.A. Wieninger, M. ElAyeub, M. Nilges, and N. Srairi-Abid. In Silico prediction of the molecular basis of ClTx and AaCTx interaction with matrix metalloproteinase-2 (MMP-2) to inhibit glioma cell invasion. *J. Biomol. Struct. Dyn.* 2017; 35(13): 2815-29.
28. Zhu, Q., S. Liang, L. Martin, S. Gasparini, A. Menez, and C. Vita. Role of disulfide bonds in folding and activity of leiurotoxin I: just two disulfides suffice. *Biochemistry.* 2002; 41(38): 11488-94.
29. Drakopoulou, E., et al. Consequence of the removal of evolutionary conserved disulfide bridges on the structure and function of charybdotoxin and evidence that particular cysteine spacings govern specific disulfide bond formation. *Biochemistry.* 1998; 37(5): 1292-301.
30. Vranken, W.F., et al. The CCPN data model for NMR spectroscopy: development of a software pipeline. *Proteins.* 2005; 59(4): 687-96.
31. Wüthrich, K. NMR studies of structure and function of biological macromolecules (Nobel Lecture). *J. Biomol. NMR.* 2003; 27(1): 13-39.
32. Chan, L.Y., et al. Engineering pro-angiogenic peptides using stable, disulfide-rich cyclic scaffolds. *Blood.* 2011; 118(25): 6709-17.
33. Chan, L.Y., V.M. Zhang, Y.H. Huang, N.C. Waters, P.S. Bansal, D.J. Craik, and N.L. Daly. Cyclization of the antimicrobial peptide gomesin with native chemical ligation: influences on stability and bioactivity. *Chembiochem.* 2013; 14(5): 617-24.
34. Page, B., M. Page, and C. Noel. A new fluorometric assay for cytotoxicity measurements *in vitro*. *Int. J. Oncol.* 1993; 3(3): 473-6.
35. Diaz-Perlas, C., M. Varese, S. Guardiola, J. Garcia, M. Sanchez-Navarro, E. Giralt, and M. Teixido. From venoms to BBB-shuttles. MiniCTX3: a molecular vector derived from scorpion venom. *Chem. Commun.* 2018; 54(90): 12738-41.
36. Selo, I., L. Negroni, C. Creminon, J. Grassi, and J.M. Wal. Preferential labeling of alpha-amino N-terminal groups in peptides by biotin: application to the detection of specific anti-peptide antibodies by enzyme immunoassays. *J. Immunol. Methods.* 1996; 199(2): 127-38.
37. Knupfer, M.M., H. Poppenborg, M. Hotfilder, K. Kuhnel, J.E. Wolff, and M. Domula. CD44 expression and hyaluronic acid binding of malignant glioma cells. *Clin. Exp. Metastasis.* 1999; 17(1): 71-6.
38. Wishart, D.S., et al. <sup>1</sup>H, <sup>13</sup>C and <sup>15</sup>N chemical shift referencing in biomolecular NMR. *J. Biomol. NMR.* 1995; 6(2): 135-40.

39. Akcan, M., M.R. Stroud, S.J. Hansen, R.J. Clark, N.L. Daly, D.J. Craik, and J.M. Olson. Chemical re-engineering of chlorotoxin improves bioconjugation properties for tumor imaging and targeted therapy. *J. Med. Chem.* 2011; 54(3): 782-7.
40. Gstraunthaler, G. Alternatives to the use of fetal bovine serum: serum-free cell culture. *Altex.* 2003; 20(4): 275-81.
41. Falahat, R., M. Wiranowska, R. Toomey, and N. Alcantar. ATR-FTIR analysis of spectral and biochemical changes in glioma cells induced by chlorotoxin. *Vib. Spectrosc.* 2016; 87: 164-72.
42. Park, T., K.A. Min, H. Cheong, C. Moon, and M.C. Shin. Genetic engineering and characterisation of chlorotoxin-fused gelonin for enhanced glioblastoma therapy. *J. Drug Target.* 2018; 11, DOI: 10.1080/1061186x.2018.1516221.
43. Futaki, S., I. Nakase, A. Tadokoro, T. Takeuchi, and A.T. Jones. Arginine-rich peptides and their internalization mechanisms. *Biochem. Soc. Trans.* 2007; 35(Pt 4): 784-7.
44. Ojeda, P.G., S.T. Henriques, Y. Pan, J.A. Nicolazzo, D.J. Craik, and C.K. Wang. Lysine to arginine mutagenesis of chlorotoxin enhances its cellular uptake. *Biopolymers.* 2017; 108, DOI: 10.1002/bip.23025.
45. Tatenhorst, L., U. Rescher, V. Gerke, and W. Paulus. Knockdown of annexin 2 decreases migration of human glioma cells *in vitro*. *Neuropathol. Appl. Neurobiol.* 2006; 32(3): 271-7.
46. MacGrath, S.M. and A.J. Koleske. Cortactin in cell migration and cancer at a glance. *J. Cell Sci.* 2012; 125(Pt 7): 1621-6.
47. Banon-Rodriguez, I., J. Monypenny, C. Ragazzini, A. Franco, Y. Calle, G.E. Jones, and I.M. Anton. The cortactin-binding domain of WIP is essential for podosome formation and extracellular matrix degradation by murine dendritic cells. *Eur. J. Cell Biol.* 2011; 90(2-3): 213-23.
48. Hashimoto, S., et al. Targeting AMAP1 and cortactin binding bearing an atypical src homology 3/proline interface for prevention of breast cancer invasion and metastasis. *Proc. Natl. Acad. Sci. U.S.A.* 2006; 103(18): 7036-41.

**Chapter 3. Development of a Potent  
Wound Healing Agent Based on the  
Liver Fluke Granulin Structural Fold**

### 3.1 Abstract

Granulins are a family of protein growth factors that are involved in cell proliferation. An orthologue of granulin from the human parasitic liver fluke *Opisthorchis viverrini*, known as *Ov*-GRN-1, induces angiogenesis and accelerates wound repair. Recombinant *Ov*-GRN-1 production is complex, and poses an obstacle for clinical development. To identify the bioactive region(s) of *Ov*-GRN-1, four truncated N-terminal analogues were synthesized and characterized structurally using NMR spectroscopy. Peptides that contained only two native disulfide bonds lack the characteristic granulin  $\beta$ -hairpin structure. Remarkably, the introduction of a non-native disulfide bond was critical for formation of  $\beta$ -hairpin structure. Despite this structural difference, both two and three disulfide-bonded peptides drove proliferation of a human cholangiocyte cell line and demonstrated potent wound healing in mice. Peptides derived from *Ov*-GRN-1 are leads for novel wound healing therapeutics, as they are likely less immunogenic than the full-length protein and more convenient to produce.

### 3.2 Introduction

Granulins are a family of protein growth factors involved in a wide range of physiological functions and disease processes including embryogenesis, wound repair, inflammation and tumour growth (1). The human parasitic liver fluke *Opisthorchis viverrini* secretes a granulin family member called *Ov*-GRN-1, which was originally isolated from the excretory/secretory (ES) products of the carcinogenic trematode (2, 3). *Ov*-GRN-1 was the first growth factor described from a pathogen to cause proliferation of both human and murine cells (4, 5). We have shown that picomolar concentrations of recombinant *Ov*-GRN-1 induce angiogenesis and accelerate wound repair in mice upon topical administration, findings that indicate that liver fluke granulin might be developed as a treatment for wounds (6).

An understanding of the structure-activity relationship for *Ov*-GRN-1 would enable design of the most efficacious form of this granulin for healing wounds. The three-dimensional structure of *Ov*-GRN-1 has not been experimentally determined, but structures for granulins of several species have been reported. The initial granulin structure determined was that of carp granulin-1; this comprises four  $\beta$ -hairpins cross-linked together by six disulfide bonds in a ladder-shaped arrangement of the disulfide bonds (7). Despite the well-defined structure observed for carp granulin-1, the structure-function relationships of granulins are complex and appear to be highly dependent on the primary sequence. This is particularly evident with the human granulins. The precursor protein of mammalian granulin (progranulin, PGRN) contains seven-and-a-half granulin domains that are approximately 6 kDa in molecular mass and are proteolytically processed into individual granulin modules after secretion of PGRN from the cell (1). The “half-granulin” unit, termed paraganulin, contains only six cysteine residues (8).

The seven human granulin modules have been expressed individually and the structures analyzed by NMR spectroscopy (9). Three contain relatively well-defined three-dimensional structures in solution (A, C and F), whereas the others are mainly mixtures of poorly structured disulfide isomers (9). The structure of human granulin A includes a  $\beta$ -hairpin structure similar to carp granulin-1 but there is significant structural disorder in the C-terminal region. Of the well folded human granulin

modules, granulin A demonstrates potent inhibition of proliferation of a breast cancer cell line, while by contrast, human granulin F stimulates cell proliferation (9). The poorly folded peptides exhibit weak or no inhibitory or activity. It should be noted, however, that the limited activity may be due to the absence of key signaling pathways in the target cells, and/or that the production of the recombinant peptides in bacteria induced incomplete/incorrect folding. To date, the range of granulin activities and binding partners is broad, and seemingly organ- and co-factor-dependent (10-13).

Structural analysis with NMR spectroscopy has shown that the N-terminal regions of carp granulin-1 and human granulin A can fold independently of the C-terminal regions (14, 15). Truncated analogues of these two granulins containing only two-disulfide bonds, have  $\beta$ -hairpin structures, as shown for a 30-residue N-terminal domain of carp granulin-1 (Figure 3-1). In the current study we synthesized truncated versions of *Ov*-GRN-1 to determine if this region can fold independently, and to determine if the N-terminal region contributes to cell proliferation and wound healing. We show for the first time that the N-terminal region of *Ov*-GRN-1 displays novel folding properties, and notably from a drug design perspective, peptides derived from the N-terminus are as potent as the full-length protein and Regranex, a clinically used wound-healing agent, in healing cutaneous wounds in laboratory mice.

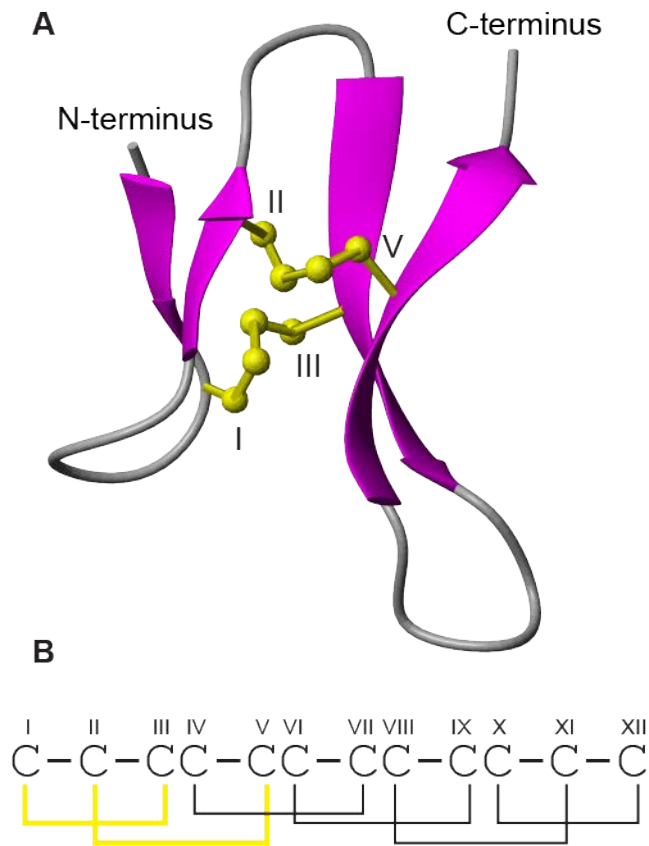


**Figure 3-1 Three-dimensional structure of a 30 residue N-terminal domain of carp granulin-1.** (A) PDB code 1QGM, the  $\beta$ -strands are shown as purple arrows and the disulfide bonds in yellow ball and stick format. The image was generated using MolMol. (B) The disulfide connectivity in the full length carp granulin-1 protein(7). Cysteines are designated with sequential roman numerals I-XII. The two bonds in the truncated carp granulin-1 are highlighted in yellow.

### 3.3 Experimental section

#### 3.3.1 Peptide synthesis and purification

Truncated granulin peptides were synthesised using manual solid-phase peptide synthesis using fluorenylmethyloxycarbonyl (Fmoc) chemistry. Peptides were assembled on 2-chlorotrityl chloride resin (Auspep, Australia). Amino acids were activated using 2-(1H-benzotriazol-1-yl)-1,1,3,3-tetramethyluronium hexafluorophosphate (HBTU-Iris Germany) in peptide grade dimethylformamide (DMF -Auspep, Australia). Peptides were cleaved using a mixture of 95% TFA/2.5% TIPS/2.5% H<sub>2</sub>O. The TFA was removed by evaporation with nitrogen and ice-cold diethyl ether was added to the residue. Ether was removed by filtration and the peptide was dissolved in 40% acetonitrile/water mixture containing 0.1% trifluoroacetic acid (TFA) and subsequently freeze-dried. The resulting crude peptides were purified with reverse phase high performance liquid chromatography (RP-HPLC) on a C<sub>18</sub> preparative column (Phenomenex Jupiter 10µm C<sub>18</sub> 300Å 250x21.2 mm). Gradients of 1%/min of 0%-80% solvent B (90% acetonitrile in 0.045% TFA in H<sub>2</sub>O) and solvent A (aqueous 0.045% TFA in H<sub>2</sub>O) were used and the eluent was monitored at 215 and 280 nm. Peptides were oxidised by stirring a solution of the peptide in 100 mM ammonium bicarbonate (pH 8.2) containing 5 mM reduced glutathione and left overnight at room temperature and purified using RP-HPLC on a C<sub>18</sub> preparative column (Phenomenex Jupiter 10µm C<sub>18</sub> 300Å 250x21.2 mm). The purity of the peptides was assessed using analytical RP-HPLC and all peptides had ≥95% purity.

To confirm the disulfide connectivity of the truncated peptides, *Ov*-GRN<sub>12-34</sub> was synthesised with selective protection of the cysteine residues. Cys1 and Cys14 were side-chain protected with ACM groups and Cys8 and Cys23 with (Trt) protecting groups. Following cleavage and purification of the crude peptide the disulfide bond between Cys8 and Cys23 was formed in 100 mM ammonium bicarbonate and the peptide was purified using the procedure described above. The S-ACM groups were subsequently removed by stirring 2 mg of peptide in 0.5 mL TFA, 10 µL anisole and 25 mg silver trifluoromethanesulfonate at 4°C for 1.5 h. Cold ether (10 mL) was added to the mixture and the precipitate collected by centrifugation. The precipitate



was washed twice with ether and oxidized, without further purification, overnight using a solution of 50% DMSO in 0.5 M HCl. The solution was diluted 15 times with water and the fully folded peptide was purified by HPLC using 1% ACN gradient on a C-18 preparative column (Phenomenex Jupiter 10 $\mu$ m C<sub>18</sub> 300Å 250x21.2 mm).

### **3.3.2 Auto-induction of recombinant protein expression in *E. coli***

*Ov-grn-1* pET41a or *Escherichia coli* thioredoxin (*trx*) cDNAs contained within the pET32a (Novagen) plasmid were transfected into BL21 *E. coli* cells (Life Technologies) and used to create recombinant proteins with auto-induction as described (5, 16). Briefly, ZYM-5052 culture media were supplemented with 100  $\mu$ M Fe(III)Cl<sub>3</sub> and 100  $\mu$ g/L kanamycin to produce recombinant protein (rOv-GRN-1) or 50  $\mu$ g/L ampicillin to produce TRX. Two hundred (200) ml of inoculated media in a one-litre baffled Erlenmeyer flask was incubated overnight at 37°C at 300 rpm rotation to induce expression with auto-induction.

### **3.3.3 Recombinant protein purification**

Purification of rOv-GRN-1 was achieved using an AKTA10 purification system at 4°C (GE Healthcare) (4). The BL21 *E. coli* pellet was lysed with 3 freeze/thaw cycles followed by sonication on ice with a Q4000 unit (Qsonix). Twenty (20) g of the resulting insoluble pellet was solubilized in 400 ml urea-containing nickel binding buffer (8 M urea/300 mM NaCl/50 mM imidazole/50 mM sodium phosphate pH 8 [Sigma]) at 4°C for 24 h with slow agitation. The 0.22  $\mu$ M filtered supernatant was passed over 2  $\times$  5 ml HisTrap IMAC nickel columns (GE Healthcare) and washed with increasing imidazole concentrations (two column volumes [CV] at 50 mM/5 CV at 100 mM) and eluted with 500 mM imidazole in binding buffer. The control TRX protein was expressed in the same fashion but under native conditions (without chaotropic agents) and purified with HisTrap IMAC Nickel columns (4).

### **3.3.4 Protein refolding and purification**

Refolding of urea-denatured rOv-GRN-1 was performed with 28 mL of G10 Sephadex (GE) resin on a XK16/20 column (GE) as described (4). A 120 ml Superdex 30 XK16/60 column (GE) was used to fractionate 3 ml of refolded rOv-

GRN-1 into 150 mM NaCl, 50 mM sodium phosphate, pH 6, at a flow rate of 1 ml/min. Fractions containing rOv-GRN-1 monomer eluting at a size equivalent of ~1 kDa (based on the fold of granulin proteins despite a denatured molecular size of 10.4 kDa) were pooled. Protein concentration was determined by a combination of microplate Bradford assay (Biorad) and absorbance at 280 nm.

### 3.3.5 NMR spectroscopy and structure determination

Purified peptides were dissolved in 90% H<sub>2</sub>O/10% D<sub>2</sub>O to provide a ~0.2 mM stock. 2D <sup>1</sup>H-<sup>1</sup>H TOCSY, <sup>1</sup>H-<sup>1</sup>H NOESY, <sup>1</sup>H-<sup>1</sup>H DQF-COSY, <sup>1</sup>H-<sup>15</sup>N HSQC, and <sup>1</sup>H-<sup>13</sup>C HSQC spectra were acquired at 290 K using a 600 MHz AVANCE III NMR spectrometer (Bruker, Karlsruhe, Germany) equipped with a cryogenically cooled probe. Spectra were recorded with an interscan delay of 1 s. NOESY spectra were acquired with a mixing time of 200 ms, and TOCSY spectra were acquired with an isotropic mixing period of 80 ms. All spectra were assigned using CCPNMR (17) based on the approach described by Wüthrich (18) The αH secondary shifts were determined by subtracting the random coil <sup>1</sup>H NMR chemical shifts of Wishart from experimental αH chemical shifts (19).

The three-dimensional structures of Ov-GRN<sub>12-34</sub> and Ov-GRN<sub>12-35\_3s</sub> were determined. The 2D NOESY spectra were automatically assigned and an ensemble of structures calculated using the program CYANA (20). Torsion-angle restraints predicted using TALOS+ were used in the structure calculations. Disulfide-bond connectivities (Cys1-Cys14, Cys8-Cys23) were included in the calculations for Ov-GRN<sub>12-34</sub> because these bonds were confirmed by selective protection of the cysteine residues. Selective protection of the cysteine residues was not used for Ov-GRN<sub>12-35\_3s</sub> in an attempt to isolate the most energetically favourable form. Consequently, the structures were calculated with the 15 possible disulfide connectivities. An analysis of the CYANA target functions was carried out to determine the most likely connectivity. Structures were visualised using MOLMOL (21).

### 3.3.6 Mammalian cell culture

The non-malignant cholangiocyte cell line H69 is a SV40-transformed human bile duct epithelial cell line derived from human liver, kindly provided by Dr. Gregory J.

Gores, Mayo Clinic, Rochester, Minnesota. H69 cells (4, 22, 23) were maintained in T75 cm<sup>2</sup> vented flasks (Corning) as monolayers as described (24) with minor modifications. Cells were maintained with regular splitting using 0.25% trypsin (Life Technologies) every 2–5 days in complete media [RPMI (Sigma) with growth factor-supplemented specialist complete media (23) [DMEM/F12 with high glucose, 10% FCS, 1×antibiotic/antimycotic, 25 µg/ml adenine, 5 µg/ml insulin, 1 µg/ml epinephrine, 8.3 µg/ml holo-transferrin, 0.62 µg/ml, hydrocortisone, 13.6 ng/ml T3 and 10 ng/ml EGF – Life Technologies]. Low nutrient media for cell proliferation assays was 5% complete media, i.e. 0.5% FCS and 1/20<sup>th</sup> of the growth factor concentrations listed above for complete media. The identities (human-derived) of the cell line were confirmed with single tandem repeat (STR) analysis in January 2015 (15/15 positive loci across 2 alleles) and mycoplasma free at the DNA Diagnostics Centre (DDC)–medical (U.S.A.), accredited/certified by CAP, ISO/IEC 17025:2005 through ACLASS.

### **3.3.7 Cell proliferation monitoring in real time using xCELLigence**

Cells were seeded at 1,500 cells/well in 180 µl complete media (above) in E-plates (ACEA Biosciences) and grown overnight while monitored with an xCELLigence SP system (ACEA Biosciences) which monitors cellular events in real time by measuring electrical impedance across interdigitated gold micro-electrodes integrated into the base of tissue culture plates (25). Cells were washed three times with PBS prior to addition of 180 µl of low nutrient media (above) and incubated for a minimum of 6 h before further treatment. Treatments were prepared at 10× concentration and added to each well in a total volume of 20 µl. The xCELLigence system recorded cell indexes at intervals of one hour for 5-6 days following treatment. Readings for the cell index were normalized prior to treatment and cell proliferation ratios represent the relative numbers of cells compared to control cells at day 4. Dose response curves for each peptide were generated from 3-6 independent experiments each with 4-6 replicates. Comparisons of induction of cell proliferation in response to treatments were accomplished using two-way ANOVA test with Dunnett's multiple comparison correction, using GraphPad Prism 6.02.

### 3.3.8 Mouse wounding assay

These studies were conducted with the approval of the James Cook University Small Animal Ethics Committee, applications A1806 and A2204, as described (6). Briefly, female 11-12 week old BALB/c mice weighing 19-23 g were sourced from the Australian ARC (Animal Resources Centre) and randomly allocated into groups of 4-5 mice. Mice were anesthetized (intraperitoneal xylazine 16 mg/kg; ketamine 80 mg/kg), after which a skin-deep wound on the crown of the head was inflicted using a 5 mm biopsy punch (Zivic instruments). Betadine liquid antiseptic (Sanofi) was applied followed by application of 50  $\mu$ l that contained either 71 pmoles of Regranex (treatment of 71 pmoles equals 1  $\mu$ g per 0.25 cm<sup>2</sup> wound, as recommended by manufacturer Smith and Nephew), 56 pmoles of rOv-GRN-1, Ov-GRN-1 peptides, control peptide (EADRKYDEVARKLAMVEADL), TRX or PBS suspended in 1.5% methylcellulose (Sigma). Wounds were photographed daily and after blinding treatment groups the area of the lesion was measured with ImageJ software and plotted as percent of wound closure from original wound images. Wound healing rates were compared with two-way ANOVA test with Dunnett's correction for multiple comparisons, using GraphPad prism 6.02. Each mouse wounding study was conducted at least twice to provide reproducibility.

## 3.4 Results

### 3.4.1 Design and synthesis of truncated *Ov*-GRN-1 peptides

To determine if the N-terminal region of *Ov*-GRN-1 can fold independently several truncated peptides were designed and synthesized using Fmoc chemistry. The sequences of the synthetic peptides are shown in Figure 3-2A.

*Ov*-GRN<sub>1-35</sub>, *Ov*-GRN<sub>8-38</sub> and *Ov*-GRN<sub>12-34</sub> all contain four cysteine residues equivalent to Cys I, Cys II, Cys III and Cys V in the full-length protein (for the remainder of the report, Roman numerals refer to the numbering present in the full length protein). Cys IV and Cys VI were predicted to form disulfide bonds with Cys VII and Cys IX respectively, based on the three-dimensional structure of carp granulin-1(7). In the truncated analogues Cys IV and Cys VI were replaced with alanine residues to prevent disulfide bond formation between these residues. Selective protection of the cysteine residues was used to direct the folding to form the predicted disulfide connectivity (i.e. Cys I-Cys III and Cys II-Cys V).

*Ov*-GRN-1 contains an extended N-terminal tail (11 residues prior to the first cysteine residue) not present in the majority of granulins, and these residues were included in *Ov*-GRN<sub>1-35</sub> to determine if they play a role in the bioactivity. The N-terminus was truncated and the C-terminus extended in *Ov*-GRN<sub>8-38</sub> to provide an analogue with a similar number of residues to the carp granulin-1 truncated peptide. *Ov*-GRN<sub>12-34</sub> is the minimal sequence that contains the four cysteine residues (Cys I, Cys II, Cys III and Cys V) and was designed to determine if the N- and C-terminal regions are required for folding and activity.

An additional peptide was synthesised (*Ov*-GRN<sub>12-35\_3s</sub>) with a truncated N-terminus but containing the first six cysteines of *Ov*-GRN-1 (the “3s” refers to the presence of three-disulfide bonds in the peptide). This peptide is analogous to mammalian paraganulin (above) in terms of the cysteine residues. It was synthesized without selective protection of the cysteine residues and the major conformation was purified for analysis of its structure and activity.

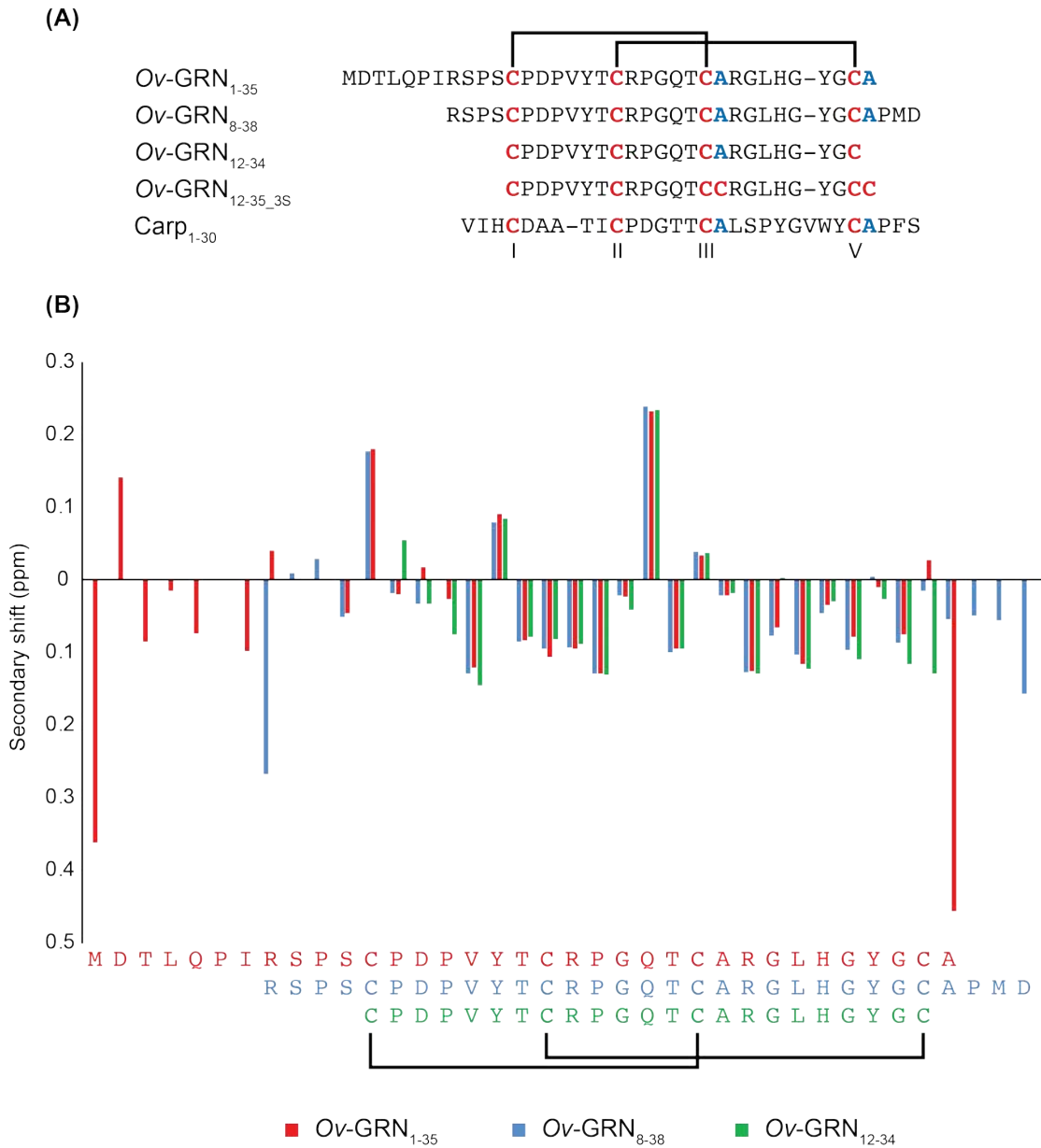


**Figure 3-2 Sequences and secondary shifts of the *Ov*-GRN-1 truncated analogues.** (A) Sequences show Cys IV and Cys VI were replaced with alanine residues; the cysteines are highlighted in red and the substitutions are shown in blue. The N-terminal 30 residues of carp granulin-1 is also provided, with Cys IV and VI replaced with alanine residues. (B) Secondary shifts of *Ov*-GRN-1 peptides with four cysteine residues (*Ov*-GRN<sub>1-35</sub>, *Ov*-GRN<sub>8-38</sub> and *Ov*-GRN<sub>12-34</sub>). The secondary shifts were derived by subtracting random coil shifts (19) from the  $\alpha$ H shifts. The similarity in the secondary shifts for the conserved residues indicates that the overall fold is the same in the three peptides. Color scheme is retained in Figures (3-2)-(3-5). Both panels: black connecting lines represent disulfide bond connectivity.

### 3.4.2 Structural analysis with NMR spectroscopy

NMR spectroscopy was employed to analyse the structure of the peptides. The one-dimensional spectra of *Ov*-GRN<sub>1-35</sub>, *Ov*-GRN<sub>8-38</sub> and *Ov*-GRN<sub>12-34</sub> have limited dispersion in the amide regions consistent with a lack of  $\beta$ -sheet structures despite formation of the two native disulfide bonds. Two-dimensional spectra (TOCSY and NOESY) were used to assign the resonances, and the secondary shifts were determined by subtracting random coil shifts (19) from the  $\alpha$ H shifts. The secondary shifts are similar over the equivalent residues for these three peptides, as shown in Figure 3-2B, indicating that the structures were similar and consequently, that the differences in the N- and C-termini of these peptides did not influence the overall fold. Furthermore, the secondary shifts were consistent with a lack of  $\beta$ -sheet structure as they are primarily negative and  $\beta$ -sheet structures are characterised by positive secondary shifts. The three-dimensional structure of *Ov*-GRN<sub>12-34</sub> was determined using NMR spectroscopy, as shown in Figure 3-3. In contrast to the characteristic granulin fold, the structure comprised turns and a region of  $3_{10}$  helix. The structure statistics are provided in Table 3-1.

In contrast to the two-disulfide bond-containing *Ov*-GRN-1 peptides, *Ov*-GRN<sub>12-35\_3s</sub>, with three-disulfide bonds has more dispersion in the amide region in the one-dimensional NMR spectrum. Furthermore, additional peaks were present in the spectra, likely due to isomerisation of the proline residues. Despite these additional peaks, the major conformation was fully assigned, and the secondary shifts were similar to the truncated carp granulin-1(14) (Figure 3-3B), which indicates the similarity of the overall structures. Truncated carp granulin-1, comprising residues 1-30, has previously been synthesised with Cys IV and Cys VI replaced with serine residues, and was shown to form a  $\beta$ -sheet structure(14). Here we synthesised carp granulin<sub>1-30</sub> with Cys IV and Cys VI replaced with alanine residues to be consistent with the truncated peptides of *Ov*-GRN-1. Only minor variations were evident between the published (14) chemical shifts of carp granulin-1 with the serine substitutions and the peptide with the alanine substitutions (Figure 3-4), indicating that the overall fold is still maintained.

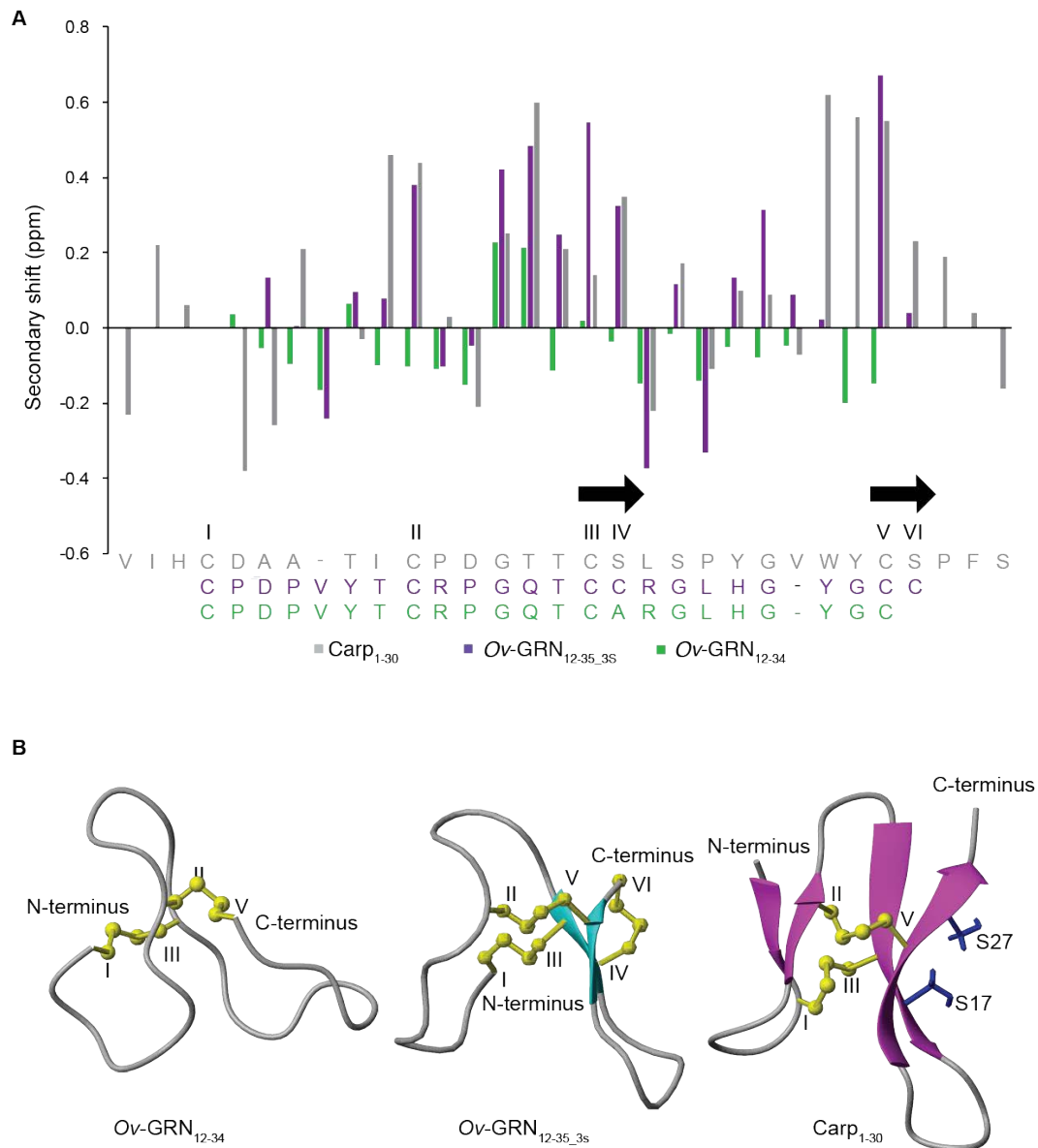


**Figure 3-3 Structural analysis of *Ov-GRN*<sub>12-34</sub> and *Ov-GRN*<sub>12-35\_3s</sub>.** (A) Secondary shifts of *Ov-GRN*<sub>12-34</sub> and *Ov-GRN*<sub>12-35\_3s</sub> compared to carp granulin<sub>1-30</sub>. The secondary shifts were derived by subtracting random coil shifts (19) from the  $\alpha$ H shifts. *Ov-GRN*<sub>12-34</sub> has significantly different secondary shifts compared to *Ov-GRN*<sub>12-35\_3s</sub> and carp<sub>1-30</sub>, and lacks positive shifts indicating a lack of  $\beta$ -sheet structure. Despite the differences in sequence the trends for the secondary shifts between *Ov-GRN*<sub>12-35\_3s</sub> and carp<sub>1-30</sub> are similar indicating that the  $\beta$ -sheet present in carp granulin-1 is also present in *Ov-GRN*<sub>12-35\_3s</sub> (black arrows). (B) The structures of *Ov-GRN*<sub>12-34</sub> and *Ov-GRN*<sub>12-35\_3s</sub> were determined using NMR spectroscopy and confirms that *Ov-GRN*<sub>12-34</sub> does not contain  $\beta$ -sheet structure but *Ov-GRN*<sub>12-35\_3s</sub> does (blue arrows). Disulfide bonds are shown as yellow ball and stick representations and the structure of carp<sub>1-30</sub> are shown for comparison. The side-chains of residues Ser17 and Ser27 are highlighted on the carp<sub>1-30</sub> structure, to indicate the Cys-Ser substituted sites of Cys IV and Cys VI. Based on this structure it appears likely that Cys IV and Cys VI of carp<sub>1-30</sub> could form a disulfide bond, consistent with the likely connectivity in *Ov-GRN*<sub>12-35\_3s</sub>.



**Table 3-1 Structural statistics for the *Ov*-GRN-1 peptides ensemble**

	<i>Ov</i> -GRN <sub>12-34</sub>	<i>Ov</i> -GRN <sub>12-35_3s</sub>
<b>Experimental restraints</b>		
Interproton distance restraints	252	113
<i>Intraresidue</i>	78	46
<i>Sequential</i>	139	52
<i>Medium range (i-j &lt; 5)</i>	21	4
<i>Long range (i-j ≥ 5)</i>	14	44
Disulfide-bond restraints	6	9
Dihedral-angle restraints	14	10
<b>R.m.s. deviations from mean coordinate structure (Å)</b>		
Backbone atoms	0.32 ± 0.15	0.65 ± 0.2*
All heavy atoms	0.93 ± 0.27	1.65 ± 0.33*
<b>Ramachandran Statistics</b>		
% in most favoured region	71.4	78.2
% in additionally allowed region	28.6	21.8

- RMSD for residues 12-24.

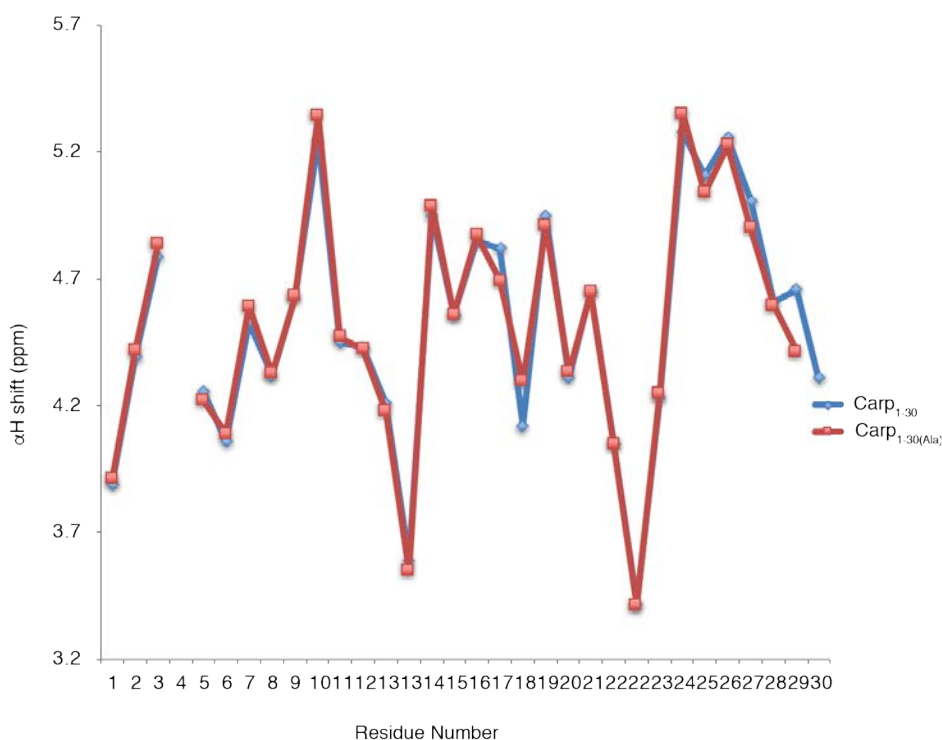


**Figure 3-4 Chemical shift comparison between the published shifts of a truncated form of carp granulin (14) and the mutant with C17A and C27A mutations.**

To confirm if the structure of *Ov*-GRN<sub>12-35\_3s</sub> was similar to carp granulin<sub>1-30</sub>, three-dimensional structures were calculated using CYANA. Structures were initially calculated without disulfide bond restraints. In these structures a  $\beta$ -hairpin was present from residues 14-23, but residues 1-8 were not defined. The lack of definition for residues 1-8 prevented an analysis of the sulfur-sulfur distances providing insight

into the most likely connectivity. Therefore, an alternative approach was used whereby the structures were calculated with the 15 possible disulfide bond connectivities. This approach has previously been used for disulfide-rich peptides such as the cyclotides to analyse the disulfide bond connectivities (26, 27). The CYANA target functions for the 15 connectivities for *Ov*-GRN<sub>12-35\_3s</sub> are shown in Table 3-2. The connectivity with the lowest CYANA target function was Cys I-Cys III, Cys II-Cys V and Cys IV-Cys VI. The three-dimensional structure of *Ov*-GRN<sub>12-35\_3s</sub> with this connectivity is shown in Figure 3-3A and the structure statistics provided in Table 3-2. The most well defined region of the molecule was the  $\beta$ -hairpin between residues 14-23. The N-terminal region, encompassing Cys I and Cys II displayed marked structural disorder.

**Table 3-2 CYANA target functions for the 15 possible disulfide bond connectivities present in *Ov*-GRN<sub>12-35\_3s</sub>.**

Set Number	Disulfide bonds connectivity	Average Target Function $\pm$ SD
1	1-14, 8-23,15-24	*0.016 $\pm$ 0.003
2	1-14, 8-24, 15-23	3.08 $\pm$ 0.18
3	1-14, 8-15, 23-24	3.59 $\pm$ 0.15
4	1-8, 14-23, 15-24	3.72 $\pm$ 0.02
5	1-8, 14-15, 23-24	5.71 $\pm$ 0.32
6	1-8, 14-24, 15-23	5.21 $\pm$ 0.25
7	1-15, 8-14, 23-24	3.31 $\pm$ 0.04
8	1-15, 8-23, 14-24	1.58 $\pm$ 0.37
9	1-15, 8-24, 14-23	1.28 $\pm$ 0.2
10	1-23, 8-14, 15-24	*0.018 $\pm$ 0.01
11	1-23, 8-15, 14-24	0.32 $\pm$ 0.05
12	1-23, 8-24, 14-15	2.53 $\pm$ 0.23
13	1-24, 8-14, 15-23	2.61 $\pm$ 0.11
14	1-24, 8-15, 14-23	1.18 $\pm$ 0.12
15	1-24, 8-23, 14-15	2.49 $\pm$ 0.29

\*The two connectivities with the lowest target functions are highlighted with an asterisk. The connectivity corresponding to Set Number 1 has the lowest target function indicating that the distance and angle restraints satisfy this connectivity better than the other connectivities, and it is therefore the most likely connectivity present in *Ov*-GRN<sub>12-35\_3s</sub>.

### 3.4.3 Cell proliferation

The influence of the *Ov*-GRN-1 peptides on proliferation of H69 cholangiocytes in real time was assessed using xCELLigence technology and dose response curves were determined for the peptides. *Ov*-GRN<sub>12-35\_3s</sub> at a final concentration of 2  $\mu$ M resulted in a 41% increase in cell growth compared to control peptide ( $P < 0.0001$ ) (Figure 3-5A). A dose response curve similar to that obtained for *Ov*-GRN-1 was observed with *Ov*-GRN<sub>12-35\_3s</sub> treatment, characterized by significantly increased cell proliferation at final concentrations of  $\geq 15$  nM ( $P < 0.05$ ). The two-disulfide bonded *Ov*-GRN-1 peptides were less potent at nanomolar concentrations, but at 2  $\mu$ M promoted significant cell proliferation (14-25% above peptide control;  $P < 0.01$ ) with dose response curves typified by *Ov*-GRN<sub>12-34</sub> (Figure 3-5A). No cell cytotoxicity was observed for any of the peptides tested at concentrations up to 2  $\mu$ M.

The cell proliferation observed for the *Ov*-GRN peptides is in contrast to carp granulins<sub>1-30</sub> that induced minimal cell proliferation (non-significant) at all concentrations tested, and maximum proliferation of 9% over peptide controls at 32 nM. The response at 400 nM of all the *Ov*-GRN peptides (Figure 3-5B) highlights the enhanced potency of the three-disulfide bonded peptide (*Ov*-GRN<sub>12-35\_3s</sub>) compared to the two-disulfide bonded peptides. *Ov*-GRN<sub>12-35\_3s</sub> promoted a highly significant ( $P < 0.0001$ ) increase in cell proliferation (26% over peptide controls) compared to the remaining peptides that induced minimal proliferation, of which the most potent was *Ov*-GRN<sub>1-35</sub> (9% non-significant increase over peptide control).

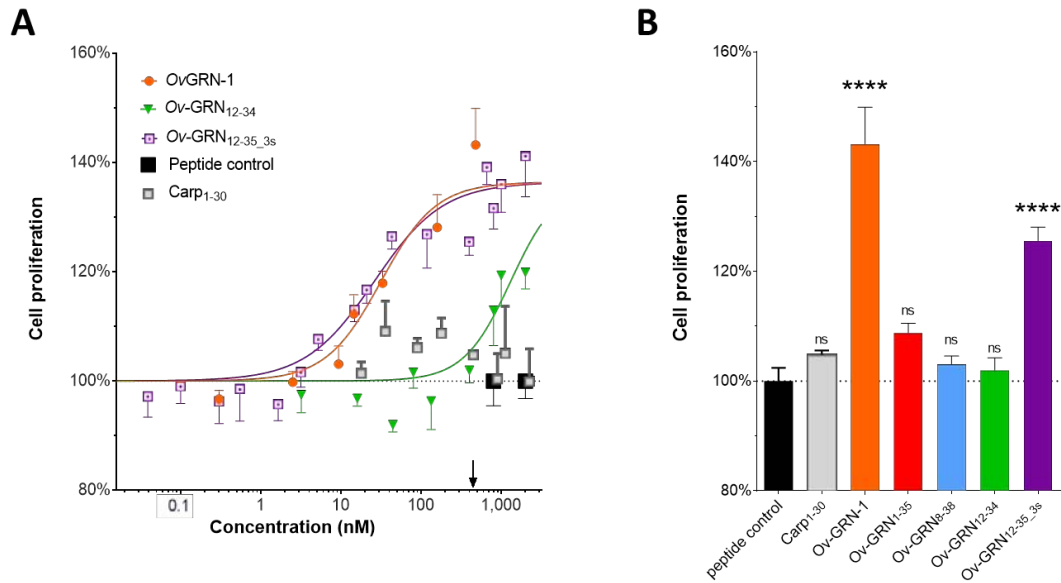


**Figure 3-5 Liver fluke granulin peptides induce cell proliferation.** (A) *Opisthorchis viverrini* granulin peptides but not carp granulin<sub>1-30</sub> induced proliferation of H69 human cholangiocytes at a range of concentrations as monitored using xCELLigence. Only selected treatments are graphed to aid visualization. Variable slope dose response lines of best fit show proliferation four days after a single application of treatment. *Ov-GRN*<sub>12-35\_3s</sub> potency characterized by significantly increased cell proliferation observed at final concentrations of  $\geq 15$  nM ( $P < 0.05$ ). Black arrow denotes 400-483 nM concentration used in panel B. (B) Mean proliferation at 400 nM of all *Ov-GRN*-1 synthesized peptides and 483 nM *Ov-GRN*-1 protein from panel A. ns = not significant, \*\*\*\*  $P < 0.0001$ . Both Panels: 2-way ANOVA test with Dunnett's correction for multiple comparisons was used to compare treatments with relevant treatment controls (*Ov-GRN*-1 protein relative to thioredoxin expression matched recombinant protein control and peptides relative to peptide control (20-residue peptide derived from tropomyosin). Mean values from 4-6 replicates pooled from 2-4 experiments with SEM bars shown either above or below for clarity.

### 3.4.4 Mouse wound healing model

The truncated *Ov*-GRN-1 peptides formulated with methylcellulose were tested in a mouse model of wound healing. All *Ov*-GRN-1 peptides exhibited potent activity (Figure 3-5A, B) when applied topically compared to control peptide in methylcellulose. The *Ov*-GRN-1 peptides, *Ov*-GRN-1 protein and Regranex significantly improved healing compared to peptide control on days 2-4 ( $P < 0.05$ ). As wounds closed, differences among treatments waned and significant differences were unapparent beyond day 4. Regranex and the various granulin peptides showed near identical best-fit curves and intact *Ov*-GRN-1 was the only compound tested here that provided significant improvement over Regranex on days 3 and 4 ( $P < 0.05$ ; Figure 3-6B).

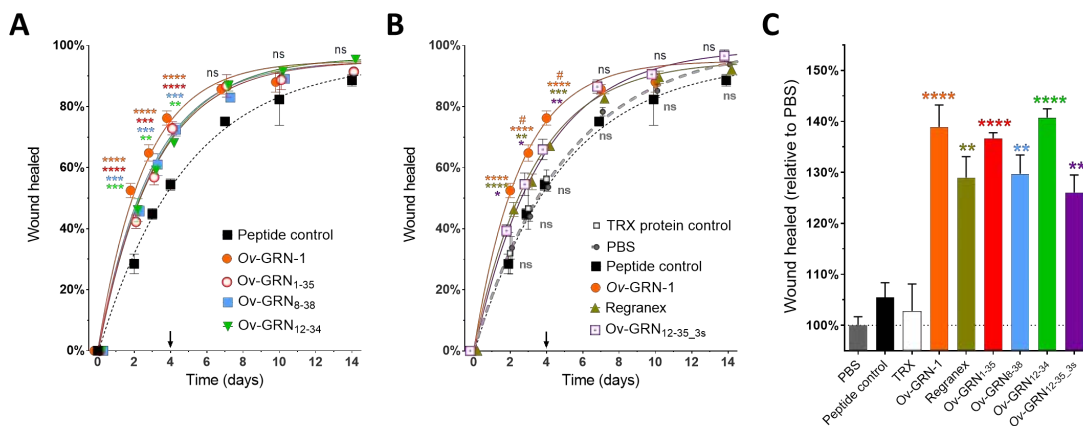


**Figure 3-6 Mouse wound healing activity of *Ov*-GRN-1 and peptides.** (A+B) Wound healing outcomes from treatments with 56 pmoles of recombinant *Ov*-GRN-1, *Ov*-GRN-1 peptides, unrelated peptide, thioredoxin (TRX) protein controls and 71 pmoles Regranex in 1.5% methylcellulose gel applied daily in 50  $\mu$ l volume from days 0-4 to a  $\sim 0.2$   $\text{cm}^2$  wound arising from biopsy punch to the scalp between the ears. To aid visualisation, data were split across two graphs with the *Ov*-GRN-1 and peptide control groups shown in both panels. No significant differences between the unrelated peptide control, PBS, or TRX protein control were noted at any time point. Black arrows denote the day 4 time point used in panel C. (C) Wound healing relative to PBS vehicle control from day 4. All panels: mean healing rates of 2-6 biological replicates of groups of 4-5 animals plotted with SEM bars. Groups have been marginally shifted left or right to aid viewing. Repeated measure 2-way ANOVA test with Dunnett's correction for multiple comparisons compare each group against each other group. Significance against peptide/protein control signified by \*\*\*\* =  $P < 0.0001$ , \*\*\* =  $P < 0.001$ , \*\* =  $P < 0.01$ , \* =  $P < 0.05$ , ns=not significant. Significant treatments against Regranex signified by # =  $P < 0.05$ . Color of asterisk or hash represents the relevant group. The colors and symbols are maintained across Figures (3-2)-(3-5).

Significant differences were not observed between the various negative control groups formulated with methylcellulose, including PBS vehicle control, peptide control, and thioredoxin (TRX) recombinant protein control.

When healing at day 4 (Figure 3-6C, Figure 3-7) was evaluated relative to PBS vehicle from each biological replicate, treatment of wounds with *Ov*-GRN-1 protein and peptides significantly accelerated wound healing compared to controls ( $P < 0.01$  at day 4: 26-41% over PBS). Although the *Ov*-GRN-1 protein, *Ov*-GRN<sub>1-35</sub> and *Ov*-GRN<sub>12-34</sub> (37-41% over PBS) provided improved healing compared to Regranex (29% over PBS), none of these comparisons reached significance at the day 4 time point.

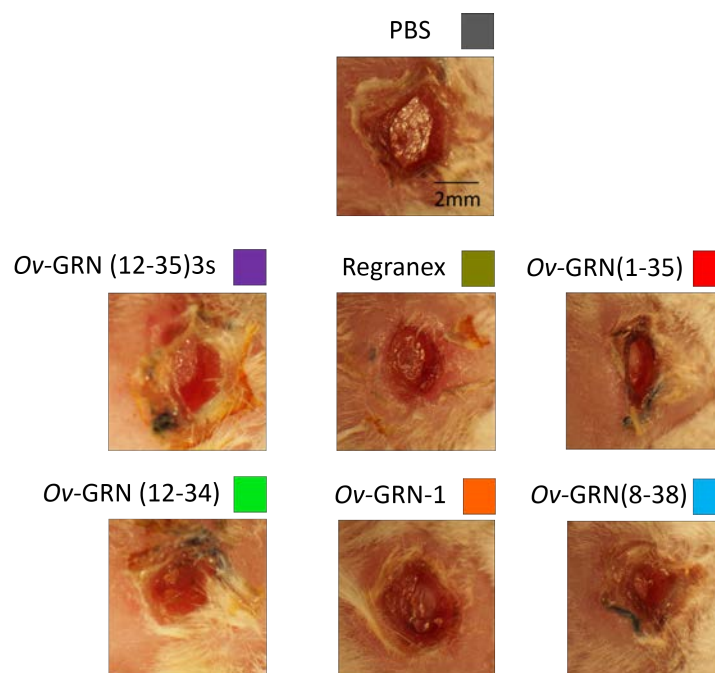


**Figure 3-7 Mouse wound healing day 4 images.** Representative images from mouse wound healing study presented in Figure 3-6. Wound healing outcomes from treatments with 56 pmoles of recombinant *Ov*-GRN-1, *Ov*-GRN-1 peptides, unrelated peptide, thioredoxin (TRX) protein controls and 71 pmoles Regranex in 1.5% methylcellulose gel applied daily in 50  $\mu$ l volume from days 0-4 to a  $\sim 0.2$  cm<sup>2</sup> wound arising from biopsy punch to the scalp between the ears. The treatment colors are maintained across Figures (3-2)-(3-5).

### 3.5 Discussion

Elucidating the structure-activity relationships of granulins has been challenging given the sequence and structural variations in this protein family. Regions with bioactivity are poorly understood, and uncertainty remains about potential receptors for this growth factor (28, 29).

*Ov*-GRN-1 appears to have distinct folding pathways compared to other granulins. The N-terminal region of *Ov*-GRN-1, comprising two native disulfide bonds (Cys I-Cys III and Cys II-V), does not fold independently into a native-like  $\beta$ -hairpin structure, in contrast to carp granulin-1 and human granulin A. It is noteworthy that the introduction of a third, non-native disulfide bond in *Ov*-GRN<sub>12-35\_3s</sub> results in a  $\beta$ -hairpin structure similar to that present in the carp granulin-1 and human granulin A peptides (14, 15). The disulfide bond connectivity of *Ov*-GRN<sub>12-35\_3s</sub> appears to comprise the two native disulfide bonds (Cys I-Cys III and Cys II-V) in addition to the Cys IV-Cys VI disulfide bond. If the bond pairs are conserved across species (7, 9), the latter bond is predicted not to be present in the full length *Ov*-GRN-1, as Cys IV is predicted to bond to Cys VII and Cys VI to Cys IX.

The paraganulin (half-granulin) domain of mammal progranulin contains the equivalent six cysteine residues present in *Ov*-GRN<sub>12-35\_3s</sub> and is biologically active (30), which suggests that *Ov*-GRN<sub>12-35\_3s</sub> potentially contains the same disulfide connectivity. Carp granulin<sub>1-30</sub> peptide might accommodate this Cys I-Cys III, Cys II-Cys V, Cys IV-Cys VI connectivity (14). Although carp granulin<sub>1-30</sub> peptide contains only the two native disulfide bonds (Cys I-Cys III and Cys II-Cys V), analysis of the structure indicates that the side-chains of the serine residues, which replace Cys IV and Cys VI, are in close proximity, and suggest that it is feasible for these cysteine residues to form a disulfide bond.

The disulfide connectivity in *Ov*-GRN<sub>12-35\_3s</sub> has implications for the structure of full-length *Ov*-GRN-1, which has not been experimentally determined because sufficient quantities of correctly folded recombinant material remain unavailable. Therefore, the disulfide connectivity of the native protein has not been shown to conform to the connectivity originally shown for carp granulin-1 (7). It is conceivable that the protein



contains a disulfide domain comprising the first six cysteine residues (equivalent to that seen in *Ov*-GRN<sub>12-35\_3s</sub>), and a second domain containing the last six cysteine residues. Without the structure of the full-length protein and a comparison to the native protein secreted by the parasite, this remains speculation. However, previous reports revealed ambiguity in the disulfide connectivity of granulins (15). The structures of human granulin A and F have well-defined N-terminal regions, but disordered C-terminal regions prevented characterisation of all the disulfide bonds. Furthermore, chemical analysis of the disulfide connectivity of human granulin A was inconclusive (15).

In addition to providing insight into the folding of *Ov*-GRN-1, the current study revealed that the N-terminal region contributes to the bioactivity and the  $\beta$ -hairpin of *Ov*-GRN<sub>12-35\_3s</sub> further enhanced cell proliferation activity. However, the  $\beta$ -hairpin structure is far from the complete story in regard to proliferative activity, as the carp granulin<sub>1-30</sub> peptide contains dual  $\beta$ -hairpins and in contrast to the *Ov*-GRN-1 peptides, showed no substantial proliferation at the eight concentrations tested (10 nM - 2  $\mu$ M). A comparison of the sequences of carp granulin-1 with *Ov*-GRN-1 reveals that there are only two conserved non-cysteine residues between Cys I and Cys VI. This lack of conservation in the loop sequences likely accounts for the differences in both folding and bioactivity.

Despite the lack of native structure, the two-disulfide bond containing *Ov*-GRN-1 peptides promoted cell proliferation at high concentrations (>800 nM) and stimulated significant healing of cutaneous wounds in mice. *Ov*-GRN<sub>12-35\_3s</sub> was the most potent peptide in the cell proliferation assay, but was no more active *in vivo* than the other *Ov*-GRN-1 peptides. If the  $\beta$ -hairpin of *Ov*-GRN<sub>12-35\_3s</sub> is involved in wound healing *in vivo* we did not observe a difference in mice. Cell proliferation activity may be cell line-specific, or alternatively the concentrations tested in mouse wound repair were not optimal. In either case, the activity observed in mice may be of greater biological and therapeutic consequence than findings from the *in vitro* analysis. In the future, we envision exploring a range of cells from diverse organs and tissues and investigation of mice that exhibit deficits in wound healing in order to increase our understanding of the role of *Ov*-GRN-1 structure-activity relationships.

To conclude, structural analysis with NMR spectroscopy suggested that *Ov*-GRN-1 exhibits unique folding properties compared with other granulins, presumably resulting from primary sequence. We have identified a bioactive region of *Ov*-GRN-1, which is likely to be less immunogenic and more readily produced than the full-length recombinant protein. Peptides and derivatives of liver fluke granulin that maintain the bioactivity represent a key advance towards identification of a novel therapies for treatment of wounds.

### 3.6 Acknowledgements

**Funding:** This research was supported by an R01 grant from the National Cancer Institute, U.S.A (R01CA164719) and a program grant from National Health and Medical Research Council, Australia (NHMRC) (1037304). Fellowship support was provided to AL from NHMRC (1020114) and NLD from the Australian Research Council (FF110100226). The content is solely the responsibility of the authors and does not necessarily represent the official views of the NCI or NIH. The funders had no role in study design, data collection and analysis, decision to publish, or preparation of the manuscript.

The PDB ID codes are 5UJH and 5UJG for *Ov*-GRN<sub>12-34</sub> and *Ov*-GRN<sub>12-35\_3s</sub> respectively. Authors will release the atomics coordinates and experimental data upon article publication.

### 3.7 Supporting information

Structure statistics for *Ov*-GRN<sub>12-34</sub> and *Ov*-GRN<sub>12-35\_3s</sub>. Chemical shift analysis of carp granulin-1. Analysis of different disulfide connectivities for *Ov*-GRN<sub>12-35\_3s</sub>. Wound healing photos.

### 3.8 Non-standard abbreviations

FMOC, Fluorenylmethyloxycarbonyl; *Ov*-GRN, *Opisthorchis viverrini* granulin; PBS, phosphate buffered saline; PGRN, progranulin, TRX, thioredoxin.

### 3.9 References

1. He, Z., C.H. Ong, J. Halper, and A. Bateman. Progranulin is a mediator of the wound response. *Nat. Med.* 2003; 9(2): 225-9.
2. Mulvenna, J., et al. The secreted and surface proteomes of the adult stage of the carcinogenic human liver fluke *Opisthorchis viverrini*. *Proteomics*. 2010; 10(5): 1063-78.
3. Laha, T., et al. Gene discovery for the carcinogenic human liver fluke, *Opisthorchis viverrini*. *BMC Genomics*. 2007; 8, DOI: 10.1186/1471-2164-8-189.
4. Smout, M.J., J.P. Mulvenna, M.K. Jones, and A. Loukas. Expression, refolding and purification of *Ov*-GRN-1, a granulin-like growth factor from the carcinogenic liver fluke, that causes proliferation of mammalian host cells. *Protein Expr. Purif.* 2011; 79(2): 263-70.
5. Smout, M.J., et al. A granulin-like growth factor secreted by the carcinogenic liver fluke, *Opisthorchis viverrini*, promotes proliferation of host cells. *PLoS Pathog.* 2009; 5, DOI: 10.1371/journal.ppat.1000611.
6. Smout, M.J., et al. Carcinogenic parasite secretes growth factor that accelerates wound healing and potentially promotes neoplasia. *PLoS Pathog.* 2015; 11, DOI: 10.1371/journal.ppat.1005209.
7. Hrabal, R., Z. Chen, S. James, H.P. Bennett, and F. Ni. The hairpin stack fold, a novel protein architecture for a new family of protein growth factors. *Nat. Struct. Biol.* 1996; 3(9): 747-52.
8. Ong, C.H. and A. Bateman. Progranulin (granulin-epithelin precursor, PC-cell derived growth factor, acrogranin) in proliferation and tumorigenesis. *Histol. Histopathol.* 2003; 18(4): 1275-88.
9. Tolkathev, D., et al. Structure dissection of human progranulin identifies well-folded granulin/epithelin modules with unique functional activities. *Protein Sci.* 2008; 17(4): 711-24.
10. Alquezar, C., A. de la Encarnacion, F. Moreno, A. Lopez de Munain, and A. Martin-Requero. Progranulin deficiency induces overactivation of WNT5A expression via TNF-alpha/NF-kappaB pathway in peripheral cells from frontotemporal dementia-linked granulin mutation carriers. *J. Psychiatry Neurosci.* 2016; 41(4): 225-39.
11. Park, B., et al. Granulin is a soluble cofactor for toll-like receptor 9 signaling. *Immunity*. 2011; 34(4): 505-13.
12. Yeh, J.E., et al. Granulin, a novel STAT3-interacting protein, enhances STAT3 transcriptional function and correlates with poorer prognosis in breast cancer. *Genes Cancer*. 2015; 6(3-4): 153-68.

13. Yip, C.W., P.F. Cheung, I.C. Leung, N.C. Wong, C.K. Cheng, S.T. Fan, and S.T. Cheung. Granulin-epithelin precursor interacts with heparan sulfate on liver cancer cells. *Carcinogenesis*. 2014; 35(11): 2485-94.
14. Vranken, W.F., Z.G. Chen, P. Xu, S. James, H.P. Bennett, and F. Ni. A 30-residue fragment of the carp granulin-1 protein folds into a stack of two beta-hairpins similar to that found in the native protein. *J. Pept. Res.* 1999; 53(5): 590-7.
15. Tolkmachev, D., A. Ng, W. Vranken, and F. Ni. Design and solution structure of a well-folded stack of two beta-hairpins based on the amino-terminal fragment of human granulin A. *Biochemistry*. 2000; 39(11): 2878-86.
16. Studier, F.W. Protein production by auto-induction in high density shaking cultures. *Protein Expr. Purif.* 2005; 41(1): 207-34.
17. Vranken, W.F., et al. The CCPN data model for NMR spectroscopy: development of a software pipeline. *Proteins*. 2005; 59(4): 687-96.
18. Wüthrich, K. *NMR of proteins and nucleic acids*. New York: Wiley-Interscience; 1986. 320p.
19. Wishart, D.S., C.G. Bigam, A. Holm, R.S. Hodges, and B.D. Sykes. <sup>1</sup>H, <sup>13</sup>C and <sup>15</sup>N random coil NMR chemical shifts of the common amino acids. I. Investigations of nearest-neighbor effects. *J. Biomol. NMR*. 1995; 5(1): 67-81.
20. Güntert, P. Automated NMR structure calculation with CYANA. *Methods Mol. Biol.* 2004; 278: 353-78.
21. Koradi, R., M. Billeter, and K. Wüthrich. MOLMOL: a program for display and analysis of macromolecular structures. *J. Mol. Graph.* 1996; 14(1): 51-5.
22. Grubman, S.A., et al. Regulation of intracellular pH by immortalized human intrahepatic biliary epithelial cell lines. *Am. J. Physiol.* 1994; 266(6 Pt 1): 1060-70.
23. Matsumura, T., et al. Establishment of an immortalized human-liver endothelial cell line with SV40T and hTERT. *Transplantation*. 2004; 77(9): 1357-65.
24. Papatpremsiri, A., M.J. Smout, A. Loukas, P.J. Brindley, B. Sripa, and T. Laha. Suppression of *Ov*-GRN-1 encoding granulin of *Opisthorchis viverrini* inhibits proliferation of biliary epithelial cells. *Exp. Parasitol.* 2015; 148, DOI: 10.1016/j.exppara.2014.11.004.
25. Xing, J.Z., L. Zhu, J.A. Jackson, S. Gabos, X.J. Sun, X.B. Wang, and X. Xu. Dynamic monitoring of cytotoxicity on microelectronic sensors. *Chem. Res. Toxicol.* 2005; 18(2): 154-61.
26. Saether, O., D.J. Craik, I.D. Campbell, K. Sletten, J. Juul, and D.G. Norman. Elucidation of the primary and three-dimensional structure of the uterotonic polypeptide kalata B1. *Biochemistry*. 1995; 34(13): 4147-58.

27. Daly, N.L., A. Koltay, K. Gustafson, R., M.R. Boyd, J.R. Casas-Finet, and D.J. Craik. Solution structure by NMR of circulin A: a macrocyclic knotted peptide having anti-HIV activity. *J. Mol. Biol.* 1999; 285(1): 333-45.
28. Chen, X., et al. Progranulin does not bind tumor necrosis factor (TNF) receptors and is not a direct regulator of TNF-dependent signaling or bioactivity in immune or neuronal cells. *J. Neurosci.* 2013; 33(21): 9202-13.
29. Etemadi, N., A. Webb, A. Bankovacki, J. Silke, and U. Nachbur. Progranulin does not inhibit TNF and lymphotoxin-alpha signalling through TNF receptor 1. *Immunol. Cell Biol.* 2013; 91(10): 661-4.
30. Rollinson, S., K. Young, J. Bennion-Callister, and S.M. Pickering-Brown. Identification of biological pathways regulated by PGRN and GRN peptide treatments using transcriptome analysis. *Eur. J. Neurosci.* 2016; 44(5): 2214-25.

**Chapter 4. Structural Variants of a  
Liver Fluke Derived Granulin  
Peptide Potently Stimulate Wound  
Healing**

## 4.1 Abstract

Granulins are a family of growth factors involved in cell proliferation. The liver-fluke granulin, *Ov*-GRN-1, isolated from a carcinogenic liver fluke *Opisthorchis viverrini*, can significantly accelerate wound repair *in vivo and in vitro*. However, it is difficult to express *Ov*-GRN-1 in recombinant form at high yield, impeding its utility as a drug lead. Previously we reported that a truncated analogue (*Ov*-GRN<sub>12-35\_3s</sub>) promotes healing of cutaneous wounds in mice. NMR analysis of this analogue indicates the presence of multiple conformations, most likely as a result of proline *cis/trans* isomerisation. To further investigate whether the proline residues are involved in adopting the multiple conformations we have synthesised analogues involving mutation of the proline residues. We have shown that the proline residues have a significant influence on the structure, activity and folding of *Ov*-GRN<sub>12-35\_3s</sub>. These results provide insight into improving the oxidative folding yield and bioactivity of *Ov*-GRN<sub>12-35\_3s</sub>, and might facilitate the development of a novel wound healing agent.

## 4.2 Introduction

Granulins are a large family of disulfide-rich proteins with diverse biological functions (1, 2) including wound healing (3), cell growth and proliferation modulation (1) and angiogenesis (4, 5). There is limited sequence conservation amongst the granulin domains but the majority contain twelve cysteine residues, with a conserved framework (6, 7), as shown in Figure 4-1A. The most well studied granulin in terms of structure is carp granulin-1, which has a  $\beta$ -hairpin stack stapled together with the six disulfide bonds (8), that are critical for maintaining structure (9). Despite the conserved cysteine framework, the structure-function relationships are complex with some granulin domains displaying cell proliferation activity and some having inhibitory effects on cell growth (10-12), and the effects on biological pathways also appears to vary (13).

The liver-fluke granulin, *Ov*-GRN-1, isolated from *Opisthorchis viverrini*, displays potent wound healing activity *in vivo* (14-16), but low yields in the recombinant expression have limited its development as a therapeutic (17). Elucidating the structure-function relationships has also been impacted by the difficulties in producing significant quantities for study. However, we have recently shown that truncated analogues of *Ov*-GRN-1 represent functional mimetics (18) with potential in treating chronic wounds where the normal tissue repair mechanisms are overwhelmed, such as diabetic ulcers (19, 20).

Our truncated analogues of *Ov*-GRN-1 provide insight into the folding and the bioactive region, but uncertainty remains regarding the principal features for secondary structure formation and structural stability (21, 22). For instance, the peptide (*Ov*-GRN<sub>12-35\_3s</sub>) corresponding to residues 12-35 in *Ov*-GRN-1, comprises only one  $\beta$ -hairpin in contrast to a truncated form of carp granulin-1 (18, 23, 24). Intriguingly, this peptide contains a non-native disulfide bond based on the predicted connectivity as shown in Figure 4-1B. The role of this bond in secondary structure stabilisation is not fully understood. In addition, *Ov*-GRN<sub>12-35\_3s</sub> displays evidence of additional conformations in the NMR spectra. To determine if these additional conformations are the result of proline *cis/trans* isomerisation, in the current study we have mutated the proline residues and examined the effects on structure, folding and



activity. Determining the most structurally stable and potent analogue is expected to facilitate the development of *Ov*-GRN-1 derived peptides as novel wound healing agents.

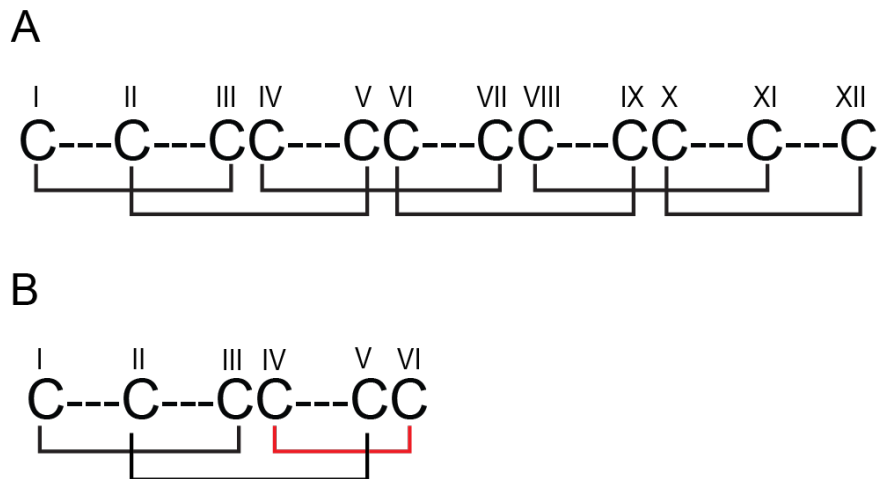


**Figure 4-1 Conserved cysteine framework in the granulin family.** Disulfide bond connectivity in full-length carp granulin-1 (A), and the synthetic N-terminal *Ov*-GRN-1 peptide (*Ov*-GRN<sub>12-35\_3s</sub>) (B). A non-native disulfide bond marked in red is predicted to be present in *Ov*-GRN<sub>12-35\_3s</sub> (18). C = cysteine residues sequentially numbered with Roman numerals, --- represents non-cysteine amino acids, solid black lines connecting cysteine residues represent disulfide bonds.

### **4.3 Experimental section**

#### **4.3.1 Peptide synthesis, purification and characterisation**

Granulin analogues were synthesised by a stepwise solid phase peptide synthesis procedure on a Protein Technologies PS3 synthesiser. The Fmoc amino acid derivatives (Auspep, Australia) were activated using HCTU (Iris, Germany) and coupled on the 2-chlorotrityl chloride resin with DIPEA/DMF. The peptide was cleaved from the resin using the following cleavage cocktail: 95% TFA:2.5% TIPS:2.5% H<sub>2</sub>O (v/v/v). The peptide was then precipitated with ice-cold diethyl ether and the ether evaporated off with a stream of nitrogen gas. Precipitated peptide was dissolved in 50% acetonitrile:50% H<sub>2</sub>O:0.1% TFA (v/v/v) and subsequently lyophilised. The resulting crude peptides were purified by reversed-phase HPLC using a C<sub>18</sub> preparative column (Phenomenex Jupiter 250 x 21.2 mm, 10 μm, 300 Å), a flow rate of 5 mL/min, and a 1% gradient (0-60%B) of solvent A (95.95% H<sub>2</sub>O:0.05% TFA (v/v)) and solvent B (90% acetonitrile:10% H<sub>2</sub>O:0.05% TFA (v/v/v)). The eluents were monitored at 214 and 280 nm and the mass determined using a 5800 MALDI TOF/TOF mass spectrometer (SCIEX, Foster city, CA). Based on analytical RP-HPLC the purified peptides had ≥95% purity.

#### **4.3.2 Disulfide formation**

Disulfide bonds were formed by overnight air oxidation of 0.1 mg/ml peptide in 0.1 M ammonium bicarbonate (pH 8-8.2) containing 5 mM reduced glutathione at room temperature for 24 h. The solution was acidified, filtered and purified on a C<sub>18</sub> preparative column using RP-HPLC and the peptide mass was analysed using a 5800 MALDI TOF/TOF spectrometer (SCIEX, Foster city, CA).

#### **4.3.3 NMR spectroscopy and structure analysis**

Samples were prepared from lyophilised peptide at concentrations of approximately 0.2 mM in 90% H<sub>2</sub>O:10% D<sub>2</sub>O. All NMR spectra were recorded on a 600 MHz AVANCE III NMR spectrometer (Bruker, Karlsruhe, Germany). 2D <sup>1</sup>H-<sup>1</sup>H TOCSY, <sup>1</sup>H-<sup>1</sup>H NOESY, <sup>1</sup>H-<sup>1</sup>H DQF-COSY, <sup>1</sup>H-<sup>15</sup>N HSQC, and <sup>1</sup>H-<sup>13</sup>C HSQC at 290 K were used for assignment. All spectra were recorded with an interscan delay of 1 s. NOESY spectra were acquired with mixing times of 200 ms, and TOCSY spectra

were acquired with isotropic mixing periods of 80 ms. All spectra were assigned using CCPNMR (25) based on the approach described in Wüthrich *et al* (26). The  $\alpha$ H secondary shifts were determined by subtracting random coil  $^1$ H NMR chemical shifts (27) from the experimental  $\alpha$ H chemical shifts. The 2D NOESY spectra were assigned and an ensemble of structures calculated using the program CYANA (28). A total of 100 initial structures were calculated using the CYANA program. Torsion-angle restraints predicted using TALOS N were used in the structure calculations (29). Structures were visualised using MOLMOL (30).

#### **4.3.4 Mammalian cell culture**

The 1BR.3.GN (ECACC 90020509), human skin normal fibroblast cell line was obtained from European Collection of Authenticated Cell Cultures (ECACC). 1BR.3.GN cells were grown and maintained in DMEM/F12 (Life Technologies) containing 1 $\times$  antibiotic/antimycotic and 1 $\times$  GlutaMAX, supplemented with 10% fetal bovine serum (FBS) (Gibco, Scotland) at 37°C and 5% CO<sub>2</sub>. Cell proliferation assays were performed with DMEM/F12 media supplemented with 10% FBS.

The H69 non-malignant cholangiocyte cell line was obtained from Dr. Gregory J. Gores, Mayo Clinic, Rochester, Minnesota (18). H69 cells were cultured and maintained as previously described (18) in DMEM/F12 (Life Technologies) containing 1 $\times$  antibiotic/antimycotic and 15 mM HEPES, supplemented with 10% fetal bovine serum (FBS) (Gibco, Scotland) at 37°C and 5% CO<sub>2</sub>. Cell proliferation assays were performed with modified DMEM/F12 media supplemented with 0.5% FBS and particular hormone and growth factors in defined concentration ranges reported (18).

#### **4.3.5 Cell proliferation monitoring in real time using xCELLigence**

Analysis of cell proliferation was performed in real time using an xCELLigence SP system (ACEA Biosciences) as described previously (18). 1BR.3.GN cells were plated into a 96-well xCELLigence E-plate (ACEA Biosciences) at a density of 7500 cells/well; then placed in the xCELLigence system with 5% CO<sub>2</sub> at 37°C and monitored overnight (31). The complete media was subsequently replaced with 150  $\mu$ L of starvation media (DMEM/F12 media supplemented with 0.5% FBS) and

incubated overnight. Treatments in 10% media were added to each well in a total volume of 20  $\mu$ L to provide 200 nM or 500 nM final concentrations and the cell index (CI) was monitored with the real time cell analysis software (RTCA, ACEA biosciences). At control peptide treatment peak cell number (peak CI) the cell proliferation rate was calculated as the relative number of treated cells compared to control cells (~120 hours in culture). H69 Cell proliferation was performed as described previously (18). GraphPad Prism 6.02 was used for comparing treatments against peptide controls with one-way ANOVA followed by Holm-Sidak's multiple comparison tests. Treatments were measured with 3-6 biological replicates from 2 independent experiments.

#### **4.3.6 Mouse wounding assay**

These studies were conducted with the approval of the James Cook University Small Animal Ethics Committee, applications A2204, as described previously (14). Briefly, female 11-12 week old BALB/c mice weighing 19-23 g were sourced from the Australian ARC (Animal Resources Centre) and randomly allocated into groups of 4 mice and fur removed on the crown of the head with small animal electric shaver. Mice were anesthetized with 3% isoflurane/air mix (Provet), after which a skin-deep wound on the crown of the head was created using a 5 mm diameter circular biopsy punch and surgical scissors (Zivic instruments). Betadine liquid antiseptic (Sanofi) was applied followed by application of 50  $\mu$ L that contained either 71 pmoles of Regranex (32, 33) (treatment of 71 pmoles equals ~1  $\mu$ g per 0.2  $\text{cm}^2$  wound, as recommended by manufacturer Smith and Nephew), 56 pmoles of rOv-GRN-1 (15), 50 pmoles Ov-GRN-1 peptides, or control peptide (EADRKYDEVARKLAMVEADL) (18), *E.coli* thioredoxin protein expression control (TRX) or PBS vehicle control suspended in 1.5% methylcellulose (Sigma). Wounds were photographed daily and treatments applied daily up until 4 days post wounding. Groups were blinded and the area of the lesion was measured with ImageJ software and plotted as percent of wound closure from original wound images. Wound healing rates of treatments were compared against controls and other treatments with one-way ANOVA test with Holm-Sidak's correction for multiple comparisons, using GraphPad prism 6.02. Wound healing assays in mice were performed in duplicat.

## 4.4 Results

### 4.4.1 Design and synthesis of *Ov*-GRN<sub>12-35\_3s</sub> mutants

To determine which proline residues are involved in adopting multiple conformations, three single mutants (GRN<sub>P2A</sub>, GRN<sub>P4A</sub>, GRN<sub>P10A</sub>) of *Ov*-GRN<sub>12-35\_3s</sub>, in which each mutant has one of the three prolines changed to an alanine residue were chemically synthesised. An analogue with all proline residues replaced with alanine residues was also synthesised and termed GRN<sub>3Ala</sub>. The sequences of the synthetic *Ov*-GRN-1 truncated peptides are given in Table 4-1.

All peptides were chemically synthesised using Fmoc solid phase peptide synthesis. The crude peptides were purified using RP-HPLC and mass analysis carried out using MALDI mass spectrometry. The peptides were oxidised to form the disulfide bonds in 0.1 M ammonium bicarbonate and 5 mM glutathione at room temperature for 24 hours. Glutathione was used as a disulfide bond shuffling reagent and generally improved the yield of the correctly folded forms (results not shown).

**Table 4-1 Sequences of *Ov*-GRN-1 peptides**

Peptide	Sequence
<i>Ov</i> -GRN <sub>12-35_3s</sub>	1 5 10 15 20 CP <u>D</u> P <u>V</u> YTCR <u>P</u> GQTCCRGLHGYGCC
GRN <sub>P2A</sub>	<b>C</b> <u>A</u> D <u>P</u> VYTCRPGQTCCRGLHGYGCC
GRN <sub>P4A</sub>	CP <u>D</u> <b>A</b> VYTCRPGQTCCRGLHGYGCC
GRN <sub>P10A</sub>	CPDPVYTCR <u>A</u> GQTCCRGLHGYGCC
GRN <sub>3Ala</sub>	<b>C</b> <u>A</u> <b>D</b> <u>A</u> VYTCR <u>A</u> GQTCCRGLHGYGCC

All *Ov*-GRN-1 truncated peptides contain the first six cysteine residues (bold) in the full-length protein. Prolines at positions 2, 4 and 10 are underlined and numbered in the native first sequence and subsequent variant sequences show proline to alanine variations underlined in bold.

A relatively sharp, early eluting peak was presented for the majority of the peptides. To describe the efficacy of the folding, the relative folding yield of this early eluting peak is given in Table 4-2. Relative folding yield is taken to mean the fraction of the integrated HPLC peak corresponding to the early eluting peak (natively folded species), relative to the total integrated HPLC area corresponding to all folding species in a given HPLC chromatogram (22, 34). For all peptides, with the exception of GRN<sub>P10A</sub>, the major early eluting peaks were isolated from each reaction for further characterisation.

The large number of peaks present in the folding reaction of GRN<sub>P10A</sub>, even following a 48-hour oxidation period, prevented the purification of a single major disulfide isomer. The yield of this early eluting peak is significantly higher in the GRN<sub>3Ala</sub> mutant (relative oxidative folding yield of 42.6%) compared to the other peptides.

**Table 4-2 Oxidative folding yields for the granulin peptides**

Peptide	Yield (%)
<i>OV</i> -GRN <sub>12-35_3s</sub>	23.0
GRN <sub>P2A</sub>	33.0
GRN <sub>P4A</sub>	31.0
GRN <sub>P10A</sub>	20.0
GRN <sub>3Ala</sub>	43.0

#### 4.4.2 Structural analysis with NMR spectroscopy

The structures of the purified or partially purified fractions for the *Ov*-GRN<sub>12-35\_3s</sub> analogues were analysed using NMR spectroscopy. The one-dimensional spectra of all peptides have significant dispersion in the amide region consistent with the presence of  $\beta$ -sheet structure. Analysis of the TOCSY (Total Correlated Spectroscopy) and NOESY (Nuclear Overhauser Effect Spectroscopy) spectra for the individual proline mutants indicates the presence of multiple conformations most likely as a result of isomerisation of the proline residues. By contrast, the GRN<sub>3Ala</sub> peptide did not appear to have multiple conformations as shown in Figure 4-2.

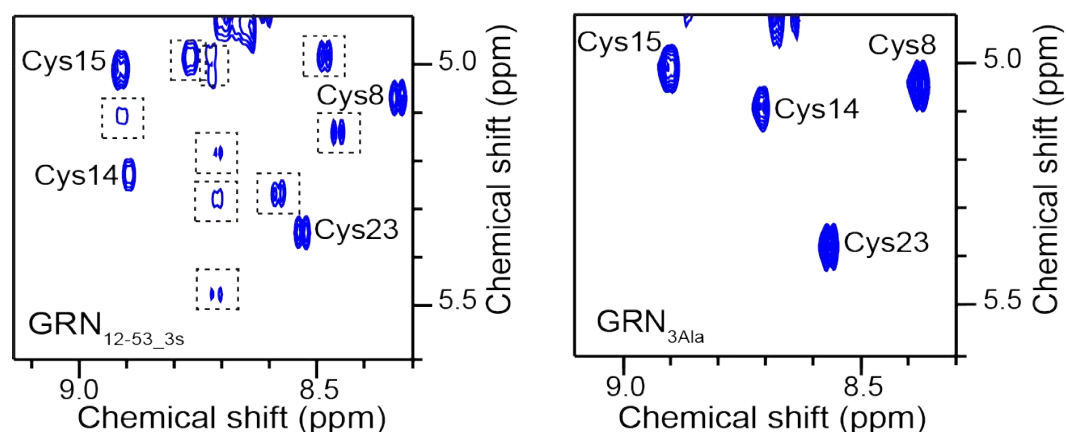


**Figure 4-2** Regions of the TOCSY spectra of *Ov*-GRN<sub>12-35\_3s</sub> and GRN<sub>3Ala</sub>. Spectra were recorded at 0.2 mM, 290 K. Assigned residues are shown with their residue name and number. Additional peaks not seen in GRN<sub>3Ala</sub> (right) resulting from multiple conformations in *Ov*-GRN<sub>12-35\_3s</sub> are boxed (left).

Two-dimensional spectra (TOCSY and NOESY) were used to assign the major conformations, and the secondary shifts were determined by subtracting random coil shifts from the experimental  $\alpha$ H shifts (27). The consecutive positive secondary shifts in Figure 4-3, particularly for residues 12-15, are consistent with the presence of  $\beta$ -sheet structure. The secondary shifts are generally similar over the equivalent residues

for all proline mutants compared to the N-terminal *Ov*-GRN-1 peptide, *Ov*-GRN<sub>12-35\_3s</sub>, indicating that the overall structures are similar.

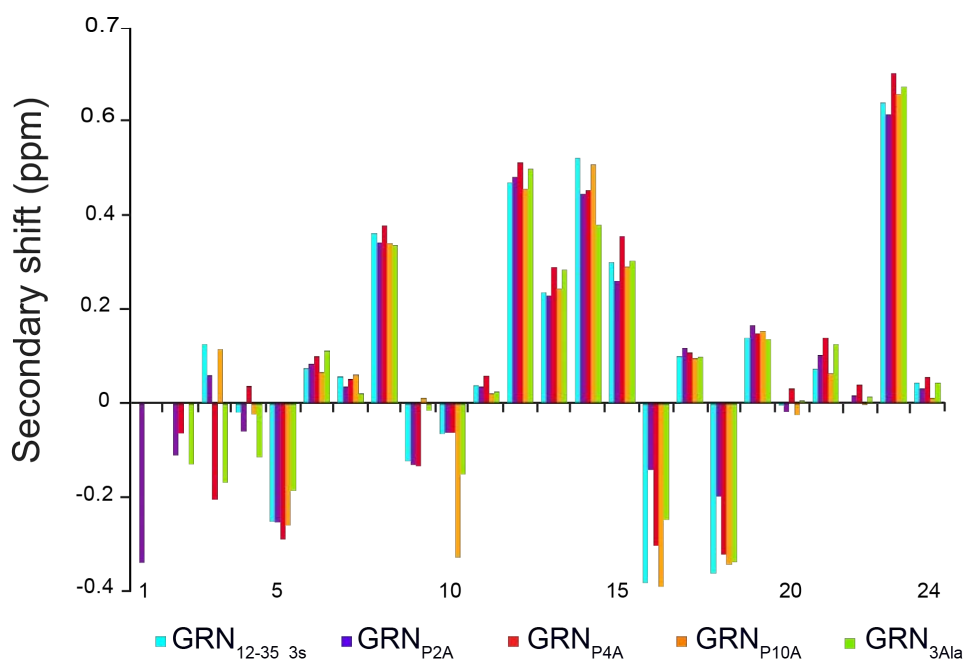


**Figure 4-3 Secondary shifts of *Ov*-GRN<sub>12-35\_3s</sub> engineered peptides.** The secondary shifts were derived by subtracting random coil shifts from the  $\alpha$ H shifts (27). The consecutive positive shifts for residues 11-14 is indicative of  $\beta$ -sheet. The trends for the secondary shifts are similar compared to *Ov*-GRN<sub>12-35\_3s</sub> indicating that the  $\beta$ -sheet present in *Ov*-GRN<sub>12-35\_3s</sub> is maintained in the proline mutant analogues.

GRN<sub>3Ala</sub> was chosen for full structural analysis because of the efficient folding, lack of conformational heterogeneity and to determine the influence of the proline residues on the overall fold. The family of structures was calculated using CYANA (28). The disulfide bonding pattern of *Ov*-GRN<sub>12-35\_3s</sub> was previously predicted to be Cys I-Cys III, Cys II-Cys V and Cys IV-Cys VI (18), and this connectivity was used in the structure calculations of GRN<sub>3Ala</sub>. Preliminary structures were calculated based on NOE (Nuclear Overhauser Effect) and dihedral angle restraint data. Hydrogen bond restraints were subsequently included for bonds that were predicted to occur in the preliminary structures and were consistent with the slowly exchanging amide protons. A family of 20 structures with the lowest CYANA target functions were chosen to



represent the structures of GRN<sub>3Ala</sub>. The structure statistics for the final ensemble of structures is given in Table 4-3.

The structures are well defined with an RMSD of 0.78 Å over the backbone atoms of all residues. Analysis of the secondary structure using MOLMOL indicates an α-helix from residues 4 to 11 and a β-hairpin involving residues 14 to 23. The β-hairpin in GRN<sub>3Ala</sub> is consistent with the structure of *Ov*-GRN<sub>12-35\_3s</sub>, but the N-terminal α-helix represents a significant structural change (Figure 4-4).

**Table 4-3 Structural statistics for GRN<sub>3Ala</sub>**

---

**Experimental restraints**

Interproton distance restraints

<i>Intraresidue,  i-j =0</i>	85
<i>Sequential,  i-j =1</i>	84
<i>Medium range, 1 &lt; i-j  &lt; 5</i>	10
Dihedral-angle restraints	28

**R.m.s. deviations from mean coordinate structure (Å)**

Backbone atoms (all)	0.78 ± 0.27
All heavy atoms (all)	1.69 ± 0.32

**Ramachandran (%)**

Residues in most favoured regions	95.9%
Residues in additionally allowed regions	4.1%

---

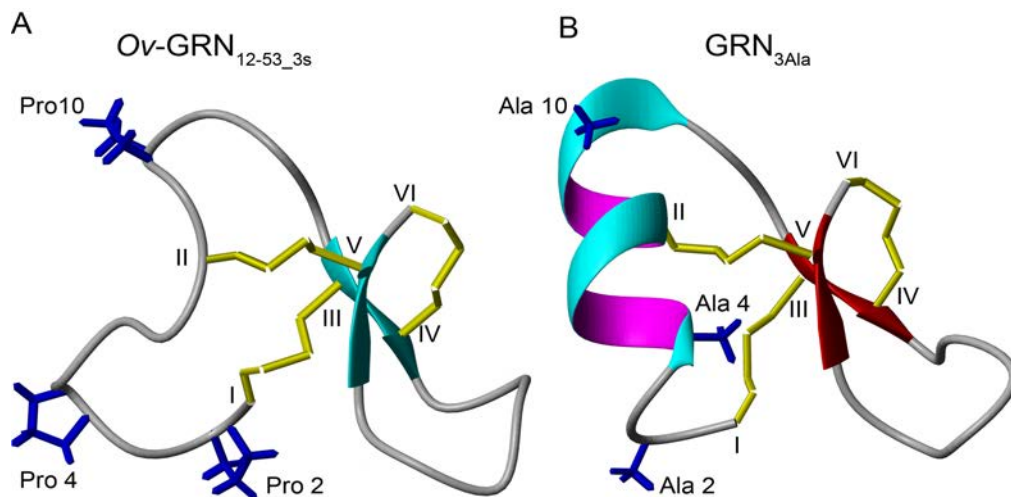


**Figure 4-4 Three-dimensional structure of *Ov-GRN*<sub>12-35\_3s</sub> (A) and *GRN*<sub>3Ala</sub> (B).** The structures were determined based on NMR spectroscopy data with cysteines numbered with Roman numerals joined by disulfide bonds in yellow,  $\beta$ -sheet represented as arrows, and  $\alpha$ -helix shown as a pink/aqua coil. The side-chains of Pro 2, Pro 4 and Pro 10 are highlighted (dark blue) on the *Ov-GRN*<sub>12-35\_3s</sub> structure (PDB ID code: 5UJH). The proline residues were replaced with alanine residues (dark blue) in *GRN*<sub>3Ala</sub> (PDB ID code: 6E1L; the coordinates are provided as supporting information).

#### 4.4.3 Cell proliferation monitoring in real time using xCELLigence

In addition to structural studies, to gain insight into the structure-function relationships of *Ov-GRN*<sub>12-35\_3s</sub>, the proline mutants were tested in an *in vitro* cell proliferation assay (17, 22). *GRN*<sub>P10A</sub> was not tested because a single isomer could not be purified. The rates of cell proliferation of H69 human bile duct (cholangiocyte) and 1BR.3.GN human fibroblast skin cells, in the presence of peptides or controls, were measured using xCELLigence technology as shown in Figure 4-5. The individual proline mutants significantly increased H69 cell proliferation compared to the negative control peptide (20 residue peptide from tropomyosin). The proliferation rates of *GRN*<sub>P2A</sub>, *P4A* were 131% ( $P < 0.0001$ ) and 141% ( $P < 0.0001$ ), respectively, relative to the control peptide (Figure 4-5A). *GRN*<sub>3Ala</sub> did not induce H69 significant cell proliferation at concentrations up to 1  $\mu$ M (data not shown).

In contrast to the H69 proliferation, *GRN*<sub>3Ala</sub> substantially promoted proliferation in 1BR.3.GN cells in a dose dependant manner by 12% ( $P < 0.01$ ) and 26% ( $P < 0.01$ ) at 200 nM and 500 nM, respectively. *GRN*<sub>P4A</sub> also promoted cell proliferation in a dose dependant manner with these cells, with proliferation rates relative to the control

peptide of 108% ( $P<0.05$ ) at 200 nM, and 125% ( $P<0.01$ ) at 500 nM. By contrast, GRN<sub>P2A</sub> was not active at 200 nM but 500 nM promoted significant cell proliferation (16% above peptide control ( $P<0.001$ )) (Figure 4-5B). It should be noted the 1BR.3.GN cells showed substantially less proliferation than the H69 cells. The differences in media in addition to the cell-type are likely to contribute to this difference.

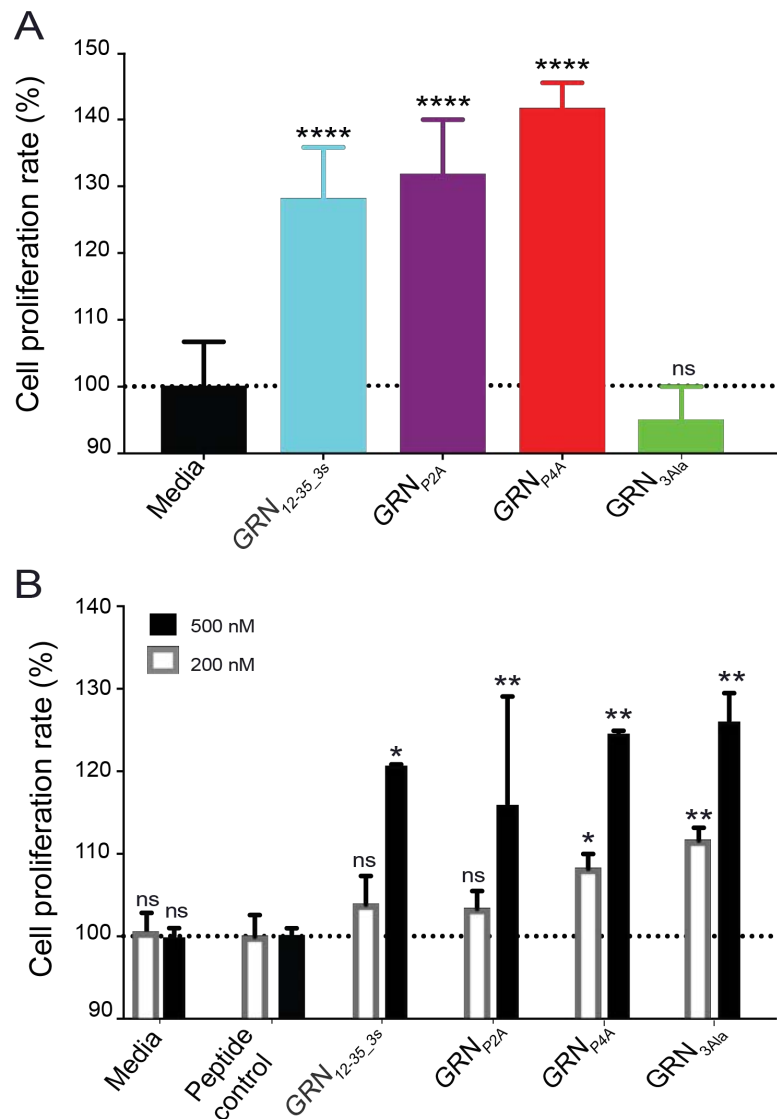


**Figure 4-5 Granulin peptide variants stimulated *in vitro* cell proliferation** (A) The H69 cells in low nutrient media (0.5% FBS) were treated with 200 nM peptide for 48 h (2 days). (B) Human fibroblast 1BR.3.GN cells were grown in complete media (10% FBS) and the various peptides were assessed for stimulation of proliferation at 200 nM and 500 nM at peak cell index (~120 hours/5 days). The proliferation rates relative to peptide controls are plotted as mean  $\pm$  SEM bars. Data were analyzed by one-way ANOVA against peptide control. Not significant = *ns*, \*  $P<0.05$ , \*\*  $P<0.01$ , \*\*\*  $P<0.001$  \*\*\*\* $P<0.0001$ .

#### 4.4.4 Mouse wounding assay

The peptides GRN<sub>P2A</sub>, GRN<sub>P4A</sub> and GRN<sub>3Ala</sub> were also tested in a mouse wound healing assay using the procedures previously reported (18). The results are shown in Figure 4-6 and highlight that both GRN<sub>P4A</sub> (142.8%,  $P<0.0001$ ) and recombinant *Ov*-GRN-1 (127.1%,  $P<0.0001$ ) stimulated more marked resolution of the cutaneous lesions on the scalp of the mice than GRN<sub>3Ala</sub> (125.1%,  $P<0.001$ ) and *Ov*-GRN<sub>12-35\_3s</sub> (119.1%,  $P<0.05$ ). GRN<sub>P4A</sub> promoted a significant ( $P<0.05$ ) increase in wound healing by 21% compared to the Regranex treatment. GRN<sub>P2A</sub> (116%) did not significantly influence wound healing compared to the control peptide.

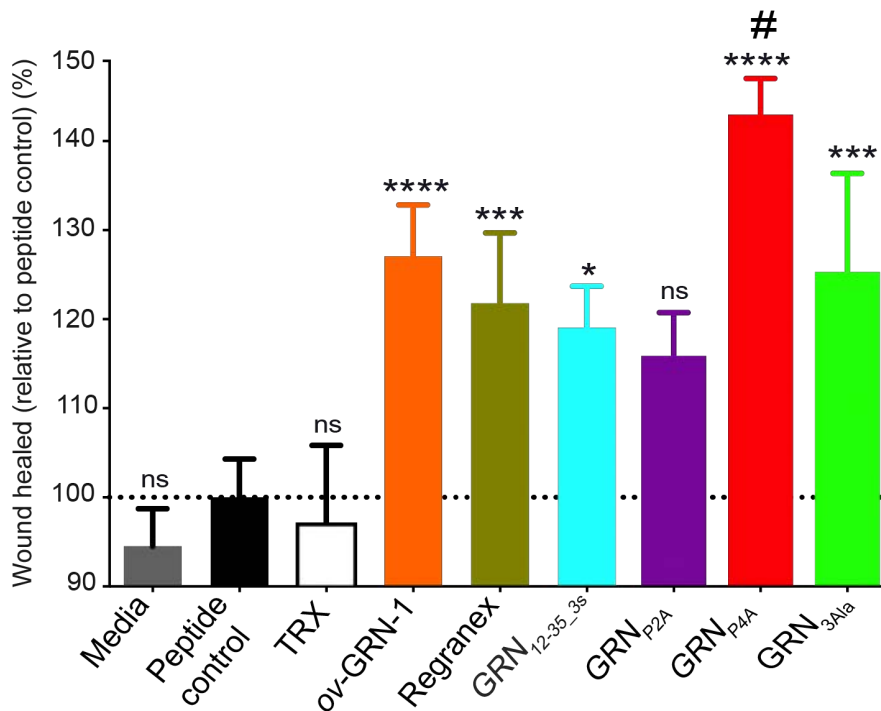


**Figure 4-6 Granulin peptides stimulated mouse wound healing.** The average wound healing rate relative to the peptide control treatment is shown after four days of 56 pmol of various granulin treatments or 76 pmol of Regranex are shown. Relative to the peptide negative control the full-length granulin protein (*Ov*-GRN-1) and Regranex stimulate wound healing by 27% and 22% respectively. Data were analyzed by one-way ANOVA from duplicated experiments with 4 female balb/c mice per group. Compared against peptide control: Not significant = *ns*, \*  $P<0.05$ , \*\*\*  $P<0.001$  \*\*\*\* $P<0.0001$ . Compared against Regranex # =  $P<0.05$ .

## 4.5 Discussion

Chronic wounds are a substantial problem affecting 1-2% of people globally and costing ~USD \$50 billion to treat annually (35, 36). Better treatments are needed desperately, especially for diabetics who suffer from a disproportionately high rate of chronic wounds (36). Regranex (recombinant human platelet-derived growth factor) is the only FDA approved treatment for chronic wounds, but increased malignancies were observed in patients (37). *Ov*-GRN-1 has potential in the development of a novel wound-healing agent, but there is still limited information on the structure-function relationships. Here we show mutation of the proline residues in *Ov*-GRN<sub>12-35\_3s</sub> can improve folding yield and wound healing properties.

Mutation of the individual proline residues did not disrupt the overall fold of *Ov*-GRN<sub>12-35\_3s</sub>, but multiple conformations were still present based on the presence of additional peaks in the NMR spectra. By contrast, when all three proline residues were mutated to alanine residues a single set of peaks corresponding to a single conformation were observed in the NMR spectra. These results indicate that all three proline residues are involved with *cis/trans* isomerisation to some extent.

*Cis/trans* isomerisation can be a rate-determining step in the folding of proteins (38, 39), and appears to be influencing the folding of *Ov*-GRN<sub>12-35\_3s</sub>. Removal of proline 2 and proline 4 in GRN<sub>P2A</sub> and GRN<sub>P4A</sub> respectively, improved the oxidative folding yields relative to *Ov*-GRN<sub>12-35\_3s</sub>. By contrast, mutation of proline 10 with an alanine residue did not improve the folding yield. Prevention of *cis/trans* isomerisation by removal of all three proline residues resulted in the highest folding yield (Table 4-2). These results indicate that the proline residues, which have a much higher propensity to form *cis* peptide bonds than other residues (40), are generally detrimental to the folding under the current conditions (41). Further study is required to determine the influence of the proline residues on folding *in vivo*.

Our findings conform with earlier reports that revealed that folding of human granulin modules is strongly influenced by sequence variations (10). In mammals, granulins are expressed as progranulin, which contains seven-and-a-half granulin modules (7, 42). The folding profiles of recombinant versions of the seven full-length granulin modules vary markedly, based on HPLC analysis (10). Analysis of the structures with

NMR spectroscopy indicate that GRN-2, GRN-4 and GRN-5 display defined structures (10). By contrast, GRN-3 and -7 did not display significant dispersion in the NMR spectra, and GRN-6 and -1, exhibit multiple signals in the NMR spectra for unique protons (10). Although the folding and structures vary amongst the different human granulin domains, the sequences responsible for these different conformations have not been defined (21). Sequence alignment (Table 4-4) of *Ov*-GRN<sub>12-35\_3s</sub> with human granulins and carp granulin-1 shows that GRN-3 and -2 both contain a proline residue immediately following the first cysteine in the sequence, consistent with proline 2 in *Ov*-GRN<sub>12-35\_3s</sub>. GRN-3 does not have a predominant, sharp peak in the HPLC profile of the folding reaction, but GRN-2 does (10). Although mutation of proline 2 in *Ov*-GRN<sub>12-35\_3s</sub> had an influence on the folding profile, the varying results for GRN-3 and GRN-2 suggest that this proline alone does not have a general influence on folding of granulin domains.

Sequence alignment of human granulin domains and carp granulin-1 also shows in all but two sequences (hGRN-1 and -7) there is a highly conserved proline residue immediately after the second cysteine in the granulin cysteine framework (Table 4-4).

*Ov*-GRN-1 does not contain this conserved “CP” sequence but rather contains a “CRP” sequence where the proline is equivalent to residue 10 in *Ov*-GRN<sub>12-35\_3s</sub>. When this proline was mutated to an alanine residue in GRN<sub>P10A</sub>, the folding profile did not contain one major isomer in contrast to the other mutants, indicating that this residue is important in the folding of *Ov*-GRN<sub>12-35\_3s</sub>.

In addition to the influence on folding, mutation of the proline residues also influenced biological activity. The single point mutants of *Ov*-GRN<sub>12-35\_3s</sub> significantly accelerated the proliferation of H69 human cholangiocytes to a similar extent to native *Ov*-GRN<sub>12-35\_3s</sub>, whereas GRN<sub>3Ala</sub> did not enhance the rate of proliferation. By contrast, GRN<sub>P4A</sub> and GRN<sub>3Ala</sub> significantly accelerated the proliferation of fibroblasts at the low concentration, whereas GRN<sub>P2A</sub> did not. The results from the *in vivo* wound healing study correlate with the fibroblast cell assay results. For example, GRN<sub>3Ala</sub> is not active on H69 cells but is active on fibroblasts and in the *in vivo* wound-healing assay. Conversely, GRN<sub>P2A</sub> induced proliferation of cholangiocytes, but only showed this effect on fibroblast cells at the highest

concentration tested and was not significantly active in the *in vivo* wound-healing assay.

**Table 4-4 Sequence alignment of human granulins.**

UniProt Entry	Peptide	N-terminal six cysteine core sequence
<a href="#">B8XSI4</a>	<i>Ov</i> -GRN <sub>12-35_3s</sub>	CPDPVY <b>T</b> <u>CRP</u> -GQT <b>C</b> CRGLHG-YG- <b>CC</b>
<a href="#">P28799</a>	*hGRN-1(G)	CQVDAH- <b>C</b> -SAGHSCIFTVSGTSS- <b>CC</b>
<a href="#">P28799</a>	hGRN-2(F)	CPDSQF <b>E</b> C- <u>P</u> DFST <b>C</b> VMVDGSWG- <b>CC</b>
<a href="#">P28799</a>	hGRN-3(B)	CPDARS <b>R</b> C- <u>P</u> DGST <b>C</b> CELPSGKYG- <b>CC</b>
<a href="#">P28799</a>	hGRN-4(A)	CDMEVS- <b>C</b> - <u>P</u> DGYT <b>C</b> RLQSGAWG- <b>CC</b>
<a href="#">P28799</a>	hGRN-5(C)	CDNVSS- <b>C</b> - <u>P</u> SSDT <b>C</b> QLTSGEWG- <b>CC</b>
<a href="#">P28799</a>	hGRN-6(D)	CDQHTS- <b>C</b> - <u>P</u> VGQT <b>C</b> PSLGGSWA- <b>CC</b>
<a href="#">P28799</a>	hGRN-7(E)	CGEGHF- <b>C</b> -HDNQ <b>T</b> CCRD <b>N</b> QG-WA- <b>CC</b>
<a href="#">P28799</a>	paraGRN	CPDGQF- <b>C</b> - <u>P</u> VA-- <b>C</b> CLDPGGASY <b>SC</b> C
<a href="#">P81013</a>	carp granulin-1	CDAATI- <b>C</b> - <u>P</u> DGTT <b>C</b> CLSPYGVWY- <b>CC</b>

Cysteine residues are marked in bold and the proline residues equivalent to proline 10 in *Ov*-GRN<sub>12-35\_3s</sub> are underlined in each sequence. hGRN-n(X) designates the individual human granulin domains from human progranulin with the two commonly used numbered (n) and alphabetized (X) designations. \*hGRN-1(G) is an unusual 5 cysteine N-terminal variant (10 cysteine residues rather than 12 in the full GRN domain).

The consistency between the mouse wound healing assay and the fibroblast cell assays is not unexpected given the role of fibroblasts in wound healing of the skin (43-46). Fibroblast numbers peak 3 days post-injury and migrate into the wound to initiate the proliferative phase differentiation (47). This is followed by deposition of new matrix proteins to restore structure and function to the injured tissue (44). Additionally, the complete 10% FBS media used with the fibroblasts is likely a closer approximation of the *in vivo* conditions encountered by cells than the low nutrient media used with the cholangiocytes.

The limited activity of GRN<sub>P2A</sub> in the fibroblast cell assay and the *in vivo* wound-healing assay, suggests that proline 2 plays an important role in the function of this protein. However, GRN<sub>3Ala</sub>, which also lacks proline 2 and has a well-defined  $\alpha$ -helix at the N-terminal region, is active in the fibroblast cells and the *in vivo* model. Collectively, these results suggest that the structure-function relationships for the granulin peptides are complex.

The lack of activity of GRN<sub>3Ala</sub> on the H69 epithelial cells compared to fibroblasts is of interest. There are many functional similarities between tumorigenesis and wound healing (44, 48). Inflammation, collagen and matrix deposition and angiogenesis are involved in both processes. While wound healing is usually a self-limiting process, rapid cellular division occurs and when uncontrolled, cell division can result in tumour formation (44, 48, 49). Developing a wound healing treatment with a growth factor can be effective but understanding the signalling pathways involved is an important step to limiting unwanted tumour stimulation, as seen with Regranex (37). Our next step to develop these peptides as potential healing stimulating treatments is to explore the underlying mechanism of action and uncover the binding partner/receptor(s) for *Ov*-GRN-1 and underlying signal transduction pathways. Nevertheless, this result might have significant implications for different receptor/mechanisms being involved in proliferation of cholangiocytes and the wound healing properties of *Ov*-GRN-1 and derivative peptides.

An area that can be explored to further the understand of the granulin peptide wound healing processes is mathematical models that break down healing steps based upon healing rates (50). Separating healing phases allows more detailed analysis and



statistical refinement. However, our data does not match the latest Cogan *et al* model that uses a 2-phase piecewise linear fit of initial stasis followed by a healing period (51). But as models adapt to a range of wound methodologies, we expect our future analysis will increasingly explore the use of these approaches.

The *in vivo* model used in the current study represents a normal (acute) wound healing process, which includes four phases: coagulation/inflammatory phase, proliferative phase, matrix remodelling and scar formation. Diabetic ulcers are classified as chronic wounds, which fail to progress through the wound healing phases in a timely manner (52, 53). In particular, the proliferative phase, which involves fibroblast cell proliferation and angiogenesis, is impaired in diabetic patients (52). Thus the prolonged inflammatory phase and persistent infections exacerbate the healing progress in diabetic ulcers (52, 53). Given the influence of the granulin peptides on the proliferation of fibroblasts we speculate that the granulin peptides will also be efficacious in diabetic wound healing models, but this remains to be determined.

#### **4.6 Conclusions**

Overall, our results highlight the importance of the proline residues in the structure, folding and function of *OV*-GRN<sub>12-35\_3s</sub>. GRN<sub>3Ala</sub> had the highest folding yield and was a potent stimulator of healing in mice. GRN<sub>P4A</sub> was the most potent peptide for healing wounds *in vivo*, and was significantly more potent than Regranex, a growth factor approved for human clinical use for this indication (32). The enhanced wound healing potency and improved folding yields of these proline mutants suggest they might be good candidates for further development as wound healing agents.

#### **4.7 Acknowledgements**

MD would like to thank James Cook University for a PhD scholarship. This work was supported by the Australian Research Council via a Future Fellowship to NLD (110100226), the National Health and Medical Research Council by a Senior Principal Research Fellowship to AL (1117504) and the Merchant Foundation. The James Cook University NMR facility was partially funded by the Australian Research Council (LE120100015, LE160100218). Support from award CA164719 from the National Cancer Institute, National Institutes of Health (NIH) to PJB, MJS and AL is gratefully acknowledged. The content is solely the responsibility of the authors and does not necessarily represent the official views of the NIH.

#### **4.8 Supporting information**

PDB ID Code for GRN<sub>3Ala</sub>: 6E1L

#### **4.9 Non-standard abbreviations**

HCTU, (2-(6-Chloro-1-H-benzotriazole-1-yl)-1,1,3,3-tetramethylammonium hexafluorophosphate); DIPEA, Ethyldiisopropylamine; TOCSY, Total Correlated Spectroscopy; USD, United States Dollar; ECACC, European Collection of Authenticated Cell Cultures; DMEM/F12, Dulbecco's Modified Eagle Medium: Nutrient Mixture F-12; HEPES, 4-(2-hydroxyethyl)-1-piperazineethanesulfonic acid; FBS, Fetal Bovine Serum; CI, Cell Index; ARC, Animal Resources Centre; TRX, thioredoxin; RP-HPLC, Reverse phase HPLC; D<sub>2</sub>O, Deuterium Oxide; DQF-COSY, Double-quantum filtered correlation spectroscopy; ANOVA, ANalysis Of Variance .

#### 4.10 References

1. Bateman, A. and H.P. Bennett. The granulin gene family: from cancer to dementia. *Bioessays*. 2009; 31(11): 1245-54.
2. Kleinberger, G., A. Capell, C. Haass, and C. Van Broeckhoven. Mechanisms of granulin deficiency: lessons from cellular and animal models. *Mol. Neurobiol.* 2013; 47(1): 337-60.
3. He, Z., C.H. Ong, J. Halper, and A. Bateman. Progranulin is a mediator of the wound response. *Nat. Med.* 2003; 9(2): 225-9.
4. Haugen, B., S.E. Karinshak, V.H. Mann, A. Popratiloff, A. Loukas, P.J. Brindley, and M.J. Smout. Granulin secreted by the food-borne liver fluke *Opisthorchis viverrini* promotes angiogenesis in human endothelial cells. *Front. Med. (Lausanne)*. 2018: 10.3389/fmed.2018.00030.
5. Eguchi, R., T. Nakano, and I. Wakabayashi. Progranulin and granulin-like protein as novel VEGF-independent angiogenic factors derived from human mesothelioma cells. *Oncogene*. 2017; 36(5): 714-22.
6. Toh, H., B.P. Chitramuthu, H.P. Bennett, and A. Bateman. Structure, function, and mechanism of progranulin; the brain and beyond. *J. Mol. Neurosci.* 2011; 45(3): 538-48.
7. Cenik, B., C.F. Sephton, B. Kutluk Cenik, J. Herz, and G. Yu. Progranulin: a proteolytically processed protein at the crossroads of inflammation and neurodegeneration. *J. Biol. Chem.* 2012; 287(39): 32298-306.
8. Hrabal, R., Z. Chen, S. James, H.P. Bennett, and F. Ni. The hairpin stack fold, a novel protein architecture for a new family of protein growth factors. *Nat. Struct. Biol.* 1996; 3(9): 747-52.
9. Ghag, G., L.M. Wolf, R.G. Reed, N.P. Van Der Munnik, C. Mundoma, M.A. Moss, and V. Rangachari. Fully reduced granulin-B is intrinsically disordered and displays concentration-dependent dynamics. *Protein Eng. Des. Sel.* 2016; 29(5): 177-86.
10. Tolkatchev, D., et al. Structure dissection of human progranulin identifies well-folded granulin/epithelin modules with unique functional activities. *Protein Sci.* 2008; 17(4): 711-24.
11. Plowman, G.D., J.M. Green, M.G. Neubauer, S.D. Buckley, V.L. McDonald, G.J. Todaro, and M. Shoyab. The epithelin precursor encodes two proteins with opposing activities on epithelial cell growth. *J. Biol. Chem.* 1992; 267(18): 13073-8.
12. Wang, X., H. Xu, X. Chen, Y. Tian, F. Wang, and X. Lin. Cloning, expression and cytotoxicity of granulin A, a novel polypeptide contained in human progranulin. *Biosci. Trends*. 2016; 10(3): 181-7.

13. Rollinson, S., K. Young, J. Bennion-Callister, and S.M. Pickering-Brown. Identification of biological pathways regulated by PGRN and GRN peptide treatments using transcriptome analysis. *Eur. J. Neurosci.* 2016; 44(5): 2214-25.
14. Smout, M.J., et al. Carcinogenic Parasite Secretes Growth Factor That Accelerates Wound Healing and Potentially Promotes Neoplasia. *PLoS Pathog.* 2015; 11(10): e1005209.
15. Smout, M.J., J.P. Mulvenna, M.K. Jones, and A. Loukas. Expression, refolding and purification of *Ov*-GRN-1, a granulin-like growth factor from the carcinogenic liver fluke, that causes proliferation of mammalian host cells. *Protein Expr. Purif.* 2011; 79(2): 263-70.
16. Smout, M.J., et al. A granulin-like growth factor secreted by the carcinogenic liver fluke, *Opisthorchis viverrini*, promotes proliferation of host cells. *PLoS Pathog.* 2009; 5, DOI: 10.1371/journal.ppat.1000611.
17. Papatpremsiri, A., M.J. Smout, A. Loukas, P.J. Brindley, B. Sripa, and T. Laha. Suppression of *Ov*-GRN-1 encoding granulin of *Opisthorchis viverrini* inhibits proliferation of biliary epithelial cells. *Exp. Parasitol.* 2015; 148, DOI: 10.1016/j.exppara.2014.11.004.
18. Bansal, P.S., et al. Development of a potent wound healing agent based on the liver fluke granulin structural fold. *J. Med. Chem.* 2017; 60(10): 4258-66.
19. Gomes, A., C. Teixeira, R. Ferraz, C. Prudencio, and P. Gomes. Wound-healing peptides for treatment of chronic diabetic foot ulcers and other infected skin injuries. *Molecules (Basel, Switzerland)*. 2017.
20. Adeghate, J., S. Nurulain, K. Tekes, E. Feher, H. Kalasz, and E. Adeghate. Novel biological therapies for the treatment of diabetic foot ulcers. *Expert Opin. Biol. Ther.* 2017; 17(8): 979-87.
21. Dastpeyman, M., M.J. Smout, D. Wilson, A. Loukas, and N.L. Daly. Folding of granulin domains. *Peptide Sci.* 2018: 10.1002/pep2.24062.
22. Jin, A.H., et al. Conotoxin  $\Phi$ -MiXXVIIA from the superfamily G2 employs a novel cysteine framework that mimics granulin and displays anti-apoptotic activity. *Angew. Chem. Int. Ed. Engl.* 2017; 56, DOI: 10.1002/anie.201708927.
23. Vranken, W.F., Z.G. Chen, P. Xu, S. James, H.P. Bennett, and F. Ni. A 30-residue fragment of the carp granulin-1 protein folds into a stack of two beta-hairpins similar to that found in the native protein. *J. Pept. Res.* 1999; 53(5): 590-7.
24. Vranken, W.F., S. James, H.P. Bennett, and F. Ni. Solution structures of a 30-residue amino-terminal domain of the carp granulin-1 protein and its amino-terminally truncated 3-30 subfragment: implications for the conformational stability of the stack of two beta-hairpins. *Proteins.* 2002; 47(1): 14-24.

25. Vranken, W.F., et al. The CCPN data model for NMR spectroscopy: development of a software pipeline. *Proteins*. 2005; 59(4): 687-96.
26. Wüthrich, K. NMR studies of structure and function of biological macromolecules (Nobel Lecture). *J. Biomol. NMR*. 2003; 27(1): 13-39.
27. Wishart, D.S., et al.  $^1\text{H}$ ,  $^{13}\text{C}$  and  $^{15}\text{N}$  chemical shift referencing in biomolecular NMR. *J. Biomol. NMR*. 1995; 6(2): 135-40.
28. Güntert, P. Automated NMR structure calculation with CYANA. *Methods Mol. Biol.* 2004; 278: 353-78.
29. Shen, Y. and A. Bax. Protein structural information derived from NMR chemical shift with the neural network program TALOS-N. *Methods Mol. Biol.* 2015; 1260, DOI: 10.1007/978-1-4939-2239-0\_2.
30. Koradi, R., M. Billeter, and K. Wüthrich. MOLMOL: a program for display and analysis of macromolecular structures. *J. Mol. Graph.* 1996; 14(1): 51-5, 29-32.
31. Xing, J.Z., L. Zhu, J.A. Jackson, S. Gabos, X.J. Sun, X.B. Wang, and X. Xu. Dynamic monitoring of cytotoxicity on microelectronic sensors. *Chem. Res. Toxicol.* 2005; 18(2): 154-61.
32. Chan, R.K., P.H. Liu, G. Pietramaggiore, S.I. Ibrahim, H.B. Hechtman, and D.P. Orgill. Effect of recombinant platelet-derived growth factor (Regranex) on wound closure in genetically diabetic mice. *J. Burn Care Res.* 2006; 27(2): 202-5.
33. Niezgoda, J.A., C.C. Van Gils, R.G. Frykberg, and J.P. Hodde. Randomized clinical trial comparing OASIS Wound Matrix to Regranex Gel for diabetic ulcers. *Adv. Skin Wound Care.* 2005; 18(5 Pt 1): 258-66.
34. Steiner, A.M. and G. Bulaj. Optimization of oxidative folding methods for cysteine-rich peptides: a study of conotoxins containing three disulfide bridges. *J. Pept. Sci.* 2011; 17(1): 1-7.
35. Graves, N. and H. Zheng. Modelling the direct health care costs of chronic wounds in Australia. *Wound Prac. Res.* 2014; 22(1): 20-33.
36. Campbell, L.V., A.R. Graham, R.M. Kidd, H.F. Molloy, S.R. O'Rourke, and S. Colagiuri. The lower limb in people with diabetes. Position statement of the Australian Diabetes Society. *Med. J. Aust.* 2000; 173(7): 369-72.
37. Weaver, J., L.L. Grenade, H. Kwon, and M. Avigan. Finding, evaluating, and managing drug-related risks: approaches taken by the US Food and Drug Administration (FDA). *Dermatol. Ther.* 2009; 22(3): 204-15.
38. Reimer, U., G. Scherer, M. Drewello, S. Kruber, M. Schutkowski, and G. Fischer. Side-chain effects on peptidyl-prolyl cis/trans isomerisation. *J. Mol. Biol.* 1998; 279(2): 449-60.

39. Eyles, S.J. Proline not the only culprit? *Nat. Struct. Biol.* 2001; 8(5): 380-1.
40. Siltari, A., R. Viitanen, S. Kukkurainen, H. Vapaatalo, and J. Valjakka. Does the cis/trans configuration of peptide bonds in bioactive tripeptides play a role in ACE-1 enzyme inhibition? *Biologics.* 2014; 8, DOI: 10.2147/btt.s54056.
41. Torbeev, V.Y. and D. Hilvert. Both the cis-trans equilibrium and isomerization dynamics of a single proline amide modulate beta2-microglobulin amyloid assembly. *Proc. Natl. Acad. Sci. U.S.A.* 2013; 110(50): 20051-6.
42. Wang, B.C., H. Liu, A. Talwar, and J. Jian. New discovery rarely runs smooth: an update on progranulin/TNFR interactions. *Protein & cell.* 2015; 6(11): 792-803.
43. Mutsaers, S.E., J.E. Bishop, G. McGrouther, and G.J. Laurent. Mechanisms of tissue repair: from wound healing to fibrosis. *Int. J. Biochem. Cell. Biol.* 1997; 29(1): 5-17.
44. Slavin, J. The role of cytokines in wound healing. *J. Pathol.* 1996; 178(1): 5-10.
45. Diegelmann, R.F. and M.C. Evans. Wound healing: an overview of acute, fibrotic and delayed healing. *Front. Biosci.* 2004; 9(1): 283-9.
46. Werner, S. and R. Grose. Regulation of wound healing by growth factors and cytokines. *Physiol. Rev.* 2003; 83(3): 835-70.
47. Darby, I.A. and T.D. Hewitson. Fibroblast differentiation in wound healing and fibrosis. *Int. Rev. Cytol.* 2007; 257: 143-79.
48. Arwert, E.N., E. Hoste, and F.M. Watt. Epithelial stem cells, wound healing and cancer. *Nat. Rev. Cancer.* 2012; 12(3): 170-80.
49. Margadant, C. and A. Sonnenberg. Integrin-TGF-beta crosstalk in fibrosis, cancer and wound healing. *EMBO reports.* 2010; 11(2): 97-105.
50. Jorgensen, S.N. and J.R. Sanders. Mathematical models of wound healing and closure: a comprehensive review. *Med. Biol. Eng. Comput.* 2016; 54(9): 1297-316.
51. Cogan, N.G., A.P. Mellers, B.N. Patel, B.D. Powell, M. Aggarwal, K.M. Harper, and M. Blaber. A mathematical model for the determination of mouse excisional wound healing parameters from photographic data. *Wound Repair Regen.* 2018, DOI: 10.1111/wrr.12634.
52. Demidova-Rice, T.N., M.R. Hamblin, and I.M. Herman. Acute and impaired wound healing: pathophysiology and current methods for drug delivery, part 1: normal and chronic wounds: biology, causes, and approaches to care. *Adv. Skin Wound Care.* 2012; 25(7): 304-14.

53. Munro, G. Causes and consideration with chronic wounds: a narrative review of the evidence. *Wound Prac. Res.* 2017; 25(2): 88-97.

# **Chapter 5. Distinct Structural and Biological Differences Between the N- and C-terminal Regions of Granulins**



## 5.1 Abstract

Granulins are a family of growth factor proteins, which generally contain six disulfide bonds and are found in most organisms. We have recently shown that the N-terminal half of *Ov*-GRN-1, a granulin derived from the parasitic human liver fluke *Opisthorchis viverrini*, can fold independently and has potent wound healing activity. This peptide contains three disulfide bonds, including a bond not present in full-length carp granulin-1, the prototypic granulin family member. Here we show using structure-based design, chemical peptide synthesis and folding analysis that the N-terminal half of the human granulin A protein also folds independently with three disulfide bonds, despite significant sequence differences to the *Ov*-GRN-1 peptide. This result indicates that accommodation of a non-native disulfide bond might be a general phenomenon in the granulin family. We also show for the first time that the equivalent C-terminal half of *Ov*-GRN-1 does not fold into a well-defined structure, but still displays some cell proliferation activity. Our results indicate that well-defined structures are not critical for granulin bioactivity

## 5.2 Introduction

*Ov*-GRN-1 is a disulfide-rich protein isolated from the excretory/secretory products of the liver fluke *Opisthorchis viverrini*. *Ov*-GRN-1 belongs to the granulin protein family (3-5) and is involved in a range of processes including wound healing (6-9), angiogenesis (10) and carcinogenesis (3, 11). The granulin protein family contains a highly conserved cysteine-rich motif, which forms six disulfide bonds (Figure 5-1A) and a series of antiparallel  $\beta$ -sheets (4, 12-15). The structure of full-length human granulin A (also referred to as hGRN-4(12)) is shown in Figure 5-1B (16).

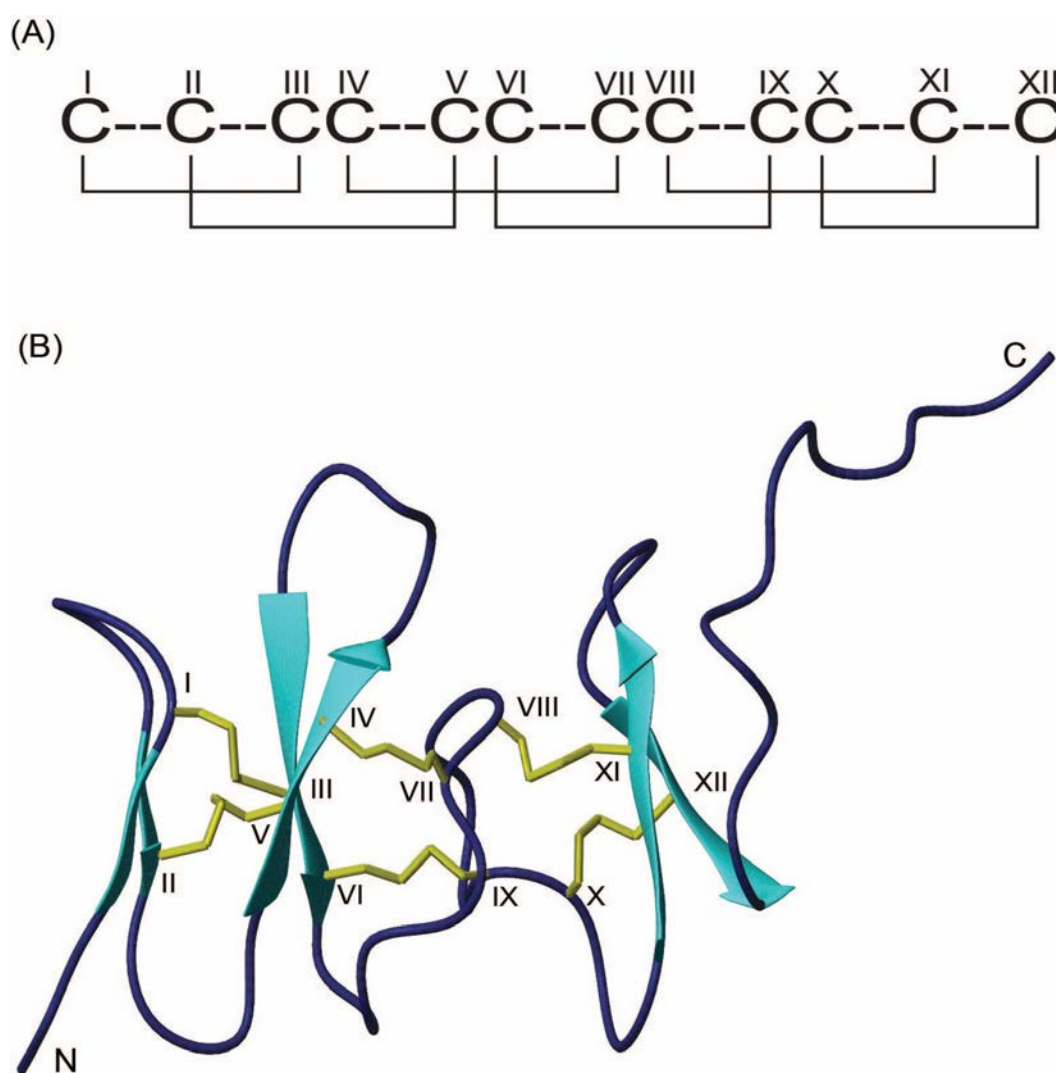


**Figure 5-1 Granulin cysteine framework and structure.** (A) Schematic representation of the highly conserved cysteine framework and disulfide bond pairing present in the granulin family; the cysteine residues are numbered using Roman numerals (I-XII). (B) The three-dimensional structure of full-length hGRN A (PDB ID: 2JYE).

Granulin proteins are found in a wide variety of organisms and possess distinct variations in the structures (12, 17). For example, the carp and zebrafish granulins display relatively well defined structures (15, 18), whereas several of the human granulins have a well-defined stack of two  $\beta$ -hairpins in the N-terminal region, and structural disorder in the C-terminal region (16). The folding pathways involved in formation of the disulfide-rich structures are unknown, but it has been shown that peptides corresponding to the N-terminal region of carp granulin-1 and a human granulin A analogue fold autonomously with two disulfide bonds (19-21). Furthermore, we have recently shown that the N-terminal half of *Ov*-GRN-1 can also fold independently (7). This peptide contains three disulfide bonds, including a bond not present in the full-length, well-defined carp granulin-1 and zebrafish granulin AaE peptides (15, 18). Despite containing a non-native disulfide bond, this peptide displays a well-defined structure, potent cell proliferation and *in vivo* wound healing properties (6, 7).

It is not clear if the folding properties of the *Ov*-GRN-1 N-terminal peptide are unique to the parasite protein, or whether granulins from other sources can also fold independently with the first six cysteine residues present. There is significant sequence variation amongst granulin peptides, making accurate prediction of different folding properties difficult. Furthermore, there is no information available on the folding and structural properties of granulin peptides containing just the C-terminal region.

In the current study we have analysed the folding of the N-terminal region of human granulin A, the most abundant of the human granulins (22), and show that it can form a well-defined structure incorporating a non-native disulfide bond. We also show that the C-terminal region of *Ov*-GRN-1 truncated peptide does not fold independently, in contrast to the N-terminal region, but still displays bioactivity, albeit with lower potency than the proline mutants of *Ov*-GRN-1 previously studied (6) .

## 5.3 Experimental section

### 5.3.1 Peptide synthesis, purification and characterisation

Truncated granulin peptides were synthesised on a Protein Technologies PS3 synthesiser, using 2-chlorotrityl-chloride resin. The Fmoc amino acid derivatives (Auspep, Australia) were activated using HCTU (Iris, Germany) and coupled on the resin with DIPEA/DMF by stepwise solid-phase peptide synthesis chemistry. Peptides were cleaved from the solid support by treatment with a mixture of TFA:TIPS:H<sub>2</sub>O at ratios of 95%:2.5%:2.5% (v/v), followed by purging with nitrogen to evaporate TFA. Peptides were then precipitated in ice-cold diethyl ether and dissolved in 50% acetonitrile:50% H<sub>2</sub>O:0.1% TFA (v/v) and subsequently lyophilised. The crude peptides were purified by reversed-phase HPLC (RP-HPLC) on a Phenomenex Jupiter C18 preparative column (300 Å, 10 µm, 250 x 21.2 mm), using a gradient of 0-60% solvent B (Solvent A: 99.95% H<sub>2</sub>O:0.05% TFA; Solvent B: 90% acetonitrile:10% H<sub>2</sub>O:0.045% TFA) over 60 minutes. The collected fractions were characterised using a SCIEX 5800 MALDI TOF/TOF mass spectrometer (SCIEX, Foster city, CA) and then lyophilized.

### 5.3.2 Disulfide bond formation

Disulfide bonds were formed as described previously (6, 7). Reduced peptide (0.1 mg/mL) was dissolved in 0.1 M ammonium bicarbonate (pH 8-8.2) containing 5mM reduced glutathione at room temperature for up to 72 h. The presence of disulfide-bonded species was examined by removing aliquots from the folding mixture at selected time points and analysing them with analytical RP-HPLC using a Phenomenex Jupiter 4 µm Proteo column (150 x 2.00 mm, 90 Å). When the oxidation was completed, the oxidation solution was acidified with TFA and loaded on a C18 preparative column with a flow rate of 5 mL/min. The separation method was as follows: a gradient of 0-50% solvent B over 50 min. Fractions were collected and the peptide mass was analysed using a SCIEX 5800 MALDI TOF/TOF spectrometer.

### 5.3.3 NMR spectroscopy

Lyophilised peptide was dissolved in 90% H<sub>2</sub>O:10% D<sub>2</sub>O at a concentration of approximately 0.2 mM. All NMR spectra were acquired on a Bruker 600 MHz AVANCE III NMR spectrometer (Bruker, Karlsruhe, Germany). 2D <sup>1</sup>H-<sup>1</sup>H TOCSY, <sup>1</sup>H-<sup>1</sup>H NOESY, <sup>1</sup>H-<sup>1</sup>H DQF-COSY, collected at 290 K were used for sequence-specific assignments and structure calculations. <sup>1</sup>H-<sup>15</sup>N HSQC and <sup>1</sup>H-<sup>13</sup>C HSQC spectra were acquired for nitrogen and carbon chemical shifts respectively. Two-dimensional homonuclear NOESY and TOCSY spectra were acquired with a mixing time of 200 ms and a spin lock time of 80 ms respectively. All spectra were processed using Bruker TopSpin (Version 3.5pl7) and assigned using CCPNMR analysis 2.1 based on the approach described in Wüthrich et al (23).

### 5.3.4 Structure calculations

The three-dimensional structures of hGRNA4-28\_3s were calculated using the CYANA program, based on automated assignment of the NOEs (24). Torsion-angle restraints predicted by TALOS-N were used in the structure calculations (25). An ensemble of 100 structures was calculated and the 20 structures with the lowest target function chosen to represent the structures of hGRNA<sub>4-28\_3s</sub>. Structures were visualised using MOLMOL and the root-mean-square derivation (RMSD) values were assessed (26). The αH secondary shifts were determined by subtracting random coil <sup>1</sup>H NMR chemical shifts from the experimental αH chemical shifts (27).

### 5.3.5 Mammalian cell culture

The human skin normal fibroblast cell line, 1BR.3.GN (ECACC 90020509), was purchased from European Collection of Authenticated Cell Cultures (ECACC). The 1BR.3.GN fibroblasts were grown and maintained in DMEM/F12 (Life Technologies) containing 1× antibiotic/antimycotic and 1× GlutaMAX, supplemented with 10% fetal bovine serum (FBS) (Gibco,

Scotland) at 37°C and 5% CO<sub>2</sub>. Cell proliferation assays were performed with DMEM/F12 media supplemented with 10% FBS.

### **5.3.6 Cell proliferation monitoring in real time using xCELLigence**

An xCELLigence Real Time Cell Analyzer – Single Plate (RTCA SP) instrument (ACEA Biosciences) was used to evaluate cell proliferation as described previously (6, 7). Briefly, 1BR.3.GN cells (7,500 cells/well) were seeded into a 96-well xCELLigence E-plate (ACEA Biosciences). The E-plate was placed into the xCELLigence station and incubated at 37°C with 5% CO<sub>2</sub> and monitored overnight. The complete media was subsequently aspirated and replaced with 150 µL of starvation media (DMEM/F12 media supplemented with 0.5% FBS) and incubated overnight. Treatments in 10% media were added to each well in a total volume of 150 µL to provide 200 nM or 1 µM final concentrations in quadruplicate. Cells treated with a 20-residue peptide from tropomyosin (EADRKYDEVARKLAMVEADL) served as the negative control peptide (6, 7). Cell proliferation was monitored every 1 h for 7 days. The cell index (CI) was normalized to CI of the time-point when the treatments were added to the cells. The cell proliferation rate was calculated as CI for the treated cells compared to CI for peptide control cells (~100-120 hours in culture). Cell proliferation rates were compared between treatment and control wells, and statistical analyses were conducted using one-way ANOVA followed by Holm-Sidak's correction for multiple comparisons, using GraphPad prism 6.02.

## 5.4 Results

### 5.4.1 Design and synthesis of granulin peptide analogues

Three granulin peptide analogues were synthesised to provide insight into the structure-function relationships of granulin peptides. The sequences of the synthetic truncated peptides are provided in Table 5-1. To determine if the N-terminal region of human granulin A can fold in a similar way to the *Ov*-GRN-1 peptides, a 24-residue peptide, termed hGRNA<sub>4-28\_3s</sub>, was chemically synthesised. The design of this peptide is equivalent to the three-disulfide, 24-residue *Ov*-GRN-1 peptide analogue we previously synthesised (*Ov*-GRN<sub>12-35\_3s</sub>) (7).

Two additional *Ov*-GRN-1-derived peptides were also synthesised. One peptide corresponded to residues 9 to 35 (*Ov*-GRN<sub>9-35\_3s</sub>) and was synthesised to determine if the additional three residues, compared to *Ov*-GRN<sub>12-35\_3s</sub> (the prefix *Ov* has been added to the *Ov*-GRN-1 derived peptides to distinguish them from the human granulin peptide), stabilize the  $\beta$ -hairpin at the N-terminus. The second peptide corresponded to residues 39-66 (*Ov*-GRN<sub>39-66\_3s</sub>) and spans the region encompassing cysteine VII to cysteine XII. All peptides were synthesised using Fmoc solid-phase peptide synthesis on 2-chlorotrityl resin. The disulfide bonds were formed by air oxidation in 0.1 M ammonium bicarbonate and 5 mM glutathione at room temperature.

The analytical RP-HPLC traces of the oxidation reactions for hGRNA<sub>4-28\_3s</sub> and *Ov*-GRN<sub>9-35\_3s</sub> both contain a relatively sharp peak that eluted earlier than the other peaks (Figure 5-2). The folding profiles are consistent with previous studies on granulin peptides and indicate that the early eluting peak is likely to have a well-folded structure (6, 16, 18, 20, 21). The relative folding yield was calculated based on the area of early eluting peak relative to the total peak area. hGRNA<sub>4-28\_3s</sub> had a better folding yield (57%) compared to *Ov*-GRN<sub>9-35\_3s</sub> (43%). The early eluting peaks for these two peptides were purified to homogeneity by semi-preparative RP-HPLC.

**Table 5-1 Sequences of granulin peptides.**

Peptide	Sequence
hGRNA	DV <b>K</b> C-DMEV <b>S</b> CPDGY <b>T</b> CCRLQSGAW <b>G</b> CCPFTQAV <b>C</b> CEDH <b>I</b> HCCPAGFT <b>C</b> DTQKG <b>T</b> CE
hGRNA <sub>4-28_3s</sub>	<b>C</b> -DMEV <b>S</b> CPDGY <b>T</b> CCRLQSGAW <b>G</b> CC
Hybrid hGRNA <sup>#</sup>	<u>V</u> <b>V</b> <u>H</u> <b>C</b> -DMEV <b>I</b> <u>C</u> PDGY <b>T</b> <u>C</u> SRLPSGAW <b>G</b> <u>C</u> SPFT
Ov-GRN-1 <sup>*</sup>	...DTLQPIRSP <b>S</b> CPDPVY <b>T</b> CRPGQ <b>T</b> CCRGLHGY-GCCPMDSAT <b>C</b> SDLL <b>H</b> CCPHGT <b>A</b> CTAYGL <b>C</b> VRGD...
Ov-GRN <sub>39-66_3s</sub>	SAT <b>C</b> SDLL <b>H</b> CCPHGT <b>A</b> CTAYGL <b>C</b> VRGD
Ov-GRN <sub>9-35_3s</sub>	SP <b>S</b> CPDPVY <b>T</b> CRPGQ <b>T</b> CCRGLHGY-G <b>C</b> C
Ov-GRN <sub>12-35_3s</sub> <sup>#</sup>	CPDPVY <b>T</b> CRPGQ <b>T</b> CCRGLHGY-G <b>C</b> C
Carp granulin-1 <sup>#</sup>	VI <b>H</b> C-DAATI <b>C</b> PDG <b>T</b> T <b>C</b> CLSPYGVWY <b>C</b> C

Hyphen (-) indicates a sequence gap. Cysteine residues are shown in bold. The sequences of the peptides synthesised in the current study are highlighted in blue. <sup>\*</sup>Residues 20-84 of the *Ov*-GRN-1 sequence are shown in this table, (...) indicates the sequence that is not presented here. <sup>#</sup>The sequences of the previously studied hybrid hGRNA(1), *Ov*-GRN<sub>12\_35\_3s</sub>(1, 2) and carp granulin-1, are cited accordingly and presented in this table just for comparison purposes. The replaced residues in hybrid hGRNA, relative to the wild type sequence, are underlined (1-5).



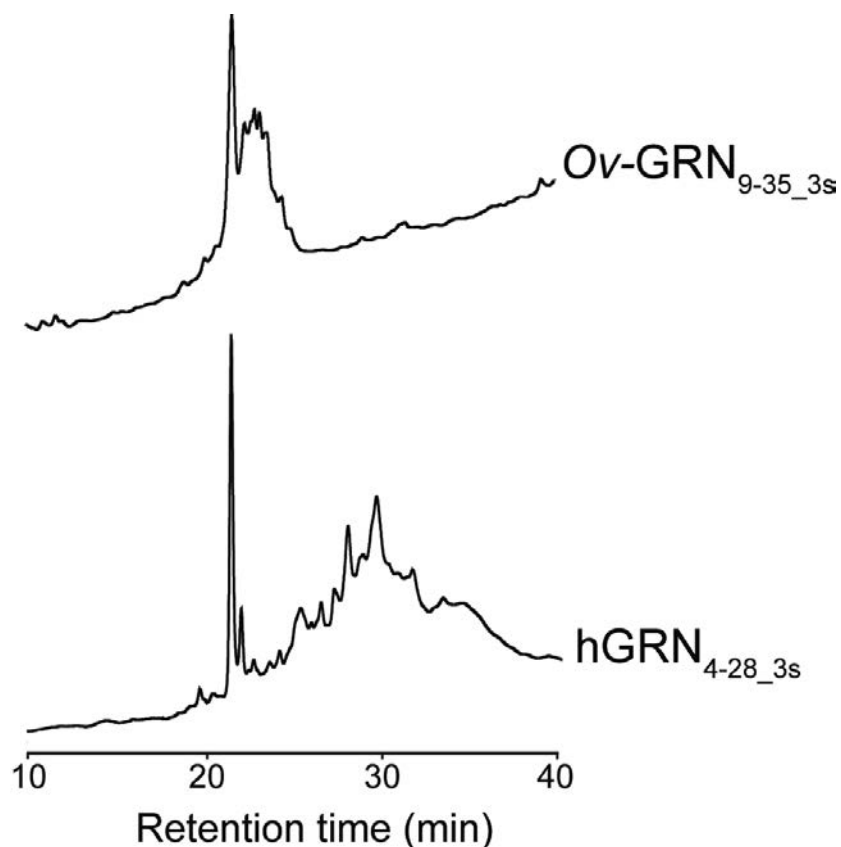


**Figure 5-2 HPLC analysis of the oxidation reaction of granulin N-terminal truncated analogues,  $Ov$ -GRN<sub>9-35\_3s</sub> and hGRN<sub>4-28\_3s</sub>.** Analytical HPLC was carried out using reversed phase HPLC with a Phenomenex Jupiter Proteo C<sub>12</sub> analytical column.

By contrast, the RP-HPLC trace for the oxidation of the C-terminal fragment of  $Ov$ -GRN-1,  $Ov$ -GRN<sub>39-66\_3s</sub>, does not contain a sharp, early eluting peak. Analysis of the fractions collected from the preparative RP-HPLC using a SCIEX 5800 MALDI TOF/TOF MS spectrometer shows that a mixture of fully oxidised and partially oxidised products are present in the oxidation solution following a 82 hour oxidation time (Figure 5-3). The purified fraction obtained for fully oxidised  $Ov$ -GRN<sub>39-66\_3s</sub> was a mixture of poorly resolved isomers, which could not be purified to homogeneity.

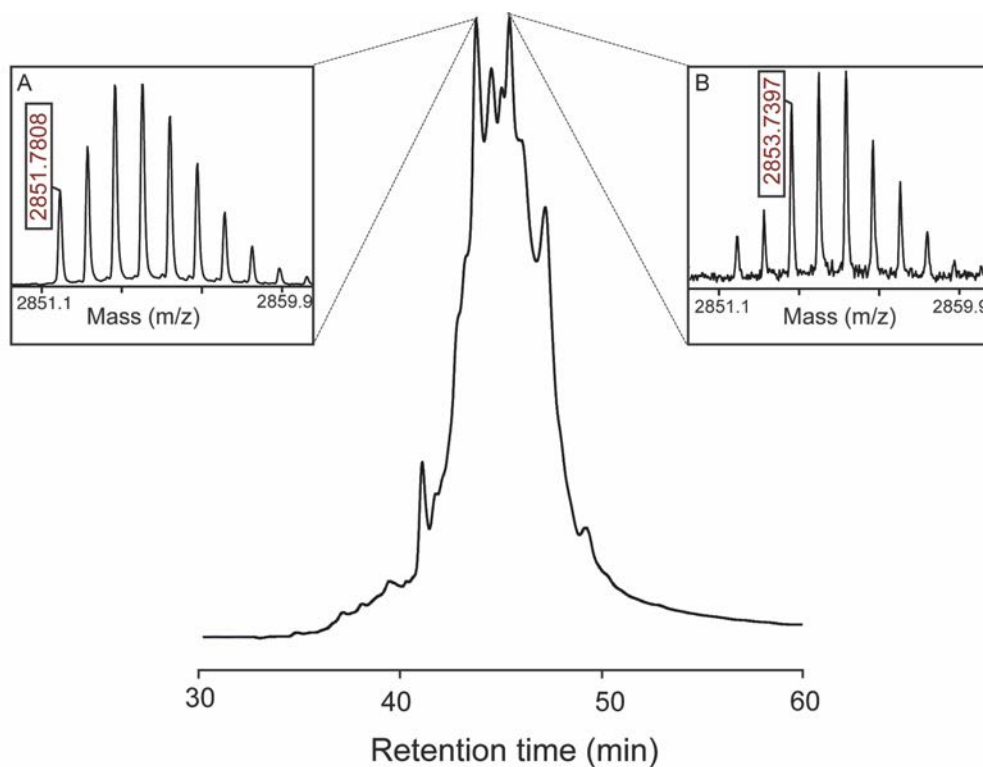


**Figure 5-3 HPLC and mass analysis of the *Ov*-GRN<sub>39-66\_3s</sub> oxidation reaction.** The oxidation mixture was fractionated using a C<sub>18</sub> preparative RP-HPLC column following 82 hours of oxidation. The masses of different *Ov*-GRN<sub>39-66\_3s</sub> disulfide bond isomers eluting at different time points are shown in boxes A and B. (A) Box A shows the ((*M* + *H*)<sup>+</sup> charged ion at (*m/z*)= 2851.7808), which corresponds to fully oxidised *Ov*-GRN<sub>39-66\_3s</sub>. (B) Box B shows the ((*M* + *H*)<sup>+</sup> charged ion at (*m/z*)= 2853.7397), which corresponds to the partially oxidised *Ov*-GRN<sub>39-66\_3s</sub> with 2 disulfide bonds. The non-symmetric isotope pattern in box B indicates the presence of some traces of fully oxidised product from adjacent peaks.

#### 5.4.2 Structural analysis with NMR spectroscopy

The structures of the purified or partially purified fractions of truncated peptides in solution were analysed using NMR spectroscopy. One-dimensional proton NMR spectra of hGRNA<sub>4-28\_3s</sub> and *Ov*-GRN<sub>9-35\_3s</sub> showed large chemical shift dispersion in the amide region (Figure 5-4), consistent with peptides containing  $\beta$ -sheet structure. By contrast, the NMR spectrum of *Ov*-GRN<sub>39-66\_3s</sub> (Figure 5-4), has limited dispersion in the amide region, and broad peaks consistent with an unstructured peptide.

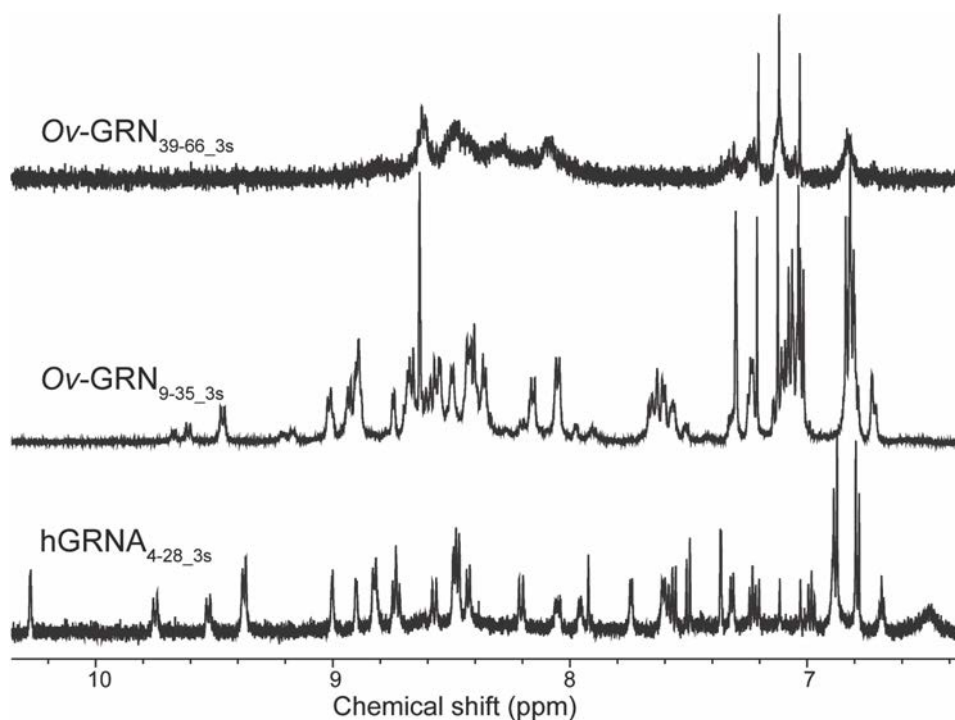


**Figure 5-4 One-dimensional proton NMR spectra for granulin N-terminal truncated analogues.** Spectra are shown from 6 to 10.5 ppm; This region contains primarily the amide protons. *Ov-GRN*<sub>9-35\_3s</sub>, and *hGRNA*<sub>4-28\_3s</sub> have significant chemical shift dispersion in this region compared to the limited dispersion for *Ov-GRN*<sub>39-66\_3s</sub>.

Secondary shift analysis suggested that the overall structure for *hGRNA*<sub>4-28\_3s</sub> and *Ov-GRN*<sub>9-35\_3s</sub> is similar to the previously studied peptide, *Ov-GRN*<sub>12-35\_3s</sub> (Figure 5-5). The *hGRNA*<sub>4-28\_3s</sub> three-dimensional structure was calculated using distance and dihedral angle restraints derived from one- and two-dimensional homonuclear <sup>1</sup>H NMR experiments. The refinement statistics are given in Table 5-2. As illustrated in Figure 5-6, *hGRNA*<sub>4-28\_3s</sub> looks similar in conformation to *Ov-GRN*<sub>12-35\_3s</sub>, in agreement with the secondary H $\alpha$  chemical shift analysis. Comparison of the 20 lowest energy structures for *hGRNA*<sub>4-28\_3s</sub> and *Ov-GRN*<sub>12-35\_3s</sub> indicates that the peptides share a  $\beta$ -hairpin structure at the C-terminal region. D<sub>2</sub>O exchange experiments indicated that *hGRNA*<sub>4-28\_3s</sub> has 12 slowly exchanging amide protons, whereas the previously studied *Ov-GRN*<sub>12-35\_3s</sub> peptide had eight slowly exchanging amide protons, indicating that *hGRNA*<sub>4-28\_3s</sub> might have a more stable structure.

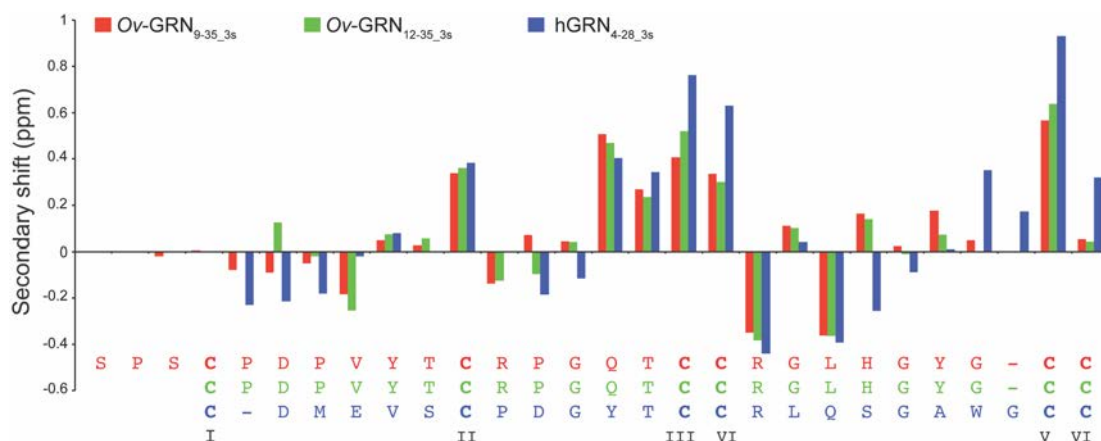


**Figure 5-5  $\alpha$ H Secondary-shift comparison for truncated granulin analogues.** The  $\alpha$ H secondary shifts were calculated by subtracting the random coil  $^1\text{H}$  NMR chemical shifts previously reported by Wishart et al. (27) from the experimental  $\alpha$ H chemical shifts. The color used for each peptide is shown at top of the diagram. The sequences of *Ov*-GRN<sub>12-35\_3s</sub> (green), *Ov*-GRN<sub>9-35\_3s</sub> (red), and hGRNA<sub>4-28\_3s</sub> (blue) are given at the bottom of the diagram.

**Table 5-2 Structural statistics for hGRNA<sub>4-28\_3s</sub>**

### Experimental restraints

Interproton distance restraints

*Intraresidue*,  $|i-j|=0$  37

*Sequential*,  $|i-j|=1$  34

*Medium range*,  $1 < |i-j| < 5$  4

*Long range*,  $|i-j| \geq 5$  17

Disulfide-bond restraints 3

Dihedral-angle restraints 32

Hydrogen bond restraints (3 restraints per bond) 9

### R.m.s. deviations from mean coordinate structure (Å)

Backbone atoms  $1.57 \pm 0.52$

All heavy atoms  $2.51 \pm 0.75$

### Ramachandran Statistics

% in most favoured region 87.8

% Residues in additionally allowed regions 12.2

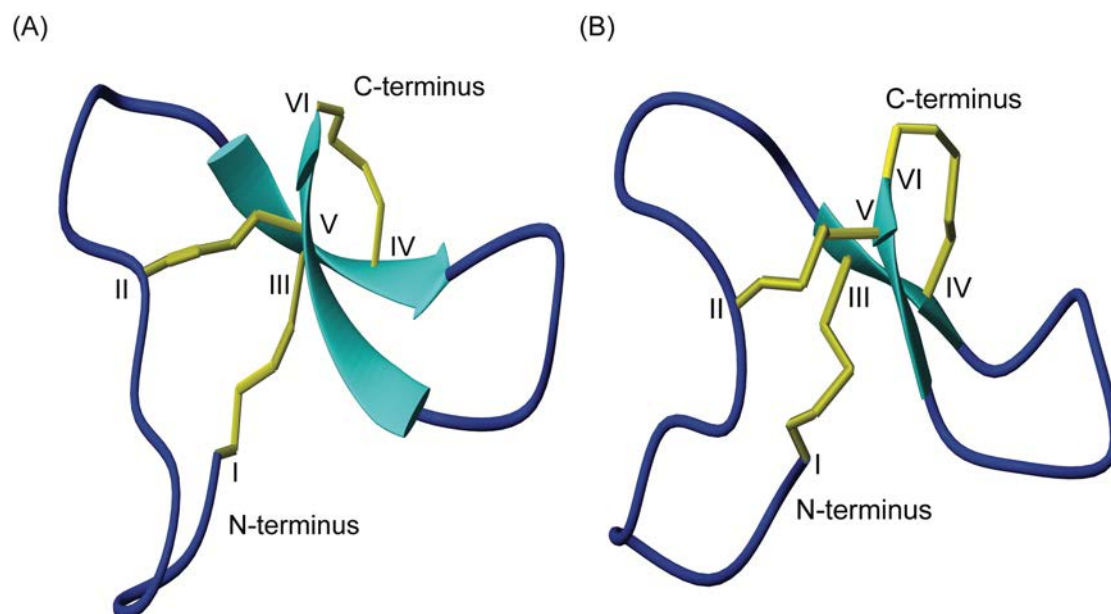


**Figure 5-6** A comparison of the three-dimensional structure of (A) hGRNA<sub>4-28\_3s</sub> (PDB ID: 6NUG) and (B) *Ov*-GRN<sub>12-35\_3s</sub> (PDB ID: 5UJG). Ribbon representations are of the lowest energy structures from ensembles of 20 structures. Disulfide bonds are shown as yellow sticks and only the backbone atoms are displayed. The figure was prepared using MOLMOL (26).

### 5.4.3 Cell proliferation monitoring in real time using xCELLigence

The effect of the truncated granulin analogues on the growth of 1BR.3.GN fibroblasts was evaluated using an xCELLigence system. 1BR.3.GN is a human fibroblast skin cell line derived from a transformed normal fibroblast. Cells were cultured with two concentrations of the peptides, 200 nM and 1  $\mu$ M (Figure 5-7). *Ov-GRN<sub>9-35-3s</sub>* showed an effect on cell proliferation with an increase in cell number by 114% ( $P<0.01$ ) and 117% ( $P<0.001$ ) at 200 nM and 1  $\mu$ M, respectively. Cells cultured in the presence of 1  $\mu$ M *Ov-GRN<sub>39-66-3s</sub>* had increased cell survival (121%,  $P<0.0001$ ) compared to the control peptide. No significant effect on cell growth was observed at 200 nM (Figure 5-7). Although the *Ov-GRN-1* truncated peptides had cell proliferation activity, *hGRNA<sub>4-28-3s</sub>* did not promote significant growth of 1BR.3.GN cells at concentrations up to 1  $\mu$ M.

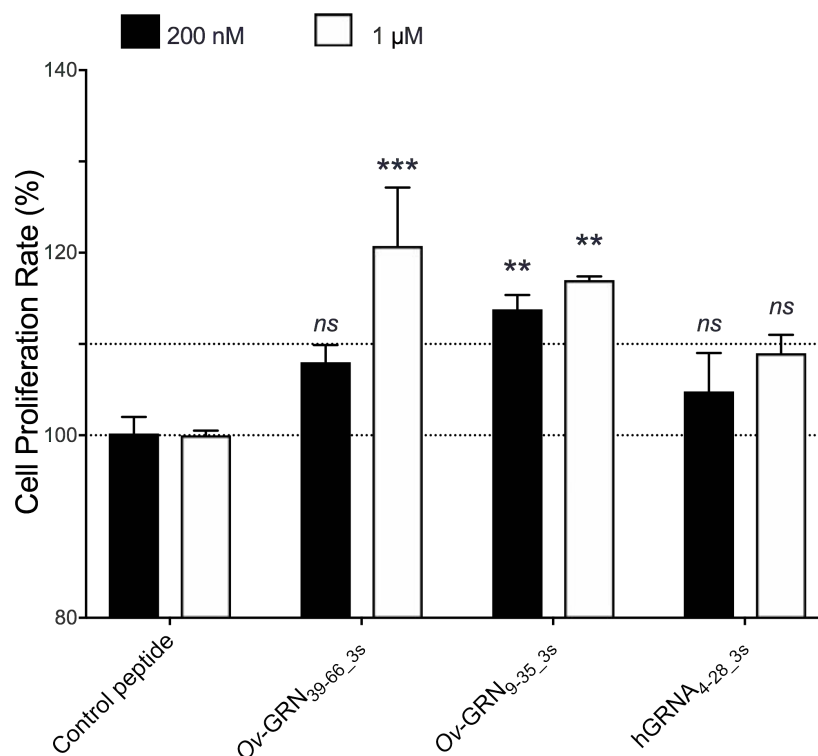


**Figure 5-7 xCELLigence fibroblasts cell proliferation assay.** Fibroblast cells were treated with peptides at 200 nM (black) and 1  $\mu$ M (white). Cell index was measured after 60-72 hour post treatment. Data represent mean  $\pm$  SEM of three independent experiments. Data were analyzed by one-way ANOVA against peptide control (Not significant = ns, \*\*  $P<0.01$ , \*\*\*  $P<0.001$ ).

## 5.5 Discussion

Insight into the structure-activity relationships of granulin proteins is just beginning to emerge, but studies have already highlighted the complexity associated with this family. Here we show that the *Ov*-GRN-1 N-terminal and C-terminal regions have distinct folding properties and that regular secondary structure is not critical for enhancing the rate of cell proliferation. Understanding the processes involved in granulin folding and bioactivity is likely to facilitate the development of novel wound healing agents based on the granulin scaffold.

We have shown that a 24-residue peptide from the N-terminal region of human granulin A, containing half of the highly conserved cysteine motif, can fold independently into a well-defined structure with a  $\beta$ -hairpin as the main element of secondary structure. This peptide contains a non-native disulfide bond (Cys IV to VI), analogous to our previous studies on a truncated form of *Ov*-GRN-1 (*Ov*-GRN<sub>12-35\_3s</sub>) (7). The structures of hGRNA<sub>4-28\_3s</sub> and *Ov*-GRN<sub>12-35\_3s</sub> are similar despite the sequence differences (the peptides have 42% sequence identity), suggesting that independent folding of the first six cysteine residues in the granulin scaffold might be a common feature.

It is not readily apparent why the N-terminal region of granulins would fold independently incorporating a non-native disulfide bond, as most granulin modules are expressed as 12 cysteine-containing proteins and appear to form a ladder arrangement of the disulfide bonds where Cys IV is bonded to Cys VII and Cys VI is bonded to Cys IX (refer to Figure 5-1A for disulfide bond connectivity) (16, 18, 28). However, this unusual folding property might be related to the paraganulin modules that contain only six cysteine residues (12, 16, 28), and which based on our results are also likely to contain the Cys IV to Cys VI bond.

Although hGRNA<sub>4-28\_3s</sub> displayed a well-defined structure, its effect on fibroblast cell proliferation was not statistically significant at concentrations up to 1  $\mu$ M. This lack of bioactivity might not be surprising given that rat

epithelin-1, a protein with a very similar sequence to hGRN A, does not induce fibroblast proliferation (29) and hGRN A inhibits the growth of several human cancer cells via an apoptotic pathway (16, 28-32) rather than promoting cell growth. The low sequence similarity between hGRNA<sub>4-28\_3s</sub> and *Ov*-GRN<sub>9-35\_3s</sub>, indicates that the *Ov*-GRN-1 cell proliferation activity is related to the peptide sequence.

Previous studies have shown that a human granulin A peptide containing only two disulfide bonds (Cys I-Cys III and Cys II-Cys V) does not form a well-defined structure, in contrast to carp granulin-1 and plant-like granulin truncated analogues (7, 16, 20, 21, 33). Hydrophobic interactions have a critical contribution to stabilization of the overall fold of carp granulin-1 and plant granulin-like analogues (20, 21, 33). Based on the importance of these interactions a fragment of hGRNA (residues 1-30) containing four substitutions was designed and shown to contain a  $\beta$ -hairpin structure. The sequence of this hybrid peptide is given in Table 5-1 (16). Interestingly, superposition of the backbone atoms of hGRNA<sub>4-28\_3s</sub> and the previously studied hybrid hGRNA peptide (19) shows the overall fold is very similar (Figure 5-8). Therefore, these findings suggest that forming a non-native disulfide bond effectively compensates for the lack of structure in a truncated version of hGRNA, in a similar manner to the hydrophobic substitutions (16).

In addition to the relatively minor substitutions in hGRNA having a significant influence on folding and structure (19), it has previously been shown that minor changes in the carp granulin-1 sequence can have an effect on structure. Analysis of carp granulin-1 peptides containing residues 1-30 and residues 3-30 showed that the former had a more well defined structure than the latter (20, 21). By contrast, in the current study we show that addition of three N-terminal residues to a truncated *Ov*-GRN-1 peptide did not influence the overall fold based on secondary structure analysis (Figure 5-5) adding to the complexity of the structure-function relationships of granulin peptides.



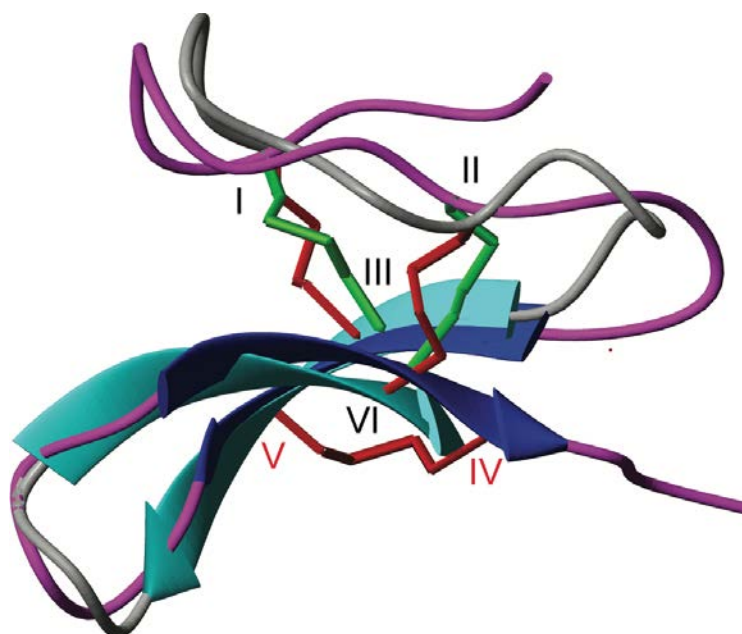


**Figure 5-8 Superposition of the structures of the hGRNA<sub>4-28\_3s</sub> and the hybrid hGRNA N-terminal truncated peptides.** The  $\beta$ -hairpins are shown as arrows, and for hGRNA<sub>4-28\_3s</sub> (PDB ID: 6NUG) it is shown in cyan, and for hybrid hGRNA (PDB: 1G26) (19) in dark blue. Disulfide bonds are shown as yellow sticks and cysteine residues are labelled using Roman numerals. The cysteine residues involved in forming the non-native disulfide bond (IV-VI) in hGRNA<sub>4-28\_3s</sub> are labelled with red letters. The figure was prepared using MOLMOL (26).

No folding or bioactivity studies have previously been reported on the C-terminal regions of granulins. We show for the first time that the C-terminal region of *Ov*-GRN-1, comprising the second half of the 12 cysteine motif (*Ov*-GRN<sub>39-66\_3s</sub>), does not fold into one major isomer following an extended oxidation time of 82 hours. It is possible that the non-native disulfide bond interferes with the correct folding in the C-terminal truncated analogue, unlike the N-terminal analogues. In addition, the highly-conserved cysteine spacing is also inverted in the C-terminal half of the molecule compared to the N-terminal region, as shown for *Ov*-GRN-1 in Table 5-1, and this is likely to influence the folding.

Although *Ov*-GRN<sub>39-66\_3s</sub> could not be purified to homogeneity, a fraction that was fully-oxidised was analysed in the fibroblast proliferation assay and displayed a similar level of activity to *Ov*-GRN<sub>9-35\_3s</sub>. This result indicates that the structure might not be critical for the cell proliferation bioactivity of *Ov*-GRN-1. Furthermore, there is limited sequence homology between the two halves of *Ov*-GRN-1 and further study is required to determine residues important for bioactivity. Our results for the C-terminal region of *Ov*-GRN-1 are consistent with previous studies on human granulin B, which indicate that this protein is intrinsically disordered but significantly induces NF- $\kappa$ B activation in SY-SH5Y human neuroblastoma cells in a dose-dependent manner (34).

Overall, this study has shown that a non-native disulfide bond has an important role in stabilising a well-defined structure in the N-terminal region of truncated granulin peptides. Furthermore, *Ov*-GRN-1-induced cell proliferation does not appear to be dependent on structure alone, but rather on the unique peptide sequence. However, the mechanism of action of granulin peptides has yet to be established, and it is possible that upon binding to a biological target, structure might be induced.

## 5.6 Acknowledgements

MD would like to thank James Cook University for a PhD scholarship. This work was supported by the Merchant Foundation and by the National Health and Medical Research Council by a Senior Principal Research Fellowship to AL (1117504) The James Cook University NMR facility was partially funded by the Australian Research Council (LE120100015, LE160100218). Support from award CA164719 from the National Cancer Institute, National Institutes of Health (NIH) to MJS and AL is gratefully acknowledged. The content is solely the responsibility of the authors and does not necessarily represent the official views of the NIH.

## 5.7 Non-standard abbreviations

HCTU, (2-(6-Chloro-1-H-benzotriazole-1-yl)-1,1,3,3-tetramethylaminium hexafluorophosphate); DIPEA, Ethyldiisopropylamine; TOCSY, Total Correlated Spectroscopy; ECACC, European Collection of Authenticated Cell Cultures; DMEM/F12, Dulbecco's Modified Eagle Medium: Nutrient Mixture F-12; HEPES, 4-(2-hydroxyethyl)-1-piperazineethanesulfonic acid; FBS, Fetal Bovine Serum; CI, Cell Index; RP-HPLC, reversed phase HPLC; D<sub>2</sub>O, Deuterium Oxide; DQF-COSY, Double-quantum filtered correlation spectroscopy; ANOVA, ANalysis Of Variance; LC-MS, Liquid chromatography-mass spectroscopy;

## 5.8 References

1. Bhutia, S.K. and T.K. Maiti. Targeting tumors with peptides from natural sources. *Trends Biotechnol.* 2008; 26(4): 210-7.
2. Edwards, C., M. Cohen, and S. Bloom. Peptides as drugs. *QJM: Int. J. Med.* 1999; 92(1): 1-4.
3. Smout, M.J., et al. A granulin-like growth factor secreted by the carcinogenic liver fluke, *Opisthorchis viverrini*, promotes proliferation of host cells. *PLoS Pathog.* 2009; 5, DOI: 10.1371/journal.ppat.1000611.
4. Smout, M.J., J.P. Mulvenna, M.K. Jones, and A. Loukas. Expression, refolding and purification of *Ov*-GRN-1, a granulin-like growth factor from the carcinogenic liver fluke, that causes proliferation of mammalian host cells. *Protein expression and purification.* 2011; 79(2): 263-70.
5. Papatpremsiri, A., M.J. Smout, A. Loukas, P.J. Brindley, B. Sripa, and T. Laha. Suppression of *Ov*-grn-1 encoding granulin of *Opisthorchis viverrini* inhibits proliferation of biliary epithelial cells. *Exp. Parasitol.* 2015; 148: 17-23.
6. Dastpeyman, M., et al. Structural Variants of a Liver Fluke Derived Granulin Peptide Potently Stimulate Wound Healing. *J. Med. Chem.* 2018; 61(19): 8746-53.
7. Bansal, P.S., et al. Development of a potent wound healing agent based on the liver fluke granulin structural fold. *J. Med. Chem.* 2017; 60(10): 4258-66.
8. Botelho, M.C., H. Alves, and J. Richter. Wound healing and cancer progression in *Opisthorchis viverrini* associated cholangiocarcinoma. *Parasitol. Res.* 2016; 115(7): 2913-4.
9. Smout, M.J., et al. Carcinogenic Parasite Secretes Growth Factor That Accelerates Wound Healing and Potentially Promotes Neoplasia. *PLoS Pathog.* 2015; 11, DOI: 10.1371/journal.ppat.1005209.
10. Haugen, B., S.E. Karinshak, V.H. Mann, A. Popratiloff, A. Loukas, P.J. Brindley, and M.J. Smout. Granulin Secreted by the Food-Borne Liver Fluke *Opisthorchis viverrini* Promotes Angiogenesis in Human Endothelial Cells. *Front. Med.* 2018; 5, DOI: 10.3389/fmed.2018.00030.
11. Zheng, S., Y. Zhu, Z. Zhao, Z. Wu, K. Okanurak, and Z. Lv. Liver fluke infection and cholangiocarcinoma: a review. *Parasitol. Res.* 2017; 116(1): 11-9.
12. Dastpeyman, M., M.J. Smout, D. Wilson, A. Loukas, and N.L. Daly. Folding of granulin domains. *Peptide Sci.* 2018: 10.1002/pep2.24062.

13. Bateman, A. and H.P. Bennett. The granulin gene family: from cancer to dementia. *BioEssays*. 2009; 31(11): 1245-54.
14. Bateman, A. and H. Bennett. Granulins: the structure and function of an emerging family of growth factors. *J. Endocrinol.* 1998; 158(2): 145-51.
15. Hrabal, R., Z. Chen, S. James, H.P. Bennett, and F. Ni. The hairpin stack fold, a novel protein architecture for a new family of protein growth factors. *Nat. Struct. Biol.* 1996; 3(9): 747-52.
16. Tolkmachev, D., et al. Structure dissection of human progranulin identifies well-folded granulin/epithelin modules with unique functional activities. *Protein Sci.* 2008; 17(4): 711-24.
17. Palfree, R.G., H.P. Bennett, and A. Bateman. The Evolution of the Secreted Regulatory Protein Progranulin. *PLoS One.* 2015; 10, DOI: 10.1371/journal.pone.0133749.
18. Wang, P., B. Chitramuthu, A. Bateman, H.P.J. Bennett, P. Xu, and F. Ni. Structure dissection of zebrafish progranulins identifies a well-folded granulin/epithelin module protein with pro-cell survival activities. *Protein Sci.* 2018; 27(8): 1476-90.
19. Tolkmachev, D., A. Ng, W. Vranken, and F. Ni. Design and solution structure of a well-folded stack of two  $\beta$ -hairpins based on the amino-terminal fragment of human granulin A. *Biochemistry.* 2000; 39(11): 2878-86.
20. Vranken, W.F., Z.G. Chen, P. Xu, S. James, H.P. Bennett, and F. Ni. A 30-residue fragment of the carp granulin-1 protein folds into a stack of two beta-hairpins similar to that found in the native protein. *J. Pept. Res.* 1999; 53(5): 590-7.
21. Vranken, W.F., S. James, H.P. Bennett, and F. Ni. Solution structures of a 30-residue amino-terminal domain of the carp granulin-1 protein and its amino-terminally truncated 3-30 subfragment: implications for the conformational stability of the stack of two beta-hairpins. *Proteins.* 2002; 47(1): 14-24.
22. Bateman, A., D. Belcourt, H. Bennett, C. Lazure, and S. Solomon. Granulins, a novel class of peptide from leukocytes. *Biochem. Biophys. Res. Commun.* 1990; 173(3): 1161-8.
23. Wüthrich, K. NMR studies of structure and function of biological macromolecules (Nobel Lecture). *J. Biomol. NMR.* 2003; 27(1): 13-39.
24. Guntert, P. Automated NMR structure calculation with CYANA. *Methods Mol. Biol.* 2004; 278: 353-78.
25. Shen, Y. and A. Bax. Protein structural information derived from NMR chemical shift with the neural network program TALOS-N. *Methods Mol. Biol.* 2015; 1260: 17-32.

26. Koradi, R., M. Billeter, and K. Wüthrich. MOLMOL: a program for display and analysis of macromolecular structures. *J. Mol. Graphics*. 1996; 14(1): 51-5, 29-32.
27. Wishart, D.S., et al.  $^1\text{H}$ ,  $^{13}\text{C}$  and  $^{15}\text{N}$  chemical shift referencing in biomolecular NMR. *J. Biomol. NMR*. 1995; 6(2): 135-40.
28. Bhandari, V., R. Palfree, and A. Bateman. Isolation and sequence of the granulin precursor cDNA from human bone marrow reveals tandem cysteine-rich granulin domains. *Proc. Natl. Acad. Sci. U.S.A.* 1992; 89(5): 1715-9.
29. Shoyab, M., V.L. McDonald, C. Byles, G.J. Todaro, and G.D. Plowman. Epithelins 1 and 2: isolation and characterization of two cysteine-rich growth-modulating proteins. *Proc. Natl. Acad. Sci. U.S.A.* 1990; 87(20): 7912-6.
30. Qiao, G., et al. Granulin A Synergizes with Cisplatin to Inhibit the Growth of Human Hepatocellular Carcinoma. *Int. J. Mol. Sci.* 2018; 19, DOI: 10.3390/ijms19103060.
31. Chen, X., et al. Interaction between granulin A and enolase 1 attenuates the migration and invasion of human hepatoma cells. *Oncotarget*. 2017; 8(18): 30305-16.
32. Wang, X., H. Xu, X. Chen, Y. Tian, F. Wang, and X. Lin. Cloning, expression and cytotoxicity of granulin A, a novel polypeptide contained in human progranulin. *Biosci. Trends*. 2016; 10(3): 181-7.
33. Tolkatchev, D., P. Xu, and F. Ni. A peptide derived from the C-terminal part of a plant cysteine protease folds into a stack of two beta-hairpins, a scaffold present in the emerging family of granulin-like growth factors. *J. Pept. Res.* 2001; 57(3): 227-33.
34. Ghag, G., L.M. Wolf, R.G. Reed, N.P. Van Der Munnik, C. Mundoma, M.A. Moss, and V. Rangachari. Fully reduced granulin-B is intrinsically disordered and displays concentration-dependent dynamics. *Protein Eng. Des. Sel.* 2016; 29(5): 177-86.

# **Chapter 6. Conclusions and Future Directions**

## 6.1 Conclusions

Disulfide-rich peptides are widely distributed in nature and the disulfide bonds generally play a crucial role in enforcing the native conformation of this class of peptides and proteins (1-4). The potential of a range of disulfide-rich peptides as novel therapeutics or diagnostic agents is currently being explored (5-9). One such promising peptide is chlorotoxin, a 36-residue peptide originally isolated from scorpion venom, which is being pursued as an imaging agent (BLZ-100) (10-13) and angiogenesis inhibitor ( $^{131}\text{I}$ -TM-601) (14-16). *Ov*-GRN-1 from the carcinogenic liver fluke *Opisthorchis viverrini*, has potential as a wound healing agent but the protein is difficult to make in high yields (17-22). Downsizing and exploring the structure-function relationships of chlorotoxin and *Ov*-GRN-1 was the focus of this thesis.

Chapter 2 of this thesis addressed the recent study that has shown fully reduced chlorotoxin, despite being unstructured in solution, has biological effects. This finding suggested that the inter-cysteine loops might be responsible for the bioactivity, and here we confirmed this hypothesis by showing small, unstructured regions of chlorotoxin displayed bioactivity and cell internalisation. The outcomes from this chapter provide insight into the structure-function relationships of chlorotoxin, which might facilitate its use as a cancer treatment agent.

Chlorotoxin has the potential to significantly increase the success of surgery, a cornerstone in the treatment of cancer (23). However, the mechanism of action of chlorotoxin is largely unknown (24). Deciphering its structure-function relationships might lead to the design of new lead molecules based on the chlorotoxin scaffold with more specific applications. Interestingly, in a study that was published while our chlorotoxin truncation study was “under review”, the C-terminal region of chlorotoxin was used to develop a cyclic peptide, miniCTX3, that effectively passes through the blood brain barrier (BBB) (25). MiniCTX3 corresponds to residues 30-35 of chlorotoxin and was conjugated to gold nanoparticles to increase the permeability of this biomedical cargo (25). This study further suggests that CTX-4, corresponding to residues 28-36 of chlorotoxin, might be useful for the development of new tumour-imaging agents.



The overall objective for Chapters 3 and 4 was to downsize *Ov*-GRN-1 into a bioactive peptide, because low yields of the recombinant protein limited its potential as a therapeutic agent. The specific aim of Chapter 3 was engineering bioactive peptides from the N-terminal region of *Ov*-GRN-1 with similar potency to the full-length protein in a mouse wound-healing assay. This aim was achieved through the development of a suite of peptides, including a 24 residue peptide, *Ov*-GRN<sub>12-35\_3s</sub>, which contains a unique structure. Although the non-native disulfide bond incorporated into this peptide was shown to be critical for formation of  $\beta$ -hairpin structure, it was not critical for wound healing bioactivity, because peptides with only two disulfide bonds also had wound healing activity.

Following on from the findings from Chapter 3, in Chapter 4 the influence of the proline residues on *Ov*-GRN<sub>12-35\_3s</sub> folding yield, structure and activity was analysed. *Ov*-GRN<sub>12-35\_3s</sub> was chosen for further study because it was the shortest peptide analysed, making it potentially cheaper to produce, and it contained the most well-defined structure, which could potentially have an impact on stability. Despite the relatively well-defined structure of *Ov*-GRN<sub>12-35\_3s</sub> compared to the two-disulfide bond analogues, it still displayed multiple conformations in solution most likely due to isomerisation of the proline residues. Mutation of the proline residues indicated that each of the three proline residues had a role in the multiple conformations, and importantly an influence on the folding yields, indicating that the proline residues have a direct influence on the folding pathways. Removal of proline 4 significantly improved the folding yield and enhanced the wound healing activity *in vivo*. Understanding why removal of this proline residue improved bioactivity will only be fully rationalised when the biological target has been elucidated, but it is possible that the conformational flexibility lowers the binding affinity. The wound healing potency of GRN<sub>P4A</sub> surpasses that observed for Regranex, a growth factor approved for human clinical use for wound healing (26, 27).

Chapter 5 shed light on the folding properties and bioactivity of the C-terminal region of *Ov*-GRN-1. This study showed that although the C-terminal region does not independently fold into a well-defined structure, in contrast to the N-terminal region, it was still able to promote fibroblast cell proliferation. Furthermore, regarding the

sequence diversity in granulin proteins it was important to determine the influence of sequence variation on wound healing properties. Hence, the other specific aim of Chapter 5 was to assess the structure and bioactivity of a fragment of human granulin A equivalent to the *Ov*-GRN-1 N-terminal fragment. The results suggest that even though the human granulin A N-terminal truncated analogue also folds independently with three disulfide bonds into a similar structure as *Ov*-GRN<sub>12-35\_3s</sub>, it does not significantly induce fibroblast cell proliferation. The results obtained from this chapter expand the knowledge of the structure activity relationships of the granulin family of protein and in particular for *Ov*-GRN-1.

The *Ov*-GRN-1 studies carried out as part of this thesis have the potential to lead to the development of a drug lead for wound healing. New treatments for wound healing are particularly needed for treating diabetic patients (28, 29). Diabetics have a 25% lifetime risk of developing foot ulcers that can develop into non-healing wounds (29-32). With diabetic foot ulcers being the second leading cause of diabetes related mortality, second only to cardiovascular disease (31, 33, 34), we need new treatments for wound healing to improve the quality of life of the significant proportion of Australians at risk of diabetic complications. Diabetes is a particularly severe health issue in Indigenous populations with higher proportions and earlier age of onset than non-Indigenous populations (35-38). There are reports in the Northern Territory that more than 90% of people with diabetes admitted to hospital with feet problems are Indigenous ([www.healthinfonet.ecu.edu.au](http://www.healthinfonet.ecu.edu.au)). Being able to engineer versions of *Ov*-GRN-1 that are smaller and therefore less likely to be immunogenic, more stable and cheaper to manufacture is likely to enhance its potential as a drug lead.

Overall, the studies in this thesis highlight the potential of disulfide-rich peptides as well as the importance of structure-function studies for developing more potent analogues and for improving production efficiency. This thesis has also expanded the studies utilizing the approach of down-sizing peptides/proteins, which has previously been applied to proteins such as DNA-binding proteins (39) and Bcl2 homology proteins (40), and confirms this approach can be valuable for the design of novel drug leads. Interestingly, in both the chlorotoxin and granulin studies, there were examples of peptides that did not have well-defined structures in solution but were still bioactive. It is often thought that the structure of disulfide-rich peptides is critical for

bioactivity (8, 41, 42), but this is not always the case and further study is required to fully understand how peptides such as chlorotoxin and granulin interact with their biological targets. Suggested future directions are outlined below.

## 6.2 Future directions

The studies on chlorotoxin suggest that a small stretch from the C-terminal region is involved in anti-migration bioactivity. Although the identification of a bioactive region in chlorotoxin has potential for the design of novel lead molecules for tumour imaging, there are limitations associated with these small, unconstrained peptides. The chlorotoxin fragments that showed binding or bioactivity (CTX-3 and CTX-4) were highly unstable in serum. Hence, improving stability is likely to be required if they are to be developed as drug leads. In this regard, a recent study has shown that the enzymatic stability of a six-residue peptide comprising residues 30-35 of chlorotoxin was successfully increased by replacing the cysteine residues with diaminopropionic acids to form a lactam bridge (25). In addition, there are several other strategies available to improve the stability of peptides, including binding acylated peptides to albumin which has been successfully done to increase the half-life of a heptapeptide in human plasma (43).

To confirm the cell internalization result observed with the chlorotoxin fragments, specific inhibitors are needed to be used such as filipin, which inhibits caveolae-dependent endocytosis, amiloride, which inhibits non-selective macropinocytosis, and chlorpromazine, which inhibits clathrin-dependent intracellular transport of coated pits (44). Extensive studies on a range of cell lines could also be carried out to further confirm that CTX-4 has tumour cell type specific activity/internalization. Moreover, synthesising and characterisation of over-lapping fragments from the C-terminal region and point mutagenesis study might be useful to discern the residues important for bioactivity.

The protein array result identifying cortactin as a binding partner for chlorotoxin has not been validated. Hence, further characterization of chlorotoxin binding to cortactin utilizing different techniques such as surface plasmon resonance (SPR) and heteronuclear NMR experiments, and determining whether different chlorotoxin fragments bind/interact with the same receptor using structure-activity relationship (SAR) by NMR will shed more light on the chlorotoxin mechanism of action (45-50).

In terms of developing *Ov*-GRN-1 as a wound-healing agent, further structural studies will provide fundamental information in this field. Determination of the structure of full-length *Ov*-GRN-1 will provide a better understanding of *Ov*-GRN-1 structure-activity relationships. Further structural characterization of other truncated human granulins in addition to GRN A will help define the fine details for the role/influence of the non-native disulfide bond in structure stabilisation of the granulin family of proteins. Moreover, critical amino acids/sequence motifs involved in inducing fibroblast cell proliferation could be identified by assessing and comparing cell proliferation bioactivity of these analogues.

Further examination of the influence of conserved residues in the *Ov*-GRN-1 bioactivity should define the minimum consensus motif and/or amino acids necessary for the cell proliferation bioactivity. In this regard, moving forward beyond the scope of this PhD study, we intend to investigate the role of inter cysteine loops in *Ov*-GRN-1 N-terminal truncated peptide. This future direction is currently being started and the preliminary results highlight the important role for the disulfide bonds in GRN<sub>9-35\_3s</sub> bioactivity.

The next phase of this study, which is beyond the scope of the PhD, is to attempt to initiate advanced studies facilitating the clinical trial studies of GRN<sub>P4A</sub>. Perhaps the most important direction of study will be related to elucidating the mechanism of action. Chemical cross-linking studies using mass spectrometry, protein array technologies and computational modelling could be used to define the interactions of *Ov*-GRN-1 and the engineered peptides with a biological target.

It would also be quite interesting to further study the wound-healing activity in the *in vivo* diabetic mouse wound model such as the genetically hyperglycemic db/db mice (51-53). The majority of chronic wounds in humans are associated with disease states, making it of significant interest to determine if the granulin peptides are still efficacious in the presence of a disease state. In addition, punch biopsy models in pigs could also be used to study wound healing and skin regeneration, as the skin of pigs is considered very similar to human skin and likely to be more relevant for subsequent clinical applications (54). Pharmacokinetics studies could also be used to predict the bioavailability, metabolism, stability and toxicity profile of GRN<sub>P4A</sub>, *in*

*vivo* and *in vitro* (55).

Overall, the future directions given in this section might further advance the potential of both chlorotoxin and *Ov*-GRN derived peptides as drug leads.

### 6.3 References

1. Gori, A., P. Gagni, and S. Rinaldi. Disulfide bond mimetics: Strategies and challenges. *Chemistry (Weinheim an der Bergstrasse, Germany)*. 2017; 23(60): 14987-95.
2. Bechtel, T.J. and E. Weerapana. From structure to redox: The diverse functional roles of disulfides and implications in disease. *Proteomics*. 2017; 17, DOI: 10.1002/pmic.201600391.
3. Chaudhuri, D., T. Aboye, and J.A. Camarero. Using backbone-cyclized Cys-rich polypeptides as molecular scaffolds to target protein-protein interactions. *Biochem. J.* 2019; 476(1): 67-83.
4. Daly, N.L. and D. Wilson. Structural diversity of arthropod venom toxins. *Toxicon*. 2018; 152: 46-56.
5. Edwards, C., M. Cohen, and S. Bloom. Peptides as drugs. *QJM: Int. J. Med.* 1999; 92(1): 1-4.
6. Bhutia, S.K. and T.K. Maiti. Targeting tumors with peptides from natural sources. *Trends Biotechnol.* 2008; 26(4): 210-7.
7. Saez, N.J., S. Senff, J.E. Jensen, S.Y. Er, V. Herzig, L.D. Rash, and G.F. King. Spider-venom peptides as therapeutics. *Toxins*. 2010; 2(12): 2851-71.
8. Gongora-Benitez, M., J. Tulla-Puche, and F. Albericio. Multifaceted roles of disulfide bonds. *Peptides as therapeutics. Chem. Rev.* 2014; 114(2): 901-26.
9. Moore, S.J., C.L. Leung, and J.R. Cochran. Knottins: disulfide-bonded therapeutic and diagnostic peptides. *Drug Discov. Today Technol.* 2012; 9, DOI: 10.1016/j.ddtec.2011.07.003.
10. Parrish-Novak, J., et al. Nonclinical Profile of BLZ-100, a Tumor-Targeting Fluorescent Imaging Agent. *Int. J. Toxicol.* 2017; 36(2): 104-12.
11. Baik, F.M., et al. Fluorescence Identification of head and neck squamous cell carcinoma and high-risk oral dysplasia with BLZ-100, a chlorotoxin-indocyanine green conjugate. *JAMA Otolaryngol. Head Neck Surg.* 2016; 142(4): 330-8.
12. Butte, P.V., et al. Near-infrared imaging of brain tumors using the Tumor Paint BLZ-100 to achieve near-complete resection of brain tumors. *Neurosurgical focus*. 2014; 36(2): E1.
13. Dintzis, S.M., et al. Real-time Visualization of Breast Carcinoma in Pathology Specimens From Patients Receiving Fluorescent Tumor-Marking Agent Tozuleristide. *Arch. Pathol. Lab. Med.* 2018.
14. Hockaday, D.C., et al. Imaging glioma extent with 131I-TM-601. *J. Nucl. Med.* 2005; 46(4): 580-6.

15. Mamelak, A.N., et al. Phase I single-dose study of intracavitary-administered iodine-131-TM-601 in adults with recurrent high-grade glioma. *J. Clin. Oncol.* 2006; 24(22): 3644-50.
16. Mamelak, A.N. and D.B. Jacoby. Targeted delivery of antitumoral therapy to glioma and other malignancies with synthetic chlorotoxin (TM-601). *Expert Opin. Drug. Deliv.* 2007; 4, DOI: 10.1517/17425247.4.2.175.
17. Smout, M.J., J.P. Mulvenna, M.K. Jones, and A. Loukas. Expression, refolding and purification of *Ov*-GRN-1, a granulin-like growth factor from the carcinogenic liver fluke, that causes proliferation of mammalian host cells. *Protein Expr. Purif.* 2011; 79(2): 263-70.
18. Smout, M.J., et al. Carcinogenic Parasite Secretes Growth Factor That Accelerates Wound Healing and Potentially Promotes Neoplasia. *PLoS Pathog.* 2015; 11(10): e1005209.
19. Haugen, B., S.E. Karinshak, V.H. Mann, A. Popratiloff, A. Loukas, P.J. Brindley, and M.J. Smout. Granulin secreted by the food-borne liver fluke *Opisthorchis viverrini* promotes angiogenesis in human endothelial cells. *Front Med (Lausanne)*. 2018: 10.3389/fmed.2018.00030.
20. Papatpremsiri, A., M.J. Smout, A. Loukas, P.J. Brindley, B. Sripa, and T. Laha. Suppression of *Ov*-GRN-1 encoding granulin of *Opisthorchis viverrini* inhibits proliferation of biliary epithelial cells. *Exp. Parasitol.* 2015; 148, DOI: 10.1016/j.exppara.2014.11.004.
21. Smout, M.J., et al. A granulin-like growth factor secreted by the carcinogenic liver fluke, *Opisthorchis viverrini*, promotes proliferation of host cells. *PLoS Pathog.* 2009; 5, DOI: 10.1371/journal.ppat.1000611.
22. Thuwajit, C., P. Thuwajit, S. Kaewkes, B. Sripa, K. Uchida, M. Miwa, and S. Wongkham. Increased cell proliferation of mouse fibroblast NIH-3T3 in vitro induced by excretory/secretory product (s) from *Opisthorchis viverrini*. *Parasitology.* 2004; 129(04): 455-64.
23. Albert, F.K., M. Forsting, K. Sartor, H.-P. Adams, and S. Kunze. Early postoperative magnetic resonance imaging after resection of malignant glioma: Objective evaluation of residual tumor and its influence on regrowth and prognosis. *Neurosurgery.* 1995; 36(4): 873-4.
24. Ojeda, P.G., C.K. Wang, and D.J. Craik. Chlorotoxin: Structure, activity and potential uses in cancer therapy. *Peptide Sci.* 2016; 106, DOI: 10.1002/bip.22748.
25. Diaz-Perlas, C., M. Varese, S. Guardiola, J. Garcia, M. Sanchez-Navarro, E. Giralt, and M. Teixido. From venoms to BBB-shuttles. MiniCTX3: a molecular vector derived from scorpion venom. *Chem. Commun.* 2018; 54(90): 12738-41.
26. Chan, R.K., P.H. Liu, G. Pietramaggiore, S.I. Ibrahim, H.B. Hechtman, and D.P. Orgill. Effect of recombinant platelet-derived growth factor (Regranex)



- on wound closure in genetically diabetic mice. *J Burn Care Res.* 2006; 27(2): 202-5.
27. Chan, R.K., P.H. Liu, G. Pietramaggiore, S.I. Ibrahim, H.B. Hechtman, and D.P. Orgill. Effect of recombinant platelet-derived growth factor (Regranex) on wound closure in genetically diabetic mice. *J. Burn Care Res.* 2006; 27(2): 202-5.
  28. Adeghate, J., S. Nurulain, K. Tekes, E. Feher, H. Kalasz, and E. Adeghate. Novel biological therapies for the treatment of diabetic foot ulcers. *Expert Opin Biol Ther.* 2017; 17(8): 979-87.
  29. Gomes, A., C. Teixeira, R. Ferraz, C. Prudencio, and P. Gomes. Wound-healing peptides for treatment of chronic diabetic foot ulcers and other infected skin injuries. *Molecules (Basel, Switzerland).* 2017, DOI: 10.3390/molecules22101743.
  30. Demidova-Rice, T.N., M.R. Hamblin, and I.M. Herman. Acute and impaired wound healing: pathophysiology and current methods for drug delivery, part 1: normal and chronic wounds: biology, causes, and approaches to care. *Adv. Skin Wound Care.* 2012; 25(7): 304-14.
  31. Graves, N. and H. Zheng. Modelling the direct health care costs of chronic wounds in Australia. *Wound Prac. Res.* 2014; 22(1): 20-33.
  32. Munro, G. Causes and consideration with chronic wounds: a narrative review of the evidence. *Wound Prac. Res.* 2017; 25(2): 88-97.
  33. Campbell, L.V., A.R. Graham, R.M. Kidd, H.F. Molloy, S.R. O'Rourke, and S. Colagiuri. The lower limb in people with diabetes. Position statement of the Australian Diabetes Society. *Med. J. Aust.* 2000; 173(7): 369-72.
  34. Vos, T., J. Goss, S. Begg, and N. Mann. Projection of health care expenditure by disease: a case study from Australia, 2003 to 2033. Canberra: AIHW; 2008. Report No.: HWE 43.
  35. Zimmet, P.Z., D.J. Magliano, W.H. Herman, and J.E. Shaw. Diabetes: a 21st century challenge. *Lancet Diabetes Endocrinol.* 2014; 2(1): 56-64.
  36. McDermott, R.A., B.A. Schmidt, A. Sinha, and P. Mills. Improving diabetes care in the primary healthcare setting: a randomised cluster trial in remote Indigenous communities. *Med. J. Aust.* 2001; 174(10): 497-502.
  37. Busfield, F., et al. A genomewide search for type 2 diabetes-susceptibility genes in indigenous Australians. *Am. J. Hum. Genet.* 2002; 70(2): 349-57.
  38. McDermott, R.A., F. Tulip, and B. Schmidt. Diabetes care in remote northern Australian Indigenous communities. *Med. J. Aust.* 2004; 180(10): 512-6.
  39. Baxter, D., et al. Downsizing Proto-oncogene cFos to Short Helix-Constrained Peptides That Bind Jun. *ACS Chem. Biol.* 2017; 12(8): 2051-61.

40. Shepherd, N.E., R.S. Harrison, G. Ruiz-Gomez, G. Abbenante, J.M. Mason, and D.P. Fairlie. Downsizing the BAD BH3 peptide to small constrained alpha-helices with improved ligand efficiency. *Org. Biomol. Chem.* 2016; 14(46): 10939-45.
41. Zhu, Q., S. Liang, L. Martin, S. Gasparini, A. Menez, and C. Vita. Role of disulfide bonds in folding and activity of leurotoxin I: just two disulfides suffice. *Biochemistry.* 2002; 41(38): 11488-94.
42. Drakopoulou, E., et al. Consequence of the removal of evolutionary conserved disulfide bridges on the structure and function of charybdotoxin and evidence that particular cysteine spacings govern specific disulfide bond formation. *Biochemistry.* 1998; 37(5): 1292-301.
43. Zorzi, A., S.J. Middendorp, J. Wilbs, K. Deyle, and C. Heinis. Acylated heptapeptide binds albumin with high affinity and application as tag furnishes long-acting peptides. *Nature Commu.* 2017; 8, DOI: 10.1038/ncomms16092.
44. Wiranowska, M., L.O. Colina, and J.O. Johnson. Clathrin-mediated entry and cellular localization of chlorotoxin in human glioma. *Cancer Cell Int.* 2011; 11, DOI: 10.1186/1475-2867-11-27.
45. Douzi, B. Protein-Protein Interactions: Surface Plasmon Resonance. *Methods Mol. Biol.* 2017; 1615: 257-75.
46. Olaru, A., C. Bala, N. Jaffrezic-Renault, and H.Y. Aboul-Enein. Surface plasmon resonance (SPR) biosensors in pharmaceutical analysis. *Crit. Rev. Anal. Chem.* 2015; 45(2): 97-105.
47. Vanderhoeven, S.J., J. Troke, G.E. Tranter, I.D. Wilson, J.K. Nicholson, and J.C. Lindon. Nuclear magnetic resonance (NMR) and quantitative structure-activity relationship (QSAR) studies on the transacylation reactivity of model 1beta-O-acyl glucuronides. II: QSAR modelling of the reaction using both computational and experimental NMR parameters. *Xenobiotica.* 2004; 34(10): 889-900.
48. Shuker, S.B., P.J. Hajduk, R.P. Meadows, and S.W. Fesik. Discovering high-affinity ligands for proteins: SAR by NMR. *Science (New York, N.Y.).* 1996; 274(5292): 1531-4.
49. Dias, D.M. and A. Ciulli. NMR approaches in structure-based lead discovery: recent developments and new frontiers for targeting multi-protein complexes. *Prog. Biophys. Mol. Biol.* 2014; 116(2-3): 101-12.
50. Sirockin, F., et al. Structure activity relationship by NMR and by computer: a comparative study. *J. Am. Chem. Soc.* 2002; 124(37): 11073-84.
51. Michaels, J.t., S.S. Churgin, K.M. Blechman, M.R. Greives, S. Aarabi, R.D. Galiano, and G.C. Gurtner. db/db mice exhibit severe wound-healing impairments compared with other murine diabetic strains in a silicone-splinted excisional wound model. *Wound Repair Regen.* 2007; 15(5): 665-70.

52. Han, X., Y. Tao, Y. Deng, J. Yu, Y. Sun, and G. Jiang. Metformin accelerates wound healing in type 2 diabetic db/db mice. *Mol. Med. Report.* 2017; 16(6): 8691-8.
53. Senturk, B., B.M. Demircan, A.D. Ozkan, S. Tohumeken, T. Delibasi, M.O. Guler, and A.B. Tekinay. Diabetic wound regeneration using heparin-mimetic peptide amphiphile gel in db/db mice. *Biomater. Sci.* 2017; 5(7): 1293-303.
54. Sullivan, T.P., W.H. Eaglstein, S.C. Davis, and P. Mertz. The pig as a model for human wound healing. *Wound Repair Regen.* 2001; 9(2): 66-76.
55. Fan, J. and I.A. de Lannoy. Pharmacokinetics. *Biochem. Pharmacol.* 2014; 87(1): 93-120.